Shock Wave Reflections off Curved Surfaces

A.E.Cohen

A dissertation submitted to the Faculty of Engineering and the Built Environment, University of the Witwatersrand, Johannesburg, in fulfilment of the requirements for the degree of Master of Science in Engineering.

Johannesburg, May 2021

Declaration

I declare that this dissertation is my own, unaided work, except where otherwise acknowledged. It is being submitted for the degree of Master of Science in Engineering in the University of the Witwatersrand, Johannesburg. It has not been submitted before for any degree or examination at any other university.

Signed this 9th day of May 2021

A.E.Cohen

Acknowledgements

This work would not have been possible without the assistance and support of the following special people:

Prof Beric W. Skews, my supervisor and mentor for this project. Your contagious passion for shock waves inspired me to complete this work with dedication and excitement. I am extremely grateful for the guidance, knowledge and assistance you have given me over the course of this work.

Dr Randall T Paton, thank you for all the assistance you have given me during the analysis and experimentation of this study.

The technical workshop staff: Andrew, Shaun and Rowan. Thank you for all the assistance you have given me with the manufacture of the test pieces, experimental set up and the repairs of the test rig and shock tube.

Miss Aurore Larroque, thank you for the assistance you gave in the experimentation and analysis of this study.

To my family, thank you for all the support, encouragement and love you have given me during this time. To my parents, thank you for encouraging me to start this project. Without you, there would be nothing to acknowledge.

Leaving the best for last, to my wife Malki. Your constant love and support for me during this journey has made it so much sweeter. I'm sure you are excited for a new topic of conversation.

Abstract

In this work two separate studies are performed on the reflections of shock waves off curved surfaces. The effect of thermal conductivity on shock wave reflection off curved surfaces and very weak shock wave reflection are investigated.

Effect of Thermal Conductivity on Shock Wave Reflection off Curved Surfaces

Previous work has shown that the properties of a shock wave reflection off a flat surface are affected by the thermal conductivity of the reflection surface. In the more complex reflection case of a curved surface, tests were done in undergraduate studies to determine whether heat transfer into the reflection surface has an effect on the shock wave reflection properties. Although the results proved promising, further testing is required to provide conclusive results.

Tests are performed on concave and convex test pieces. Test pieces of different thermal conductivities (0.19 W/mK and 401 W/mK) and hydraulically smooth surfaces are used in the experimentation. The test pieces are placed in identical positions on either side of a plane of symmetry and at the same incident angles in the shock tube. Z-configuration shadowgraph and high speed imaging is used to capture the images. Tests are performed at Mach numbers in the range of $1.26 \leq M \leq 1.5$. The images are analysed both quantitatively through reflection angle measurements and qualitatively by examining the symmetry of the reflection patterns.

Both the qualitative and quantitative analysis performed show that the thermal conductivity of the reflecting surface affects the reflection patterns off curved surfaces. The quantitative analysis showed that heat transfer into the reflecting surface affects the reflection patterns through the measurement of various reflection angles. Significant differences in the reflection angles indicate the presence of thermal conductivity effects. In the qualitative analysis asymmetry in the reflection patterns is found at all Mach numbers, supporting the findings which are found in the quantitative analysis.

Weak Shock Wave Reflection off Curved Surfaces

Little is known about the behaviour of very weak shock waves. At Mach numbers below 1.03 there is an absence of experimental data. Several attempts at achieving a Mach number below 1.03 have been unsuccessful. In a previous study, Mach numbers between 1.03 and 1.05 showed that there are variations in the accepted reflection evolution of a curved surface. The previous work indicated the existence of a regular reflection pattern in the curved shock wave reflection evolution. The aim of the current study is to perform tests at a Mach number below Mach 1.03, explore the existence of a regular reflection pattern in the reflection evolution, and investigate the evolution of very weak shock wave reflection off a curved surface.

Experimentation is performed in a large shock tube. Various diaphragm materials such as: wax paper, aluminium foil and 12μm plastic sheeting are used to obtain Mach numbers close to unity. A 520mm radius cylindrical curved test piece with zero initial ramp angle is used in the experimentation. A shadowgraph optical setup and high speed photography is used to capture the test images. The images are analysed both qualitatively and quantitatively. Novel experimental data in the form of tests at a range of $1.007 \leq M \leq 1.026$ is captured. No shear layer is present on the Mach reflection or transitioned regular reflection at Mach numbers below 1.07. A reflection pattern resembling a regular reflection exists in the evolution between the three shock reflection patterns and the transitioned regular reflection. At low Mach numbers, curved reflection waves are observed.

Published Work

The following publications have resulted from this work:

- Cohen A., Skews B. Very weak shock wave reflection off curved surfaces. Experiments in Fluids, 61:174 (2020) *https://doi.org/10.1007/s00348-020-03009-2*
- Cohen A., Skews B.Surface Conductivity effects during Shock Wave Reflection off Curved Surfaces. Experimental Thermal and Fluid Science, 124 (2021) *https://doi.org/10.1016/j.expthermflusci.2021.110353*

Contents

List of Figures

List of Tables

Chapter 1 Introduction

1.1 Background

The Effect of Wall Thermal Conductivity on Shock Wave Reflection

The reflecting surface has been regarded as being isothermal, adiabatic and smooth in classical two dimensional shock wave theory. This implies an absence of viscous and thermal boundary layers in close proximity to the reflection surface. The existence of such boundary layers would have a distinct effect on the shock wave reflection properties.

In a 2017 study by Berry and Skews [1], it was shown that heat transfer between the shock wave and the reflecting surface has an effect on the shock wave reflection topologies. In the work done by them two identical test pieces of different thermal conductivity were placed in identical positions on either side of a plane of symmetry. The reflection patterns were compared and analysed against each other. In the study, it was found that the thermal conductivity of the reflection surface affects the reflection topologies.

In 2018, work by Cohen [2] the thermal conductivity effects of shock wave reflections off curved surfaces were explored in undergraduate studies. The results of the study indicated that the thermal conductivity has an effect on the curved shock wave reflection patterns. However, due to the limited scope of the work done in undergraduate studies the results obtained were inconclusive.

This dissertation is a continuation of the work done in undergraduate studies by Cohen. In addition, it complements the work done by Berry and Skews regarding the effects of heat transfer on shock wave reflection.

Weak Shock Wave Reflection off Curved Surfaces

There is a lack in understanding of weak shock wave behaviour. This is due to a dearth of information on very weak shock waves. There is no experimental data at a Mach number

below 1.03. Several attempts have been made to generate shock waves below Mach 1.03 but have been unsuccessful.

Work done by Gruber [3] has shown that there are variations in the accepted evolution of reflection patterns off a curved surface. His study of shock waves of speeds: 1.03< M < 1.05, indicate the existence of a regular reflection pattern between the Mach and transitioned regular reflection. This is shown in Figure 1.1. The first reflection pattern is a compression reflection (CR), this evolves into a Mach reflection(MR). The MR eventually terminates into a regular reflection (RR). The final stage in the evolution process is a transitioned regular reflection (TRR).

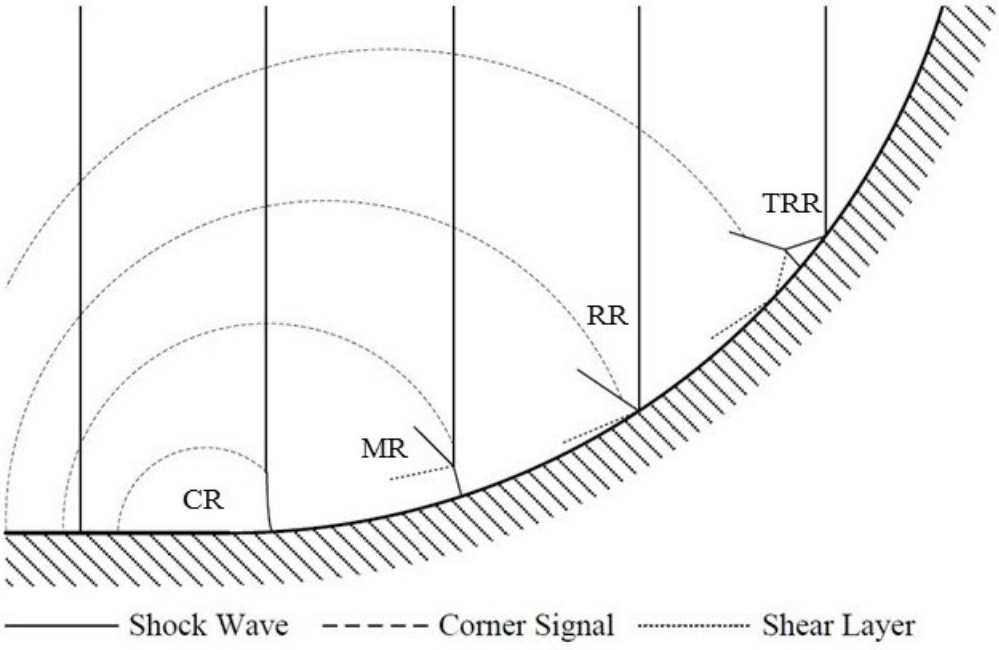

Figure 1.1: Sketch of the Curved Shock Wave Evolution.

1.2 Purpose of Study

The Effect of Wall Thermal Conductivity on Shock Wave Reflection

In classical two dimensional shock wave theory it has been assumed that the reflecting surface is adiabatic. It has been shown that reflection properties are affected by the thermal conductivity of the reflecting surface. These effects have found to be present in the reflection off a straight surface. However, the heat transfer effects off a curved surface have not been properly investigated.

Weak Shock Wave Reflection off Curved Surfaces

The purpose of this work is to gain a better understanding of very weak shock wave reflection off curved surfaces. At Mach 1, the reflection pattern will always resemble a regular reflection. Therefore, it is important to know and understand what happens as the Mach number approaches Mach 1. In addition to very weak shock wave reflection the study will focus on the transition angles of the reflection cases as well as the identification of the reflection patterns at such low Mach numbers.

1.3 Problem Statement

The Effect of Wall Thermal Conductivity on Shock Wave Reflection

It has been shown that the thermal conductivity of the reflecting surface affects the reflection patterns in the simple case of a flat surface. However, in the more complex case of reflecting waves off a curved surface the effects of thermal conductivity are unknown and will therefore be investigated.

Weak Shock Wave Reflection off Curved Surfaces

In this study the evolution of weak shock wave reflection off a curved surface will be investigated, focusing on the existence of a regular reflection stage. Methods to generate shock waves with a Mach number below 1.03 will be explored.

1.4 Assumptions

The assumption made in traditional two dimensional shock wave theory that the reflecting wall is adiabatic will be disregarded. It is also assumed that all the reflecting surfaces are hydraulically smooth and when using materials of different conductivities are identical in their design and manufacture.

Chapter 2 Literature Survey

This literature survey will cover topics relevant to this study. These include a background in compressible flow theory, shock wave theory, shock wave reflection theory, shock tube theory, flow visualisation and an exploration of the pertinent previous work.

2.1 Compressible Flow Theory

Compressible flow is defined as the flow of gas in which there are significant changes in the density between points along a streamline [4]. At a Mach number (defined below) lower than 0.3 the fluid flow can be considered to be incompressible. This is not because of an absence of compressible flow but rather the compressible effects are too small to be considered significant [4].

2.1.1 Mach Number

In compressible fluid flow the Mach number is a dimensionless velocity ratio. It is defined as the ratio of the fluid velocity to the local sonic velocity [5]. The Mach number is used to classify different flow regimes. Table 2.1 displays the different flow regimes dependant on the Mach number.

Table 2.1: Flow Regimes as Defined by Mach Number [4].

Mach Number	Flow Regime
$M < 0.3$	Incompressible
$0.3 < M < 0.8$	Subsonic
$0.8 < M < 1.2$	Transonic
$1.2 < M < 4$	Supersonic
$M > 4$	Hypersonic

If the Mach number is below 1, information about the flow can propagate upstream. If the Mach number is above 1 information about the flow cannot propagate upstream [5]. The Mach number is calculated using the following equation [5]:

$$M = \frac{v}{a} \tag{2.1}$$

Where:

- M is the Mach Number.
- v is the flow or wave speed in m/s.
- a is the local speed of sound in m/s.

2.1.1.1 Speed of Sound

The speed of sound can be explained as the propagation rate of a pressure pulse of infinitesimal strength through a stationary fluid. It can be compared to a small ripple that radially travels outward when an object is dropped into still water [5]. The speed of sound is calculated using the following equation [4]:

$$a = \sqrt{\gamma RT} \tag{2.2}$$

Where:

- a is the speed of sound in m/s.
- T is the temperature in K.
- γ is the specific heat of the gas.
- R is the universal gas constant in $\frac{J}{molK}$.

2.1.2 Ideal Gas Assumption

In many experimental, numerical and analytical solutions the assumption is made that the air behaves as an Ideal Gas. This assumption is based on a calorifically perfect gas [6]. This implies that the specific heat of the gas remains constant. This is assumed to be true at

subsonic and low supersonic flows. Since the experimentation performed in this study is at low supersonic and subsonic flows this assumption is valid. The Ideal Gas assumption is expressed as follows [5]:

$$P = \rho RT \tag{2.3}$$

Where:

- P is the absolute pressure in kPa.
- ρ is the density of the gas in $\frac{kg}{m^3}$.
- R is the universal gas constant in $\frac{J}{molK}$.
- T is the temperature in K.

A temperature difference exists across a shock wave. Dissociation and ionization of the gas may occur depending on the strength of the shock wave. However, at the speeds used in the experimentation in this study this does not occur, therefore the Ideal Gas assumption can be used to describe the physical properties of the gas during experimentation.

2.2 Shock Wave Theory

A shock wave is an irreversible occurrence which occurs in multi dimensional fluid flow. It is distinguished by discontinuous changes in temperature, pressure and density. Physically, a shock wave is a region of compressed air with a thickness of two or three mean-free paths [5]. Figure 2.1 shows the shock wave which is formed around a bullet which is travelling at supersonic speeds.

2.2.1 Normal Shock Wave

Figure 2.2 shows the properties on the upstream (1) and the downstream (2) sides of a normal shock. The downstream parameters can be found by applying the conservation laws of mass, energy and momentum [8].

Through the application of the equations, a set of relationships can be established to determine the downstream flow properties. These relationships are only valid when there is no heat addition and the flow is frictionless. It is also assumed that the air is an Ideal Gas.

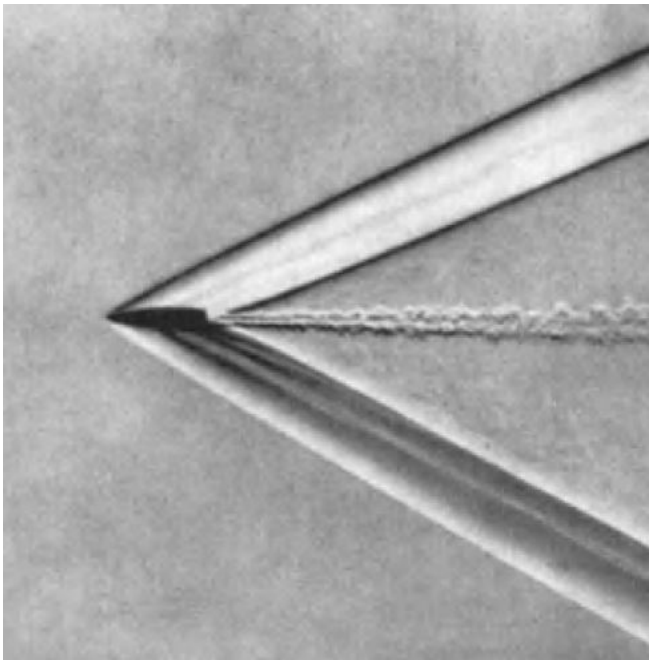

Figure 2.1: A Close Up Image of a Supersonic Bullet [7]

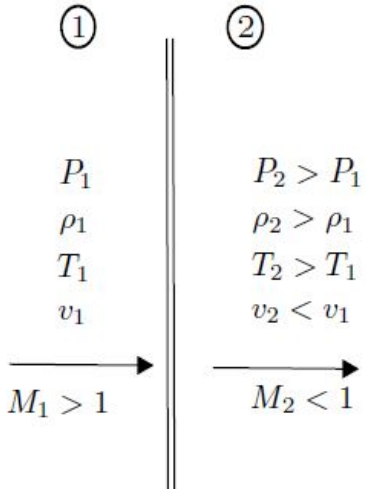

Figure 2.2: A Shock Wave [8].

Where:

- P is the air pressure in kPa.
- ρ is the air density in $\frac{kg}{m^3}$.
- T is the temperature of the air in K.
- v is the velocity of the air in m/s.

Relation between Mach numbers:

$$\frac{M_1}{M_2} = \frac{P_2}{P_1}\sqrt{\frac{T_1}{T_2}} \tag{2.4}$$

Relation between Pressures:

$$\frac{P_2}{P_1} = \frac{1+\gamma M_1^2}{1+\gamma M_2^2} \tag{2.5}$$

Relation between Temperatures:

$$\frac{T_2}{T_1} = \frac{1+\frac{\gamma-1}{2}M_1^2}{1+\frac{\gamma-1}{2}M_2^2} \tag{2.6}$$

By eliminating the pressure ratio $\frac{P_2}{P_1}$ and the temperature ratio $\frac{T_2}{T_1}$, the following equation is derived:

$$\frac{M_1^2}{M_2^2} = [\frac{(1+\gamma M_1^2)}{(1+\gamma M_2^2)}]^2 \frac{1+\frac{\gamma-1}{2}M_2^2}{1+\frac{\gamma-1}{2}M_1^2} \tag{2.7}$$

When solving equation 2.7 there are two solutions for M_2 in terms of M_1:

$$M_2 = M_1 \tag{2.8}$$

$$M_2^2 = \frac{(\frac{2}{\gamma-1}+M_1^2)}{(\frac{2\gamma}{\gamma-1}M_1^2-1)} \tag{2.9}$$

Equation 2.9 illustrates that the value of the downstream Mach number is dependant on upstream Mach number. The weakest wave possible will be existent in the case of equation 2.8 which is a sound wave. The equations above have been derived based on a derivation in the Compressible Fluids Course Notes from the University of Witwatersrand [5].

2.2.2 Moving Normal Shock Wave

The relationships and equations used to describe a stationary shock wave can also be used to describe a moving shock wave. This is done by changing the reference frame. The reference

frame can be changed from the position of a stationary observer to the shock wave itself. By doing this, the shock wave appears to be stationary. Since properties such as pressure, density and temperature are independent of the reference plane, it is simple to transform the shock wave from one reference plane to another by making adjustments for the speed of the wave.

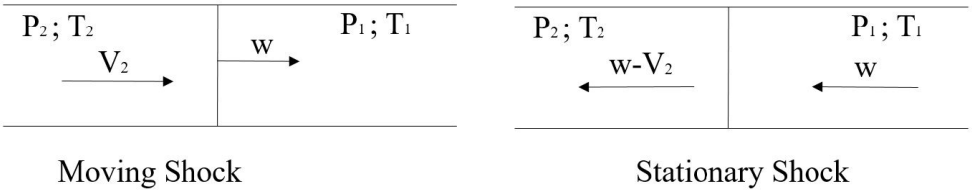

Figure 2.3: A Moving Shock Wave Into Stationary Air With Reference to an observer (Left) and to the Stationary Shock (Right) [2].

Figure 2.3 displays the transition of the shock wave from the reference plane of a stationary observer to the shock itself. The difference in the transformation is the subtraction of the speed of the shock w (m/s) from the speed of the air upstream of the shock.

2.3 Shock Wave Reflection

When a supersonic compressible flow is turned into itself, an oblique shock wave is generated [5]. Figure 2.4a shows subsonic flow travelling over a wedge. Since the flow is below Mach 1 the flow upstream can communicate to the rest of the flow about the change in the path, hence the flow path shown in Figure 2.4a.

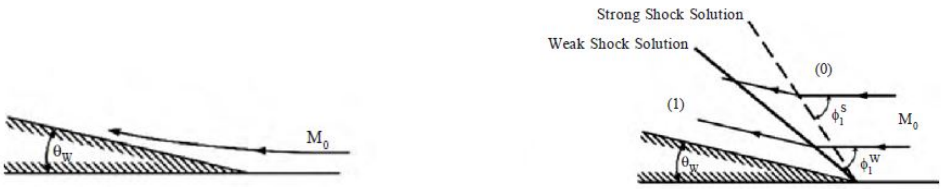

(a) Subsonic Flow

(b) Supersonic Flow

Figure 2.4: Flow Over a Wedge [9].

In the case of supersonic flow an oblique shock is formed. Figure 2.4b shows an initially supersonic compressible flow turned by an angle of θ_w. The flow upstream cannot detect the change in direction which is imposed by the wedge. Therefore, the flow adjusts to the wedge through an oblique shock wave [5]. The adjusted flow travels parallel to the wall. The oblique shock is a compressive shock wave and generates high temperature and pressures. The oblique shock reduces the speed of the gas.

A comprehensive explanation of the shock wave reflection can be found in Chapter 1 of the book Shock Wave Reflection Phenomena by G Ben Dor [9].

2.3.1 Shock Wave Reflection Off a Straight Surface

Just like an oblique shock wave will reflect when a supersonic flow encounters an edge, so too when a moving shock wave encounters a stationary surface it will reflect off that surface. The most simple case of a shock wave reflection is when a moving shock encounters a straight surface. There are two possible types of reflections that can occur. These are a regular reflection and an irregular reflection [9].

Figure 2.5 shows a regular and irregular reflection. A regular reflection simply consists of a reflected(R) and incident(I) wave. An irregular reflection is more complex than a regular reflection, this due to the addition of a Mach stem to the incident and reflected wave. The Mach stem (MS), incident wave and reflected wave meet at the triple point(TP) of the irregular reflection. A irregular reflection also exhibits a shear layer(SL) which originates from the triple point.

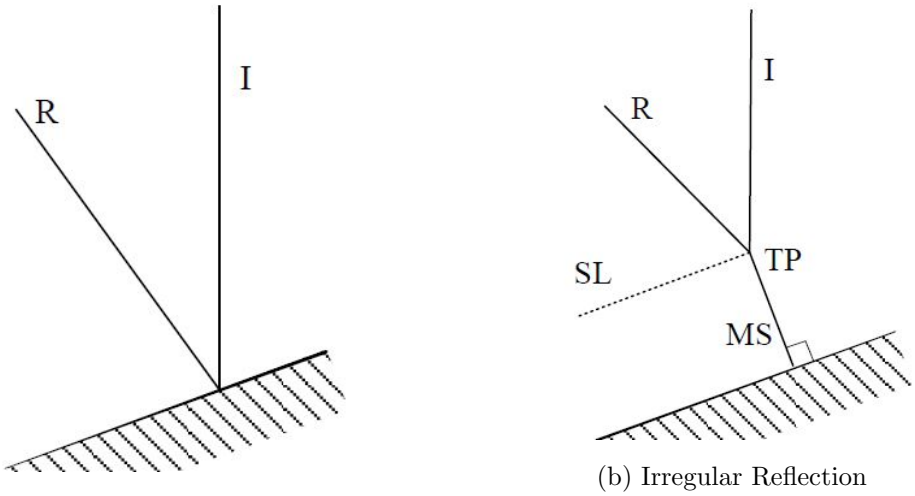

(a) Regular Reflection

(b) Irregular Reflection

Figure 2.5: A Shock Wave Reflecting off a Straight Surface [10].

A moving shock reflection off a straight surface is pseudo-stationary. The nature of the reflection pattern is that it will not change form along the reflecting surface. This remains true as long as the angle of the straight surface remains constant. The existence of a regular or irregular reflection depends on the wedge angle of the straight surface [9].

2.3.2 Shock Wave Reflection off a Curved Surface

When a moving shock reflects along a curved surface the reflection patterns exhibited are more complex than those mentioned in Section 2.3.1. This is because as the shock wave moves along the curve it is incrementally reflecting off a surface at different wedge angles. The reflection pattern is therefore transient. The reflection pattern therefore experiences an evolution as it moves along the surface of the curved surface. The evolution the shock wave experiences is different in the concave and convex cases.

2.3.2.1 Concave Surface

In the case of a concave reflection surface the reflection evolution is shown in Figure 2.6.

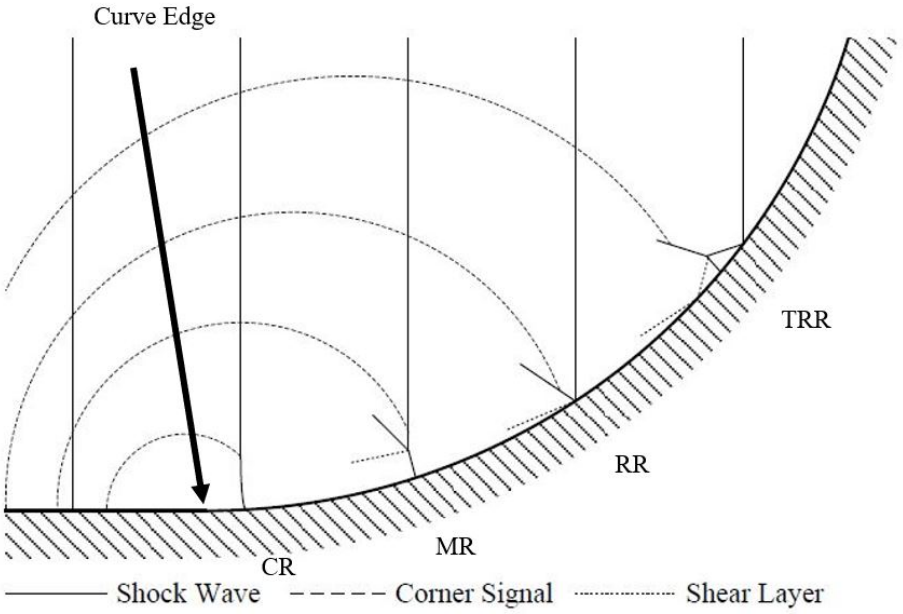

Figure 2.6: The Evolution of a Shock Wave Reflection Over a Curved Surface [10].

The incident wave is entirely planar before encountering the curve. As the shock wave encounters the curve a compression wave reflection is observed. The compression reflection evolves into a Mach reflection. The Mach reflection becomes a regular reflection which ultimately evolves into a transitioned regular reflection.

Regarding regular reflection it must be noted that in all previous studies besides for those performed by Skews and his students, have regarded the regular reflection as purely transitory and not existing for any time.

A more detailed explanation of the evolution of the Mach reflection is shown in Figure 2.7. The reflection pattern starts as a Direct Mach reflection (DiMR) which is characterized by the triple point moving away from the reflecting surface. The stationary Mach reflection (StMr) is characterized by a triple point which moves parallel to the reflecting surface. The inverse Mach reflection (InMR) is characterized by a triple point which moves toward the reflecting surface.

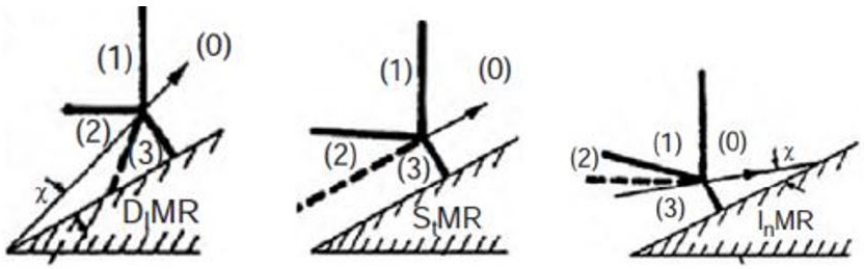

Figure 2.7: The Evolution of a Mach Reflection [9].

As the InMR terminates it develops into a Transitioned Regular Reflection. Once the triple point reaches the surface the Mach stem disappears and the incident wave and reflected wave meet at the surface. This reflected wave has the same appearance as a regular reflection. As the wave moves up the surface a new triple point is formed. The transformation process is shown in Figure 2.8.

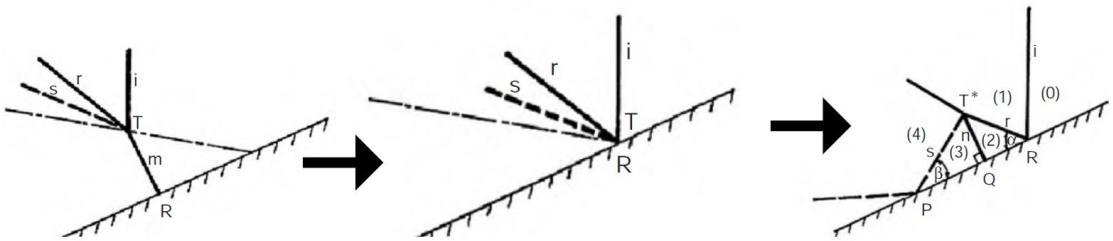

Figure 2.8: The Transition of a InMR to a TRR [9].

The final phase of the evolution of a shock wave reflecting off a curved surface is the transitioned regular reflection. In the TRR shown in Figure 2.9 a shock wave (S) is formed in the wake behind the incident wave. It meets the reflected wave, shear layer and secondary reflected wave at the triple point. Since there are two shock waves, the secondary reflected waves and shear layers are denoted as S^* and SL^* [11]. This is shown in Figure 2.9.

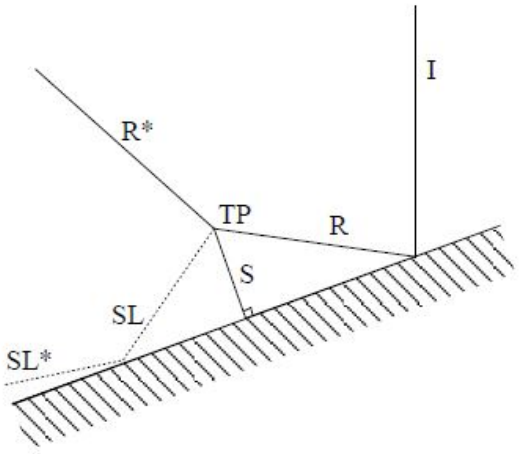

Figure 2.9: Transitioned Regular Reflection [10].

2.3.2.2 Convex Surface

The reflection exhibited when a shock wave reflects of a convex surface are different to the reflections from a concave surface. Depending on the initial wedge angle the reflection pattern is either a Mach reflection (MR) or a Regular Reflection (RR) [9]. These are shown in Figure 7.8. The reflection pattern begins as a regular reflection in Figure 2.10a and transitions into a Mach reflection in Figure 2.10b

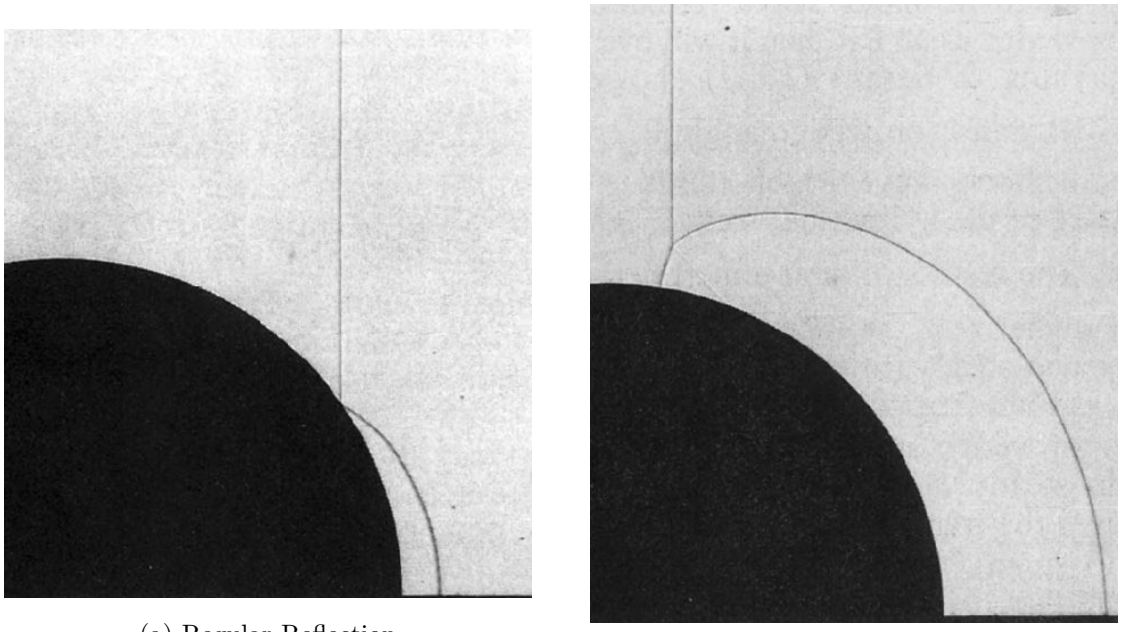

(a) Regular Reflection

(b) Mach Reflection

Figure 2.10: A Shock Wave Reflecting off a Concave Curved Surface [9].

The transition angle between RR and MR is dependant on four variables: Mach number, initial wedge angle, radius of the cylindrical surface and surface roughness. More details on the effect the radius, Mach number, surface roughness and incidence angle has on the transition point can be found in Chapter 4.1.2 in Ben Dor [9].

2.3.3 Shock Wave Reflection Patterns

Although several reflection patterns have been mentioned so far, there are many more reflection patterns. A reflection pattern tree from Ben Dor [9] is shown in Figure 2.11. The reflection tree consists of all possible reflection patterns that have been identified. All reflection patterns relevant to this study have a white background.

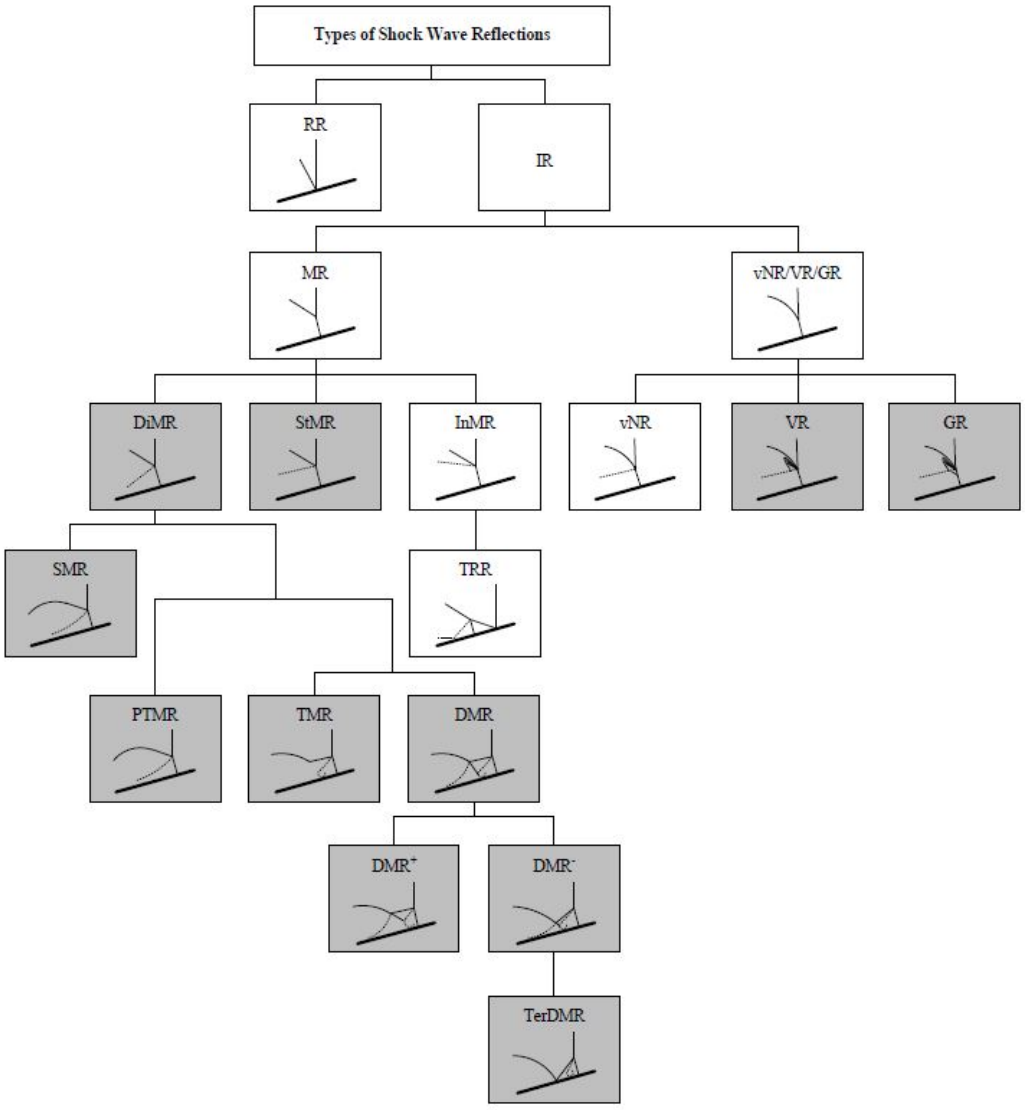

Figure 2.11: Shock Wave Reflection Pattern Tree [9].

2.3.4 Theoretical Calculation of Reflection Angles

The theoretical reflection angles can be calculated using Two Shock Theory as outlined in Chapter 1 of Ben Dor [9] and in Chapter 8 of Skews [5]. This subsection will summarize the steps taken to calculate the theoretical reflection angles. In this study the theoretical reflections are useful as they can be compared to the measured reflected angles from the experiment.

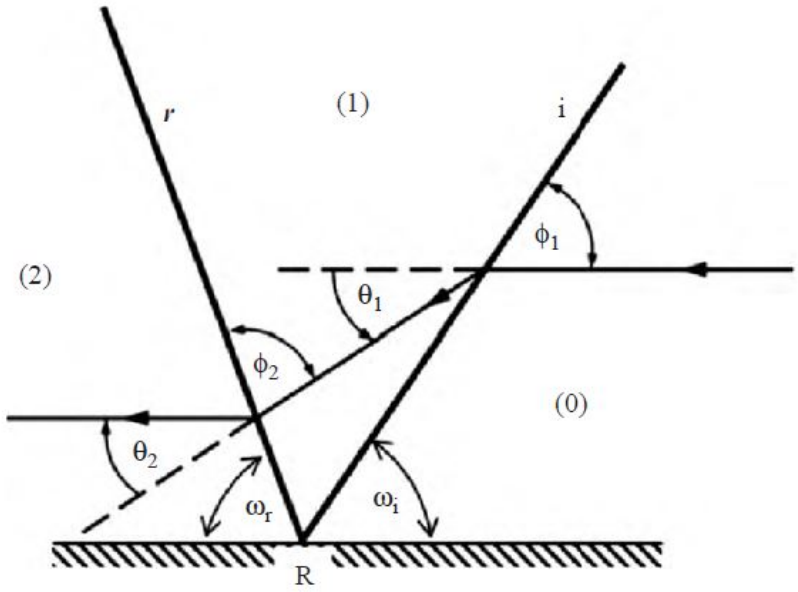

Figure 2.12: Schematic Diagram of a Regular Reflection [9].

Figure 2.12 shows a schematic of a regular reflection. When performing the calculation, it assumed that the Mach number of incident shock is known. Therefore, compressible gas tables can be used to calculate the properties across the wave. However, these tables are only valid for use when the flow is normal to the shock wave. The incident flow is normalised in a frame fixed on the reflection point:

$$M_{no} = M_o sin(\phi_1) \tag{2.10}$$

$$M_{n1} = M_1 sin(\phi_1 - \theta_1) \tag{2.11}$$

The same process is followed to normalise the flow velocity:

$$V_{no} = V_o sin(\phi_1) \tag{2.12}$$

$$V_{n1} = V_1 sin(\phi_1 - \theta_1) \tag{2.13}$$

In order to calculate the angle by which the reflection deflects the flow (θ_1):

$$V_{t1}^2 = V_1^2 - V_{n1}^2 \tag{2.14}$$

$$tan(\phi_1 - \theta_1) = \frac{V_{n1}}{V_{t1}} \tag{2.15}$$

Since the flow is parallel to the wall the following assumption must be made:

$$\phi_1 = \omega_1$$

The above calculations define the properties in state 0 and in state 1. However, determining the properties of the flow at state 2 is more complex. An iterative process can be used to calculate the properties in state 2 and hence the reflection angle. The following equations can be used in that iterative process. As illustrated in Figure 2.12 the flow before the incident wave (state 0) and the flow after the reflected wave (state 2) are parallel to the reflecting surface. Therefore, the following assumption can be made:

$$\theta_1 = \theta_2$$

The flow is normalised to the reflected shock:

$$M_{n1} = M_1 sin(\phi_2) \tag{2.16}$$

$$M_{n2} = M_2 sin(\phi_2 - \theta_2) \tag{2.17}$$

The velocities of the flow are calculated using the following equations:

$$V_{n1} = V_1 sin\phi_2 \tag{2.18}$$

$$V_{n2} = V_2 sin(\phi_2 - \theta_2) \tag{2.19}$$

$$V_{t2}^2 = V_2^2 - V_{n2}^2 \tag{2.20}$$

Finally, ϕ_2 is calculated:

$$\phi_2 = arctan(\frac{V_{n2}}{V_{t2}}) + \theta_2 \tag{2.21}$$

Once the flow properties are obtained for all three states of flow, the angle between the incident and reflected wave can be calculated.

2.4 Shock Tube Theory

In gas dynamics a shock tube is an item of experimental equipment which is used to create and replicate shock waves. The replication of these waves is used for research in gas dynamics. In order to generate a shock wave, a controlled explosion is created inside a shock tube. The generated shock wave passes down the shock tube and exits at the exhaust. The shock tube has a constant rectangular cross sectional area. A general diagram of the shock tube is shown in Figure 2.13.

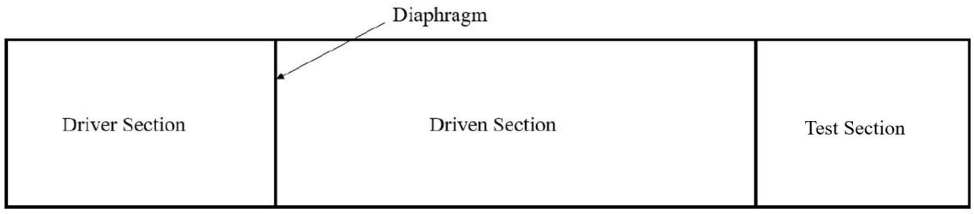

Figure 2.13: General Diagram of the Shock Tube.

In the shock tube there are three sections. These are: the driver, the driven and the test section. A diaphragm is placed in-between the driver and the driven section. In order to create a shock wave the driver section is gradually pressurized. A shock wave is generated when the diaphragm can no longer support the pressure and as a result ruptures, or when a pricker is used to burst the diaphragm. An incident shock wave passes from the driver section through the driven section and test section and exits at the exhaust which is at the very end of the shock tube. An expansion wave propagates in the opposite direction of the incident shock wave [12].

Figure 2.14 and Figure 2.15 show the pressure diagrams of the shock wave before and after the rupture of the diaphragm. Figure 2.14 shows two pressure regions, a high pressure and

low pressure region. The high pressure region is controlled by the operator while the low pressure region is air at atmospheric pressure. The Mach number of the resulting shock wave is dependant on the pressure difference between the high pressure and low pressure regions.

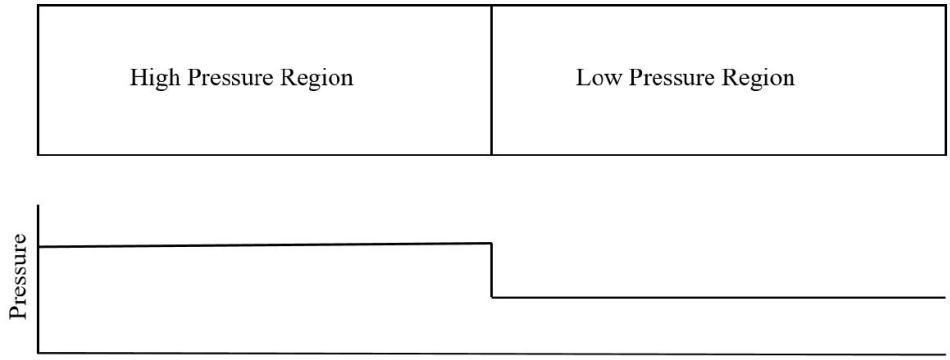

Figure 2.14: Pressure Diagram of the Shock Tube Before the Rupture of the Diaphragm

The pressure distribution in the tube after the diaphragm is burst is shown in Figure 2.15. Once the diaphragm has ruptured, a expansion wave is generated to the left of the diaphragm and a shock wave is generated to the right of the diaphragm. Depending on the initial pressure there may be regions of subsonic, sonic and supersonic speeds between these two waves. These regions may only exist for a couple of milliseconds depending on the length of the tube.

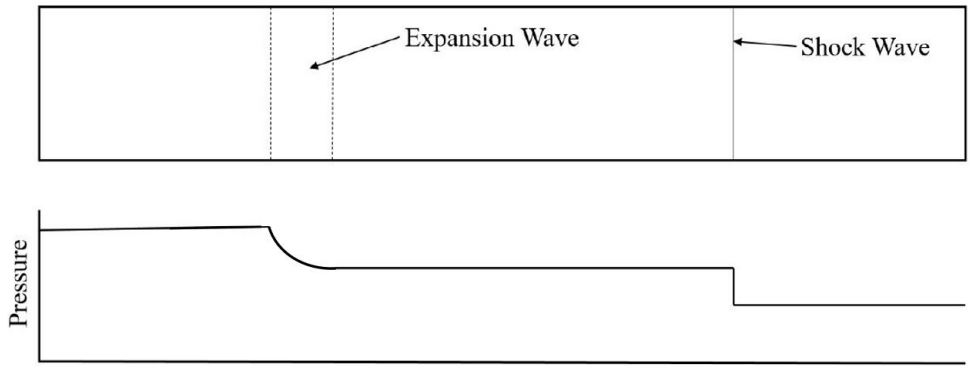

Figure 2.15: Pressure Diagram of the Shock Tube After the Rupture of the Diaphragm

Figure 2.16 is a wave diagram which describes what happens inside the tube after the rupture. The air is changed from state 1 to state 2 as a shock propagates into the driven section. At the same time an expansion wave enters the driver section changing the air from state 4 to state 3. State 2 and State 3 are at different temperatures but the same velocities.

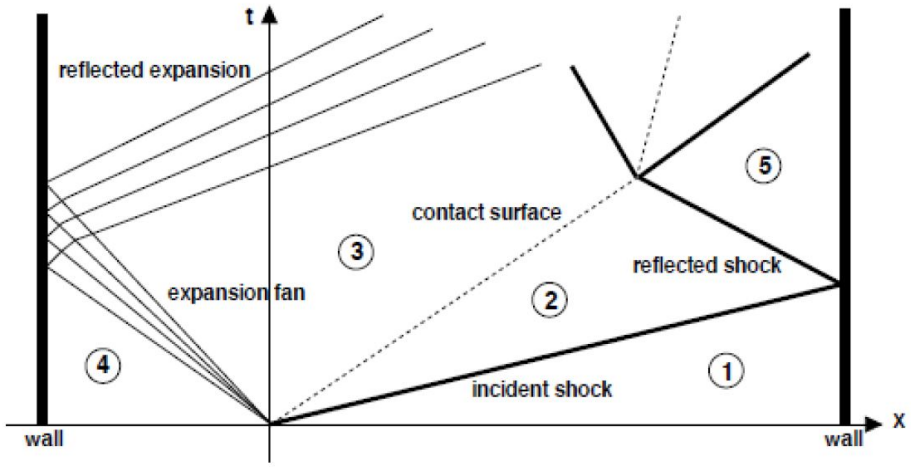

Figure 2.16: Wave Diagram of the Shock Tube [12].

2.4.1 Shock Tube Equation

The shock tube equation can be used to calculate the Mach Number of the wave. The Mach number is a function of the temperature ratio, pressure ratio and specific heat ratio. The Mach number can be calculated using the following equation [12]:

$$\frac{P_4}{P_1} = \frac{1 + (\frac{2S_1}{S_1+1})(M_s^2 - 1)}{(1 - (\frac{S_4-1}{S_1+1})(\frac{a_1}{a_4})(\frac{2S_4}{S_4-1}))^{\frac{2S_4}{S_4-1}}} \tag{2.22}$$

Where:

- P_1 and P_4 are the pressures in the low and high region respectively.
- a_1 and a_4 are the air sound speeds.
- S_1 and S_4 are the specific heats in the low and high pressure regions respectively.
- M_s is the Mach number of the shock wave.

2.5 Flow Visualisation

In the study of shock waves, the visualisation of the shock wave and it's properties is a most useful tool in the analysis of these waves. However, since the shock wave physically consists of compressed air moving at a high speed, it is invisible to the human eye. Therefore, special techniques have been developed and are used to aid the human eye in witnessing these phenomena.

The human eye and camera can only see amplitude, colour contrast and polarisation [7]. The human eye cannot see phase differences in light. However schlieren and shadowgraph methods aid the human eye. This is done by translating phase differences into amplitude. This allows the human eye to see the 'invisible'.

In a comprehensive book by G Settles [7] the history and details of various optical setups are covered. In this study a z configuration shadowgraph was used. A diagram of the setup is shown in Figure 2.17.

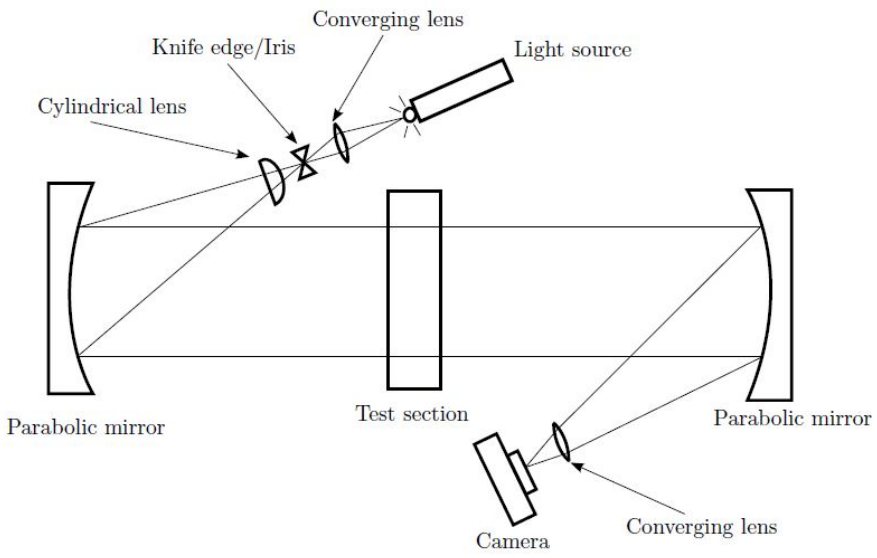

Figure 2.17: A Z configuration Shadowgraph Layout [8]

The light source emits a diverging light beam which passes through a converging lens. A pinhole is placed at the focal length of the converging lens. This is done to approximate a point source. After travelling through the pinhole the light diverges onto a parabolic mirror. The mirror transforms the beam from a diverging beam to a parallel beam and directs it through the test section onto the other parabolic mirror. This mirror converts the parallel beam to a converging beam. A knife edge is placed at the focal point of the mirror. The knife edge blocks deflected light rays from reaching the camera resulting in a more sensitive image.

The primary flow visualisation technique used in this study is shadowgraphy. However, in some instances schlieren is used as well. A diagram of a z-configuration is shown in Figure 2.18.

A Z-configuration schlieren layout is shown in Figure 2.18. The optical setup required to produce a schlieren is almost identical to a shadowgraph. It requires the addition of a knife

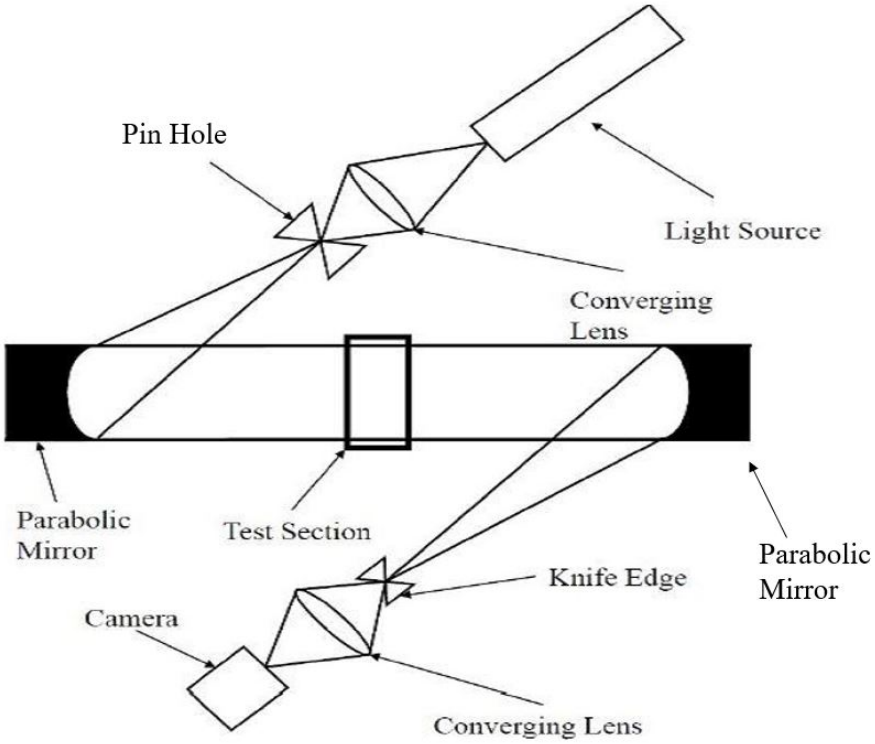

Figure 2.18: A Z configuration Schlieren Layout [8]

edge on the camera side. Figure 2.19 shows a shadowgraph and schlieren images of air passing over an aerofoil. As it is clear from the images, a shadowgraph image gives a more defined and clear image but the schlieren image provides more information about the air around the aerofoil. The primary visualisation technique used in the experiment is shadowgraphy, if necessary schlieren imaging is used in addition.

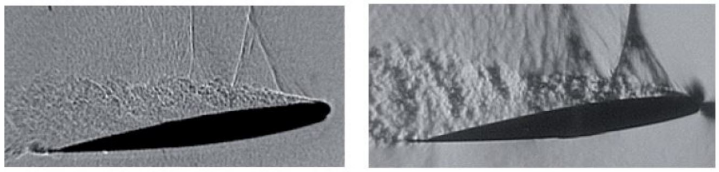

Figure 2.19: Two Images of an Aerofoil: A shadowgraph on the left and a schlieren image on the right [13].

2.6 Previous Work

The Effect of Wall Thermal Conductivity on Shock Wave Reflection

2.6.1 Reflection off a Straight Surface

In a 2017 journal paper by Berry and Skews [1], it was shown that the reflection properties of the shock wave are affected by heat flow to the reflecting surface. Two test pieces with different thermal conductivities were placed in identical positions on either side of a plane of symmetry. Both test pieces had the same incident angle and both leading edges come into contact with the shock at the exact same moment. The images were captured using single-shot high-resolution photography.

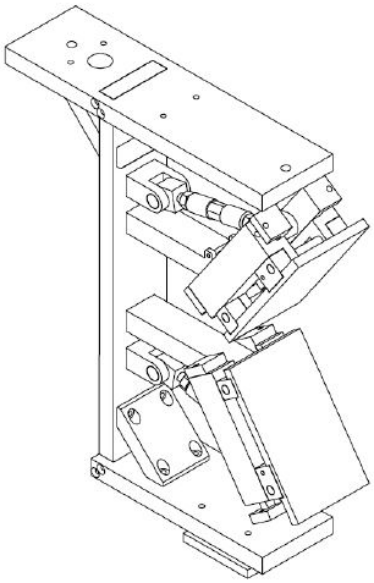

(a) The Test Rig Used by Berry.

(b) Shock Coming Into Contact With Leading Edges.

Figure 2.20: Setup of the Experiment Done by Berry [8].

The experimental configuration used by Berry [8] is shown in Figure 2.20a. The test rig is adjustable, it allows the test pieces to be rotated using sliding arms. The lateral position of the test piece can also be adjusted as the test pieces are placed on sliding mounts. An inclinometer was used to ensure that both test pieces are positioned at identical angles. This was necessary to make certain that the incident shock wave comes into contact with the leading edges at exactly the same moment in time. This is shown in Figure 2.20b.

In the work done by Berry, both Regular and Mach reflection patterns were considered. The different reflection patterns were obtained by changing the incidence angle of the straight

surfaces. Once the images had been taken, an analysis using a CAD package was performed. A qualitative and quantitative analysis was performed on each reflection case.

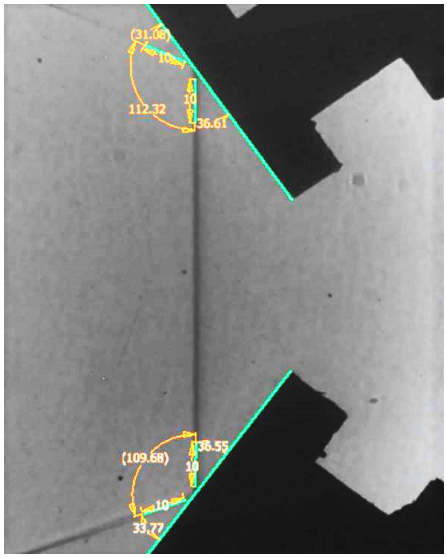

(a) Quantitative Measurement of Reflection Pattern.

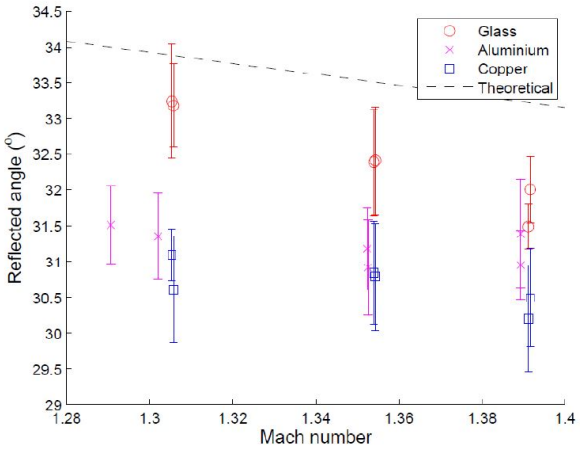

(b) Quantitative Results.

Figure 2.21: Quantitative Measurement and Results for Regular Reflection [8].

An AutoCad package was used to measure the angle between the incident and reflected waves, this is shown in Figure 2.21a. Figure 2.21b shows the results obtained by Berry. It is evident that there are significant differences between the measured angles for glass (low thermal conductivity) and copper (high thermal conductivity). From the graph, it is apparent that there is a difference of approximately 1.5^o to 2^o. The smaller reflection angles were present in the material with a lower thermal conductivity (glass).

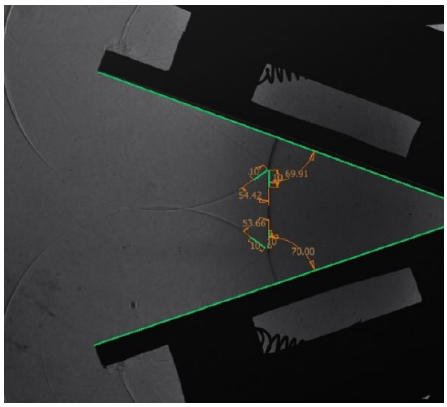

(a) Quantitative Measurement of Reflection Pattern.

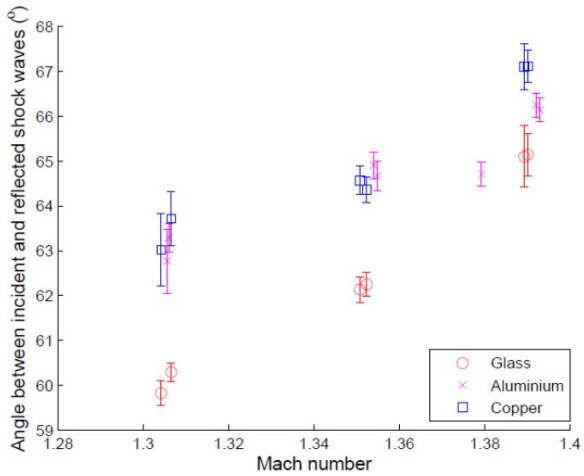

(b) Quantitative Results.

Figure 2.22: Quantitative Measurement and Results for Mach Reflection [8].

In the case of Mach reflection, the angles were measured in a similar way to the regular reflection. This is shown in Figure 2.22a. The angle between the incident wave and reflected wave is measured. As is shown in Figure 2.22b the difference between reflection angles off the two surfaces range from 1^o to 3.5^o. It is noted that in the Mach reflection case the material with a higher thermal conductivity has a higher reflected angle.

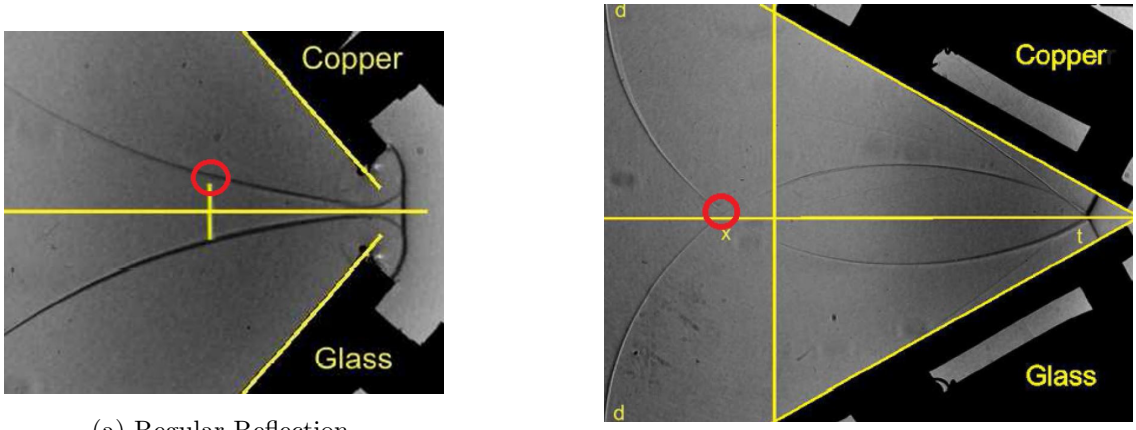

(a) Regular Reflection.

(b) Mach Reflection.

Figure 2.23: Qualitative Results [8].

The qualitative analysis is performed by drawing a line along the plane of symmetry that splits the image. The line is perpendicular to the incident shock wave. This is shown in Figure 2.23b. Figure 2.23a shows a regular reflection. At a random point, a line normal to the splitting line is drawn which touches the reflection pattern from the glass side. A line of the same distance is drawn on the other side of the splitting line. This line does not touch the reflection pattern from the copper side. This is a strong indication that the wall thermal conductivity affects the reflection pattern.

Figure 2.23b shows the qualitative measurement of the Mach reflection. In this case, just one line perpendicular to the incident shock was drawn on the image. As it can be seen in the image, the reflection patterns cross each other above the symmetry line. The image shows asymmetry in the reflection patterns.

Skews and Berry [1] have shown that reflection topologies are affected by heat flow into a flat reflecting surface. The results from the work suggest that the reflection patterns from materials with a higher thermal conductivity exhibit weaker shock waves.

2.6.2 Reflection off a Curved Surface

In undergraduate studies by the candidate [2] the effects of wall thermal conductivity off curved surfaces was investigated. The undergraduate work was a continuation of the work

done by Berry in plane walls. As explained in Section 2.3 shock wave reflection off a curved surface are more complex than reflection off a straight surface. Since the wall thermal conductivity affected the reflection properties of a reflection off a straight surface the assumption can be made that wall thermal conductivity will affect the reflection patterns off curved surfaces

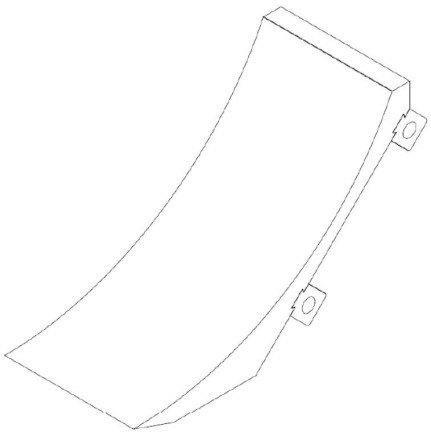

Figure 2.24: Curved Test Piece [2]

In the study, two identical curved pieces of different thermal conductivities (copper and PVC) were placed in identical positions about a plane of symmetry. The test pieces were attached onto the test rig designed by Berry. Several adjustments were made to the test rig. As in the work done by Berry, a qualitative and quantitative analysis was performed on the results. The test pieces were aligned using an inclinometer and the sliding mounts on the test rig. Figure 2.25 shows the incident shock coming into contact at the same position on both test pieces.

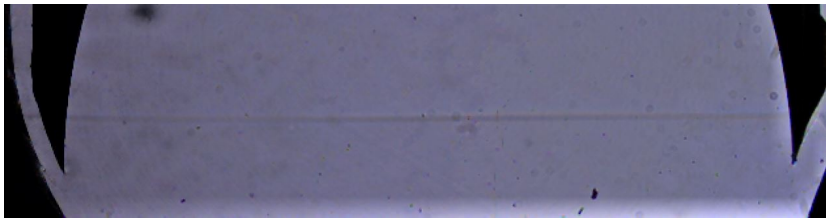

Figure 2.25: Incident Shock Wave Coming Into Contact with Curved Test Pieces [2]

Data about the reflection properties was obtained from the image using an AutoCad package. In the case of a regular reflection the angle between the incident and reflected wave was measured. This is shown in Figure 2.26. The results were obtained at Mach numbers of 1.18, 1.27, 1.37 and 1.46. In all cases, the measured angle was larger for the PVC test piece than the measured angle from the copper test piece. The differences range from 3^o to 5^o. The graph indicates that the wall thermal conductivity has a significant effect on the reflection properties of a regular reflection.

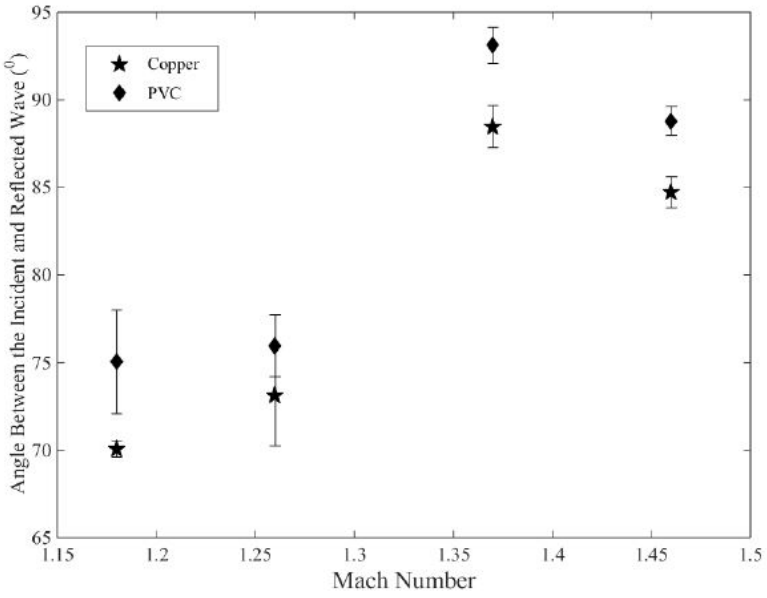

Figure 2.26: Differences Between Incident and Reflected Waves in the Case of a Regular Reflection [2].

In the case of a Mach reflection the difference in the angle between the incident and reflected wave was not as significant. Figure 2.27 shows the data obtained at Mach numbers of 1.18, 1.27, 1.37 and 1.46 of a Mach reflection. Besides for the results at Mach 1.18 the size of the measured angle is larger when reflecting off PVC than copper. Although this small difference is not as significant as the difference present in the regular reflection case, it still has merit to suggest that the reflection properties are affected by heat flow into the reflecting surface.

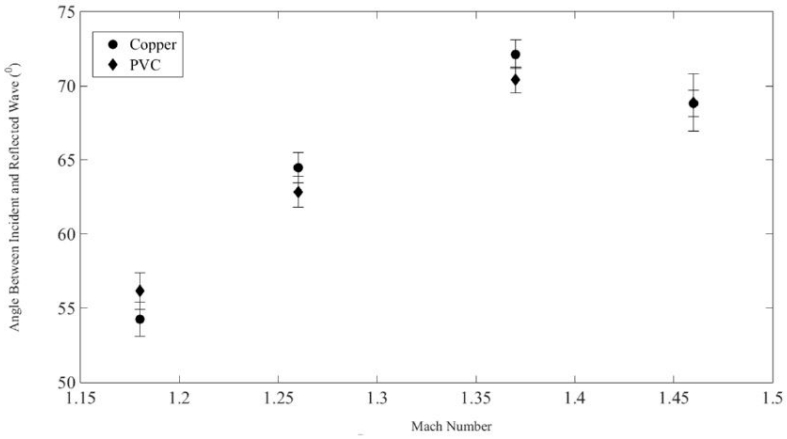

Figure 2.27: Differences Between Incident and Reflected Waves in the Case of a Mach Reflection [2].

A qualitative analysis was performed on the images. This was done by superimposing the reflection from the copper test piece onto the reflection from the PVC. The case of a transited regular reflection is shown in Figure 2.28. Clear differences in the reflection patterns are

observed. In Figure 2.28a it can be seem that the TRR off the PVC surface is larger and more developed than the TRR from the copper surface. The difference in size of the reflection patterns is even more pronounced in Figure 2.28b at Mach 1.37. The qualitative analysis had shown a distinct difference in the reflection patterns hence the reflection properties are affected by wall conductivity.

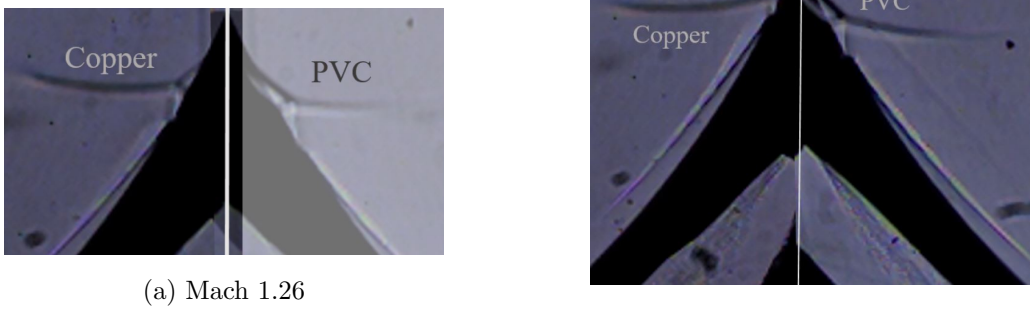

(a) Mach 1.26

(b) Mach 1.37

Figure 2.28: Superimposed Images of Copper and PVC [2].

The quantitative and qualitative analysis suggest that in the case of shock wave reflection off a curved surface the reflection properties are affected by heat transfer between the reflecting wave and the reflecting surface. Although the results from this experiment were promising they were not conclusive and therefore the need arose for more investigation.

Weak Shock Wave Reflection off Curved Surfaces

2.6.3 Skews, Kleine, Barber, et al. 2007

In a 2007 study by Skews et al. [14] tests at Mach numbers from 1.04 to 1.36 were performed on curved surfaces and cavities. In their work, both schlieren and shadowgraph images were taken of a shock wave reflecting off a cylindrical curved surface. Typical images from the experiment are shown in Figure 2.29.

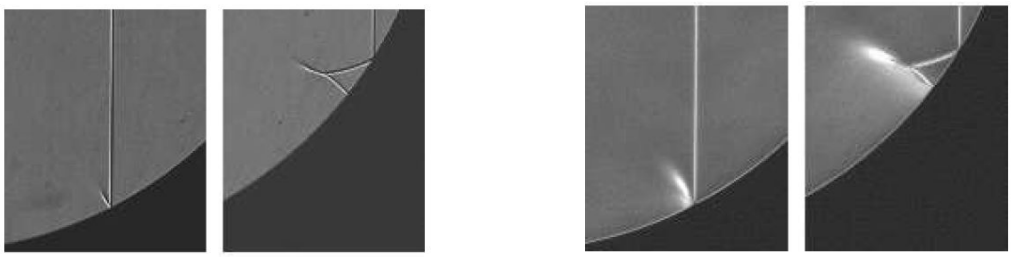

(a) Shadowgraph Image.

(b) Schlieren Image.

Figure 2.29: Shadowgraph and schlieren Images of Shock Wave at Mach 1.04[14].

Figure 2.29a shows a shadowgraph image. In the first image the reflected wave appears to be a regular reflection. However, the schlieren image in Figure 2.29b is not clear and it cannot be determined from this image whether the reflection pattern is a regular reflection or not. The reflection pattern in the second image has similarities to a TRR but an absence of shear layers and a slipstream suggests the reflection is more similar to that of a von Neumann reflection. The area behind the reflection is not clear in the schlieren image, therefore further investigation into this is required [14].

2.6.4 Skews and Gruber, 2013

A 2013 study by Skews and Gruber [10] explored weak shock wave reflections off curved surfaces. Experiments were performed at Mach < 1.1 on different curved profiles. High resolution photography was used to capture images of the reflecting patterns.

Results from the work done indicate the existence of a regular reflection in the weak shock wave case. It exists in the region between where the triple point of the Mach reflection touches the surface and the development of the transitioned regular reflection [3]. Images of the apparent regular reflection are shown in Figure 2.30.

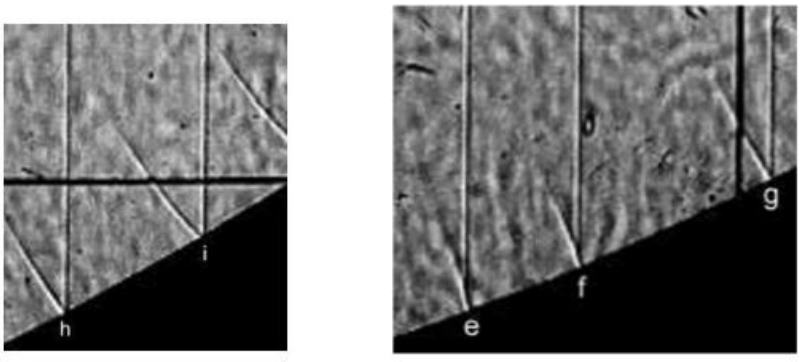

Figure 2.30: Apparent Regular Reflection at Mach 1.035 from Experiments Done by Skews and Gruber [10]

The reflection pattern (frames g, h and i) in Figure 2.30 strongly resembles that of a regular reflection. This indicates that in the weak shock wave case a regular reflection exists between the Mach reflection and TRR as is shown in the diagram in Section 2.3.2.1. However, the images do not have a high resolution. This is mainly because at such low Mach numbers the size of the reflection pattern is small and since the models used in this experiment were small the resolution of the images and the reflection pattern is lacking. The lack of clarity required more experimentation to be done in order to conclusively determine whether the regular reflection exists.

Another finding of Gruber and Skews was the absence of a shear layer, or a clear discontinuity in shock wave slope at the triple point of shock waves $1.03 < M < 1.05$. This absence represents a potential difference in the reflection properties of very weak and stronger shock wave reflection.

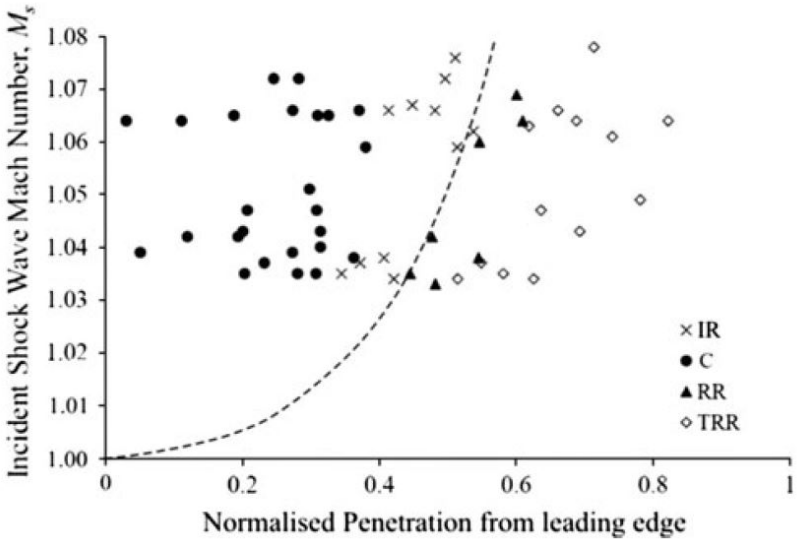

Figure 2.31: Scatter Plot Summarising the Reflection Configurations After Classification for all Circular Test Pieces [3].

In Figure 2.31 the transition cases of compression reflection (C), Mach reflection (IR), regular reflection (RR) and transitioned regular reflection (TRR) are collected in a scatter plot. A boundary line is drawn onto the graph to represent the von Neumann theory of transition between regular and Mach reflection on a plane wall at the same angle. All Mach reflection takes place on the left side of the boundary line.

It can be seen from the scatter plot that below a Mach number of 1.03 there is no data. This is due to the experimental difficulty in producing such weak waves. From the scatter plot it seems that Mach 1.03 is the lower physical limit in weak shock wave generation. If possible, obtaining data below Mach 1.03 would be useful in confirming the theoretical boundary line and establishing boundary lines for other reflection transition cases.

This literature survey has covered all theoretical topics relevant to this study. The topics covered will form the foundation for the experimentation and analysis undertaken in this work. In addition it has reviewed in detail all previous work which is pertinent to this work.

Chapter 3 Objectives

The Effect of Wall Thermal Conductivity on Shock Wave Reflection off Curved Surfaces

- Undertake both a quantitative and qualitative analysis of the effects that materials of different thermal conductivities have on the various reflection cases of curved shock reflection.
  - The effects on concave and convex cylindrical reflection patterns.
  - Confirm results from past work done by the author [2].

Weak Shock Wave Reflection off Concave Curved Surfaces

- Using high speed and high resolution photography, examine the reflection properties of weak shock waves (Mach < 1.1)
  - Perform tests below Mach 1.03.
  - Determine if the apparent regular reflection exists in weak shock reflection.
  - Investigate the evolution of weak shock wave (Mach < 1.1) reflection off a curved surface with zero initial ramp angle.

Chapter 4 Apparatus

4.1 Introduction

This section will describe all the equipment and instrumentation used in this study. All testing in this work was performed in room F7 at the Flow Research Unit (FRU). The FRU is based in the Northwest Engineering Building on the East Campus of the University of Witwatersrand in Johannesburg, South Africa. This section will discuss the following topics: the shock tube, test pieces, optics, imaging and the diaphragm materials.

The engineering drawings for all the test pieces and test components can be found in Appendix A. The appendix also contains a list of the instrumentation used in the experimentation.

4.2 Shock Tube

In this study the Large Scale Diffraction Shock Tube (Blue Tube) was used. The tube consists of three sections: a driver section, a driven section and a test section. The driver section is a 450mm diameter pipe with a wooden insert. The wooden insert matches the rectangular cross section of the tube. The wooden insert reduces the volume of air the driver section can contain. The driven section consists of three rectangular sections, the cross section is 100mm by 450mm. However, a channel is placed in the test section, giving it the same cross section as the driver and driven section. The test section has a larger cross section of 100mm by 1100mm. A diagram of the shock tube is shown in Figure 4.1.

The test section has a rotating section with two window slots that are able to rotate 360°. This rotating window allows the operator to see what happens in most of the test section. The test section is fitted with an exhaust muffler to dissipate the energy from the shock wave.

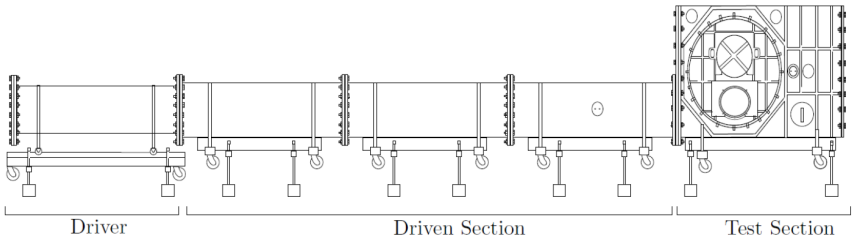

Figure 4.1: Diagram of the Large Scale Diffraction Shock Tube [8].

The test rig or test pieces connect to a test rig mount. The test rig mount attaches to the test section. The shock travels 6.6m from the driver section to the leading edge of the test pieces.

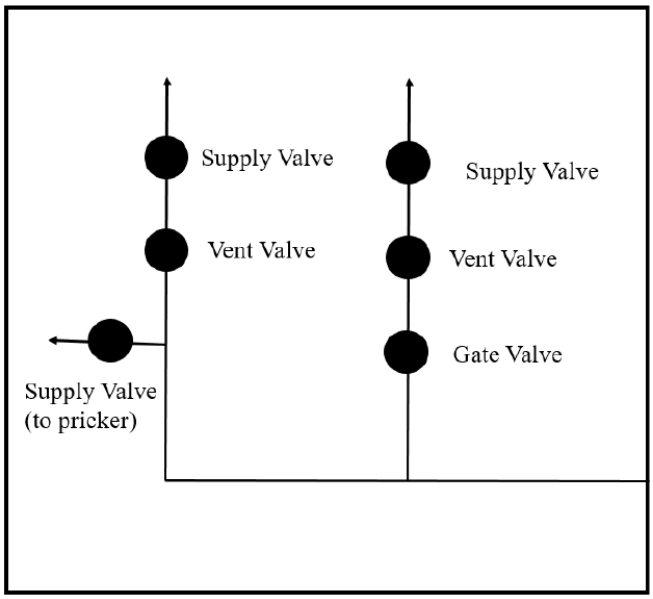

Figure 4.2: Line Diagram of the Control Board

A shock wave is created from the bursting of a diaphragm between the driver and driven sections. The bursting of the diaphragm can happen when the diaphragm cannot support the pressure inside the driver section and fails, or a pricker is used to burst the diaphragm. The driver section is pressurized using the workshop compressor.The supply pressure varies between 6.2 bar and 6.7 bar. The flow of air into the driver is controlled via a control panel. A diagram of the control panel is shown in Figure 4.2.

4.2.1 Pneumatic Pricker

A pneumatic pricker can be attached to the tube. It is operated from the control panel. Prickers of various sizes and lengths can be used. In this work prickers of lengths 180mm and 190mm were used. All prickers were sharpened before use. The pricker was used to control the burst pressure.

4.2.2 Adjustments and Repairs

Before any experimentation could be performed several adjustments and repairs were carried out. These included:

- The gaskets between the driver and driven section had to be replaced.
- All 12 of the studs used to connect the window to the test section needed replacement.
- Depending on the strength of the shock, different pressure gauges were used.

4.3 Test Pieces

Since there are two topics in this work two different test pieces are used. In the study of thermal conductivity effects on shock wave reflections on curved surfaces, concave and convex test pieces were designed. These test pieces attach onto a test rig. In the study of weak shock waves, a large curved test piece is used. This subsection will describe the test pieces used in this work.

4.3.1 Test Rig

The test rig used in the experimentation was designed by Berry [8]. The test rig is shown in Figure 4.3. The test rig was designed to hold two test pieces in identical positions across a plane of symmetry. The test rig was designed in a way which allows the test pieces to be rotated and moved along the plane of the test piece mount.

The rig has the following components: supporting structure, test pieces, spacing arms and test piece mounts. The test piece has a sliding mount and a mounting assembly. Translation of the test piece along the test mount is achieved by sliding the mounting assembly on the sliding mount. The angle of the test piece is adjusted using the spacing arms.

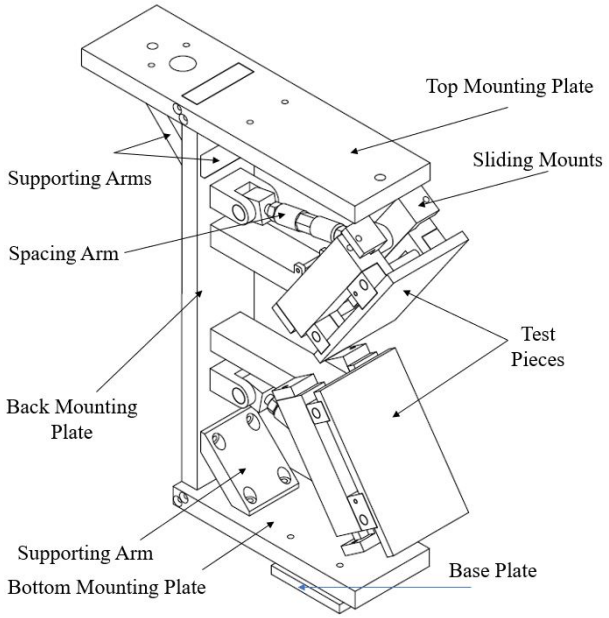

Figure 4.3: Test Rig Designed by Richard Berry [8].

4.3.2 Concave Test Pieces

The test pieces that were designed and used in an undergraduate study [2] were used in this experiment. The identical test pieces are made out of copper and PVC. Both test pieces were manufactured using a CNC milling machine. The test pieces have a radius of 223mm and are 99mm wide. There is 65^o of curvature on the test pieces. The test pieces were designed with the largest possible radius in order to increase the extent of the reflections.

Once made, both test pieces were polished using water paper of 350 to 1200 grit and then finally finished with BRASO. An isometric view of the test piece is shown in Figure 4.4.

The thermal conductivity values of the copper and PVC are listed in Table 4.1. These are the same for the convex and concave cases.

Table 4.1: Thermal Conductivity of the Test Pieces [15].

Material	Thermal Conductivity ($\frac{W}{mK}$)
Copper	401
PVC	0.19

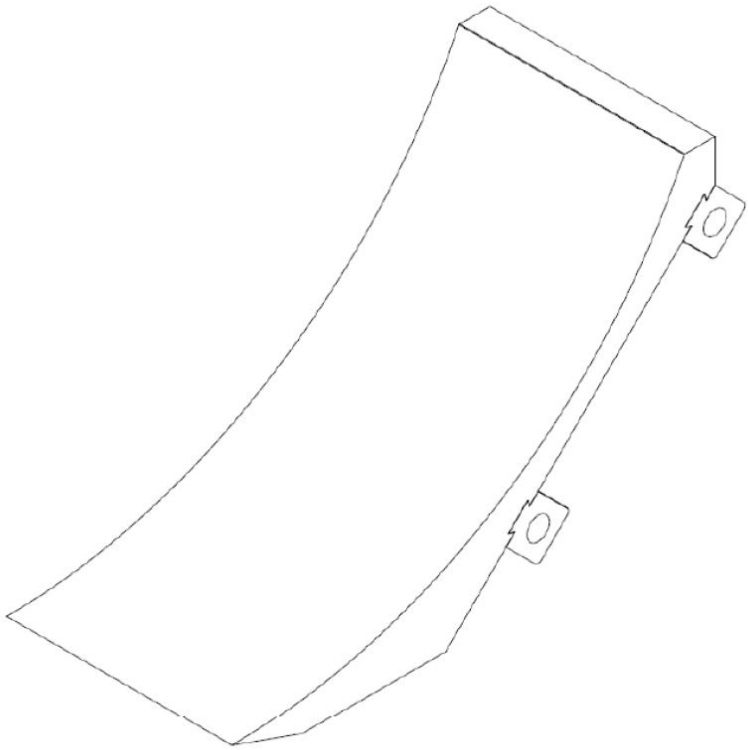

Figure 4.4: Isometric View of the Concave Test Piece

4.3.3 Convex Test Pieces

The test pieces have a circular curvature with a radius of 120mm and a width of 99mm. Due to slight space constraints, the curvature on the test piece was limited to 85^0. The test piece was designed in order to visualise all reflection patterns of the convex curved surface reflection case at the highest possible resolution. An isometric view of the convex test piece is shown in Figure 4.5.

The following design constraints existed in the design of the test piece:

- The diameter of the viewing window is only 320mm. This restricted the size of the radius.
- The proximity of the test pieces when attached to the test rig. This affected the amount of curvature of the test pieces.

The test pieces were manufactured using a CNC milling machine. The CNC is capable of providing a very smooth surface finish, but in order to ensure an ultra smooth finish water paper was used to polish the test pieces in the following order. First a 600 grit paper was used, then a 850 grit and finally 1000 grit. Thereafter the surface was further polished using

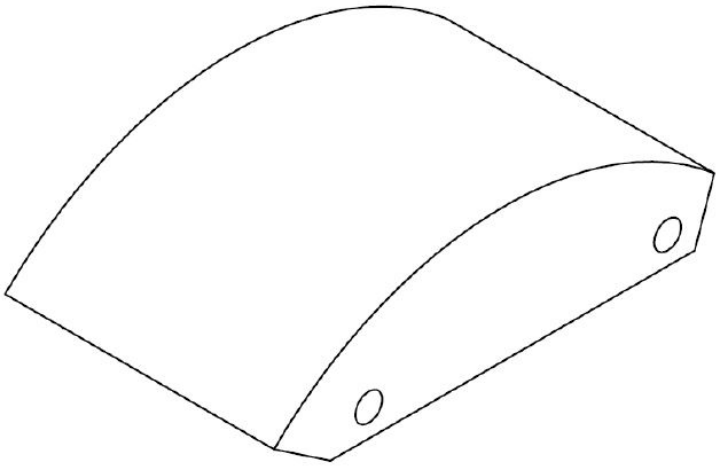

Figure 4.5: Isometric View of the Convex Test Piece.

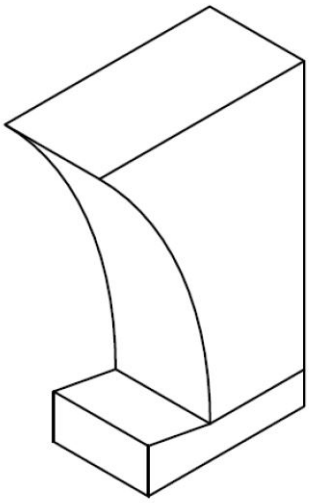

Figure 4.6: Isometric View of the Alignment Tool.

BRASO. Once this entire process had been completed, the copper test piece had a 'mirror like' finish.

An isometric view of the convex test pieces is shown in Figure 4.5. Two test pieces with different thermal conductivities, copper and PVC were made. In order to ensure that the two test pieces were aligned, an alignment block was made. This is placed on the front edge of the test piece. An inclinometer rests atop the alignment block. An isometric view of the alignment block is shown in Figure 4.6.

4.3.4 Experimental Setup

The image in Figure 4.7 shows how the test pieces were setup during the experiment. The two test pieces are attached to the test rig in the large shock tube. Protective tape is placed on the outer surfaces of the test pieces. This is done in order to protect the surface of the optical windows. Figure 4.8 is a front view of the test pieces attached to the test section.

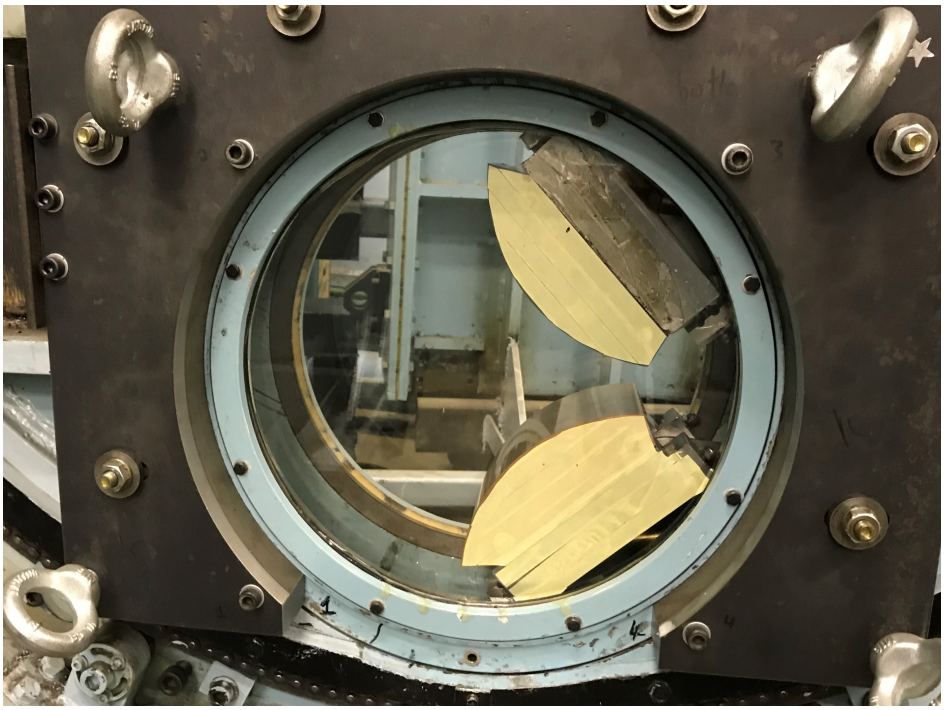

Figure 4.7: A Side View Image of the Two Convex Test Pieces in the Shock Tube.

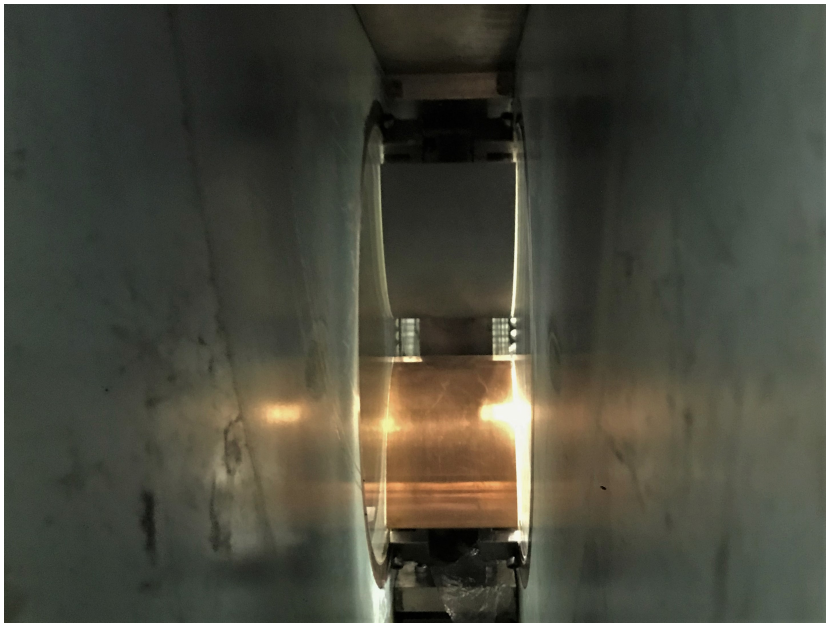

Figure 4.8: A Front View Image of the Two Convex Test Pieces in the Shock Tube.

4.3.5 Large Curve Test Piece

In the experimentation on weak shock waves, a large curved test piece was used. The large curved test piece has a radius of 520mm. This test piece was chosen to increase the resolution and size of the reflected waves at low Mach numbers. The large curved test piece attaches to the adjustment plate and is inserted inside the test section. The curve is made from mild steel and has a smooth surface. The surface is not as perfectly smooth as the test pieces for the thermal conductivity experiments but neverless the surface is not rough or sandpaper like. A diagram of the test piece is shown in Figure 4.9 below.

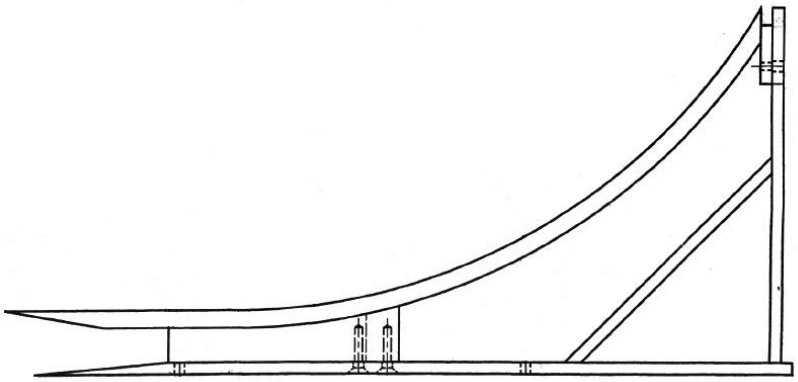

Figure 4.9: Test Rig Designed by Russell Hall.

4.4 Optics

In order to visualize the reflection process a Z-configuration shadowgraph system was used. The light source is a Megaray plasma light source. Glass lenses were used to focus the light. Two 350mm diameter parabolic mirrors were used to collate the light. The lenses, light source and camera are placed on a rail which is magnetically clamped to stands. A laser is used to align the optical system and ensure that the parabolic mirrors produce a parallel light beam which can travel through the test section.

In the setup the lenses had the following focal lengths:

- On the light source side an effective focal length of 80mm.
- On the camera side an effective focal length of 80mm.

4.5 Imaging

High speed imaging was used to record the flow features. A Photron Fastcam SA5 high speed camera is used. Images were captured at frame rates between 30000 fps and 50000 fps. The camera was triggered using a voltage trigger box using a pre-set delay. Once the shock passes the pressure transducer closest to the test pieces, a signal is sent to the delay box and thus triggering the camera. The camera is placed on an adjustable mount which allows the camera to be moved up, down, left or right with ease.

Photron Fastcam Viewer software (PFV) is used to capture and store the images. An Ethernet cable is used to connect the camera to the computer. The PFV software is used to control the frame rate, exposure, shutter speed and calibrate the image. The software is used to sort the images and save the files in the appropriate location.

4.6 Diaphragm

During the experimentation, various diaphragms were used. This was done to control the Mach number and strength of the wave. The following is a list of the different diaphragms and diaphragm configurations used in the experimentation.

Effects of Thermal Conductivity on Shock Wave Reflections

In this section of the study plastic sheeting of different thicknesses were used. The following thicknesses were used:

- 50 μm
- 100 μm
- 125 μm
- 150 μm
- 175 μm
- 200 μm

Weak Shock Wave Reflection off Curved Surfaces

In the work done on weak shock waves, the main challenge was finding a diaphragm that was weak enough to rupture and produce a wave of Mach 1.03 or less. Therefore, diaphragms of various materials were used. The results of the experiments done using these materials is outlined and explained in Section 7. The following is a list of the various types of diaphragm materials used in the experimentation:

- 12 μm plastic sheeting.
- 23 μm plastic sheeting.
- Light aluminum foil.
- Heavy aluminum foil.
- Wax paper.
- Baking paper.

This section has covered in detail all the apparatus used in the experiment. It has covered the shock tube used for experimentation, the test pieces designed and used in the experimentation, the imaging equipment, optical setup used and the chosen diaphragms.

Chapter 5 Methodology

This section will outline the methodology used in this work. This will cover: The optical setup, alignment of the test pieces and testing procedure.

5.1 Optical Setup

A Z-configuration was used in the optical setup. This includes: a light source, pinhole, lenses, parabolic mirrors and a high speed camera. To ensure that a parallel light beam passes through the test section the following procedure was followed.

1. All components are initially aligned in a Z pattern. An example of a Z-configuration is shown in Figure 2.17.
2. From the light source side, the components are placed in the following order: light source, converging lens, pinhole, parabolic mirror, test section, parabolic mirror, converging lens and high speed camera.
3. The centre of the viewing window is used as the height for the entire setup. It is measured and all other components are placed at this height.
4. The pinhole and the knife edge are placed at the focal point of the mirror on the light source and camera side respectively.
5. The light source is removed from the setup and replaced with a laser. A rotatable lens is mounted onto the laser. A straight beam from the laser can be orientated in both horizontal and vertical positions.
6. The laser is placed in a horizontal position. This is done to ensure that the laser light is level throughout the optical setup.
7. By placing the light source at the focal point of the parabolic mirror a parallel beam is achieved. This is done using a measuring tape and the focal point of the mirror.

8. In order to achieve an accurate and correct image the parallel beams must be perpendicular to the optical window.

9. The vertical lines are aligned by moving the mirror either left or right. In order to align the horizontal lines the mirrors can be either raised or lowered. Since the mirrors are placed on a stack of wooden boards, the height is changed by either adding or removing boards.

10. The above steps are first performed on the light source side and then performed on the camera side.

11. Once a parallel beam has been established, the parabolic mirror on the camera side can be used to direct the light rays onto the camera. The mirror rotates around its vertical axis and horizontal axis.

12. The final step is aligning the optics on the camera side and ensuring a clear image is present on the lens of the camera.

13. The camera software is used to see the formed image. The various optical components are adjusted in order to form a clear sharp image at the camera.

14. A threaded bolt is placed in front of the optical window. The optical system is considered to be focused once the threads of the bolt can be seen in the image.

15. If schlieren photography is required, a knife edge can be placed at the focal point of the mirror on the camera side.

An image of the two concave test pieces in position is shown in Figure 5.1.

The Effect of Wall Thermal Conductivity on Shock Wave Reflection

5.2 Alignment of the Test Pieces

In this study, shock wave reflections off curved surfaces are compared and analysed. It is therefore critical to ensure that both of the test pieces are in identical positions along a plane of symmetry to ensure the validity of the experiment. Both test pieces are required to be at the same angle and same position. This is done to ensure that the shock comes into contact with the leading edge of both test pieces at the exact same moment in time. It is also done to ensure that the incident wave is normal to the leading edge of both test pieces.

Only after experimentation has taken place can it be determined whether the test pieces are aligned or not. Therefore the alignment is a multi step process. Since two different types of

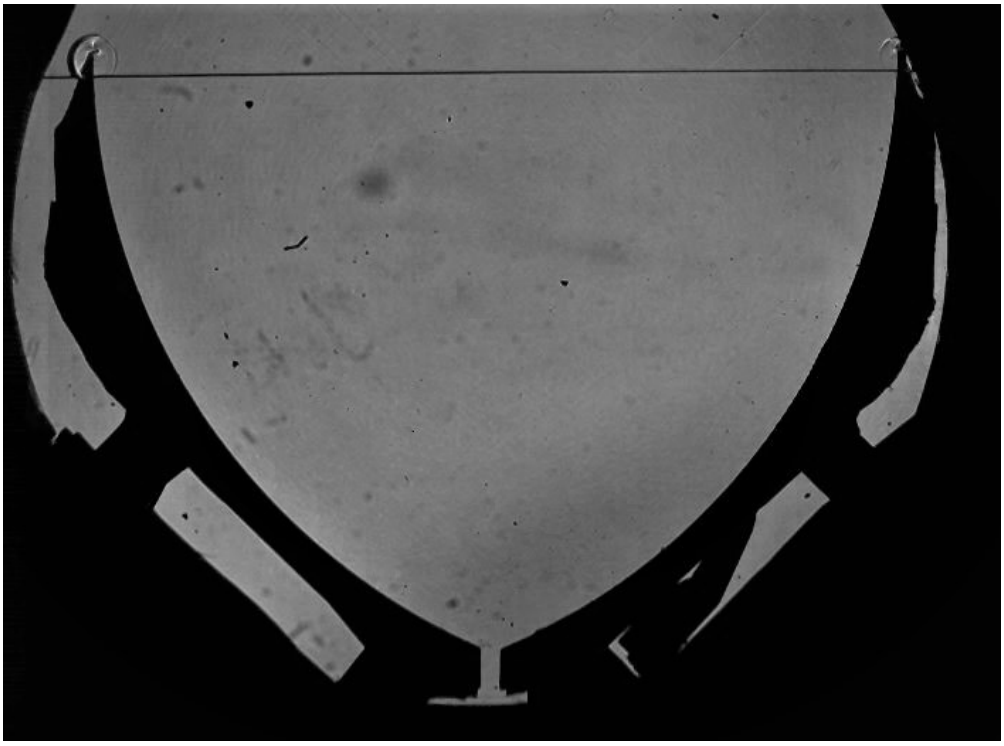

Figure 5.1: A Shock Entering the Test Rig with Concave Test Pieces Attached.

test pieces were used (convex and concave), two different alignment procedures were followed. These two procedures are listed below.

5.2.1 Concave Test Pieces

On the concave test pieces there are two flat surfaces which are used in the alignment. A diagram showing the front and back surfaces is shown in Figure 5.2. The back and the bottom surface are manufactured to be 90°to each other and the bottom surface is manufactured parallel to the inlet angle.

1. Both of the test pieces are placed in the test rig. As a starting point, the angles of the test pieces are estimated.
2. Using a digital inclinometer, the two test pieces are adjusted to be at the same angle. This is done by placing the inclinometer on the bottom surface. The angle is adjusted through the spacing arms.
3. Once the test pieces are placed at the same angle, the test pieces must be placed in an identical longitudinal position. This is done by matching the positions of the back surfaces.

4. The test pieces are moved along the sliding mount to ensure that the back surfaces are flush to each other. A set square is used to ensure this .

5. The test pieces are locked into place on the sliding mounts.

6. The angle of the test pieces is checked. This is done to ensure that the angles have not been adjusted when the test pieces are moved along the sliding mount. If required, the angles of the test pieces are adjusted and locked into place.

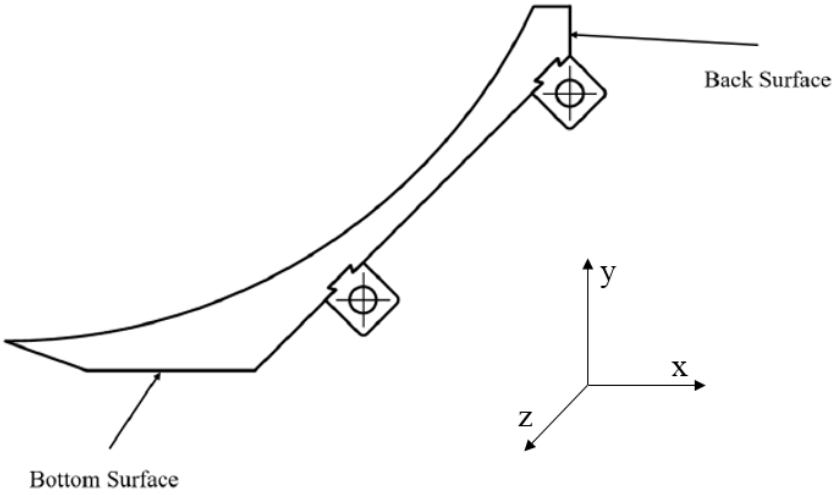

Figure 5.2: Diagram of the Test Piece

Once the above steps are followed the optical windows are secured into place and the rig is prepared for testing. In order to determine whether the alignment of the test pieces is accurate an experiment has to be done. The alignment will be considered true if the incident shock wave comes into contact with both leading edges at the same time

In the case that the test pieces are not aligned, the optical windows are removed and the above procedure is followed.

5.2.2 Convex Test Pieces

To achieve alignment of the convex test pieces, the back and bottom surfaces were used. However, as shown in Figure 5.3, the convex test piece does not have any flat surface suitable for the alignment process.

Therefore a alignment tool was designed and manufactured in order to perform the alignment of the two test pieces to each other. This tool is shown in Figure 4.6. The tool is designed to fit onto the leading edge of the convex test piece. The tool has two flat surfaces which are

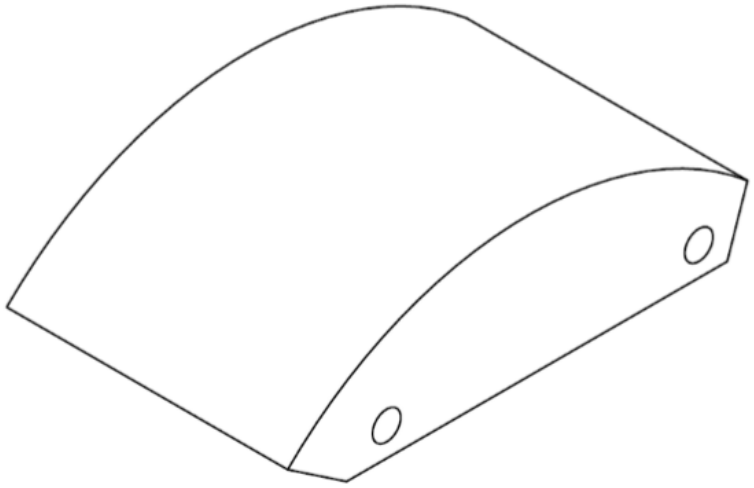

Figure 5.3: Convex Test Piece

perpendicular to each other. The following procedure was followed to ensure that the two test pieces were aligned to each other.

Initial Alignment Procedure

1. The test pieces are placed in approximately identical positions.
2. The alignment tool is placed onto the leading edge of the copper test piece. A digital inclinometer is placed on the top of the alignment tool. The angular position of the test piece is adjusted until the angle is 0° relative to the absolute reference frame.
3. The same procedure as step 2 is followed but on the PVC test piece.
4. The front surface of the alignment tool is used to ensure that both test pieces are in an identical position. A set square is placed flush onto one of the test pieces. The other test piece is moved in a lateral direction until it is flush with the set square. This is done by the test piece along the sliding mount. The sliding mount is then locked.
5. The angles are checked again to account for any changes that may have happened when the test pieces were moved. The test pieces are the locked in an angular position.
6. The optical windows are replaced and the shock tube is prepared for testing.

In order to test the accuracy of the alignment, a few experiments were done. The images from these experiments were then analysed and it is determined whether an adjustment to the test pieces is required. The adjustment may either be in a lateral direction or angular.

Using the images, it is determined what adjustment needs to be made and the value of the adjustment.

Final Alignment Procedure

1. Identify what adjustment needs to be made (angular or lateral).
2. Determine by how much the test pieces need to be adjusted.
3. Apply the changes using the methods used in the Initial Alignment Procedure.
4. Lock the test pieces into place.
5. Attach the optical windows and prepare the shock tube for testing.

Further Alignment of Convex Test Pieces

The accurate alignment of the test pieces is crucial for the integrity and validity of the study. Therefore, great care was taken during the alignment of the convex test pieces. This was done to ensure that both test pieces were in identical positions across the plane of symmetry as accurately as possible.

The alignment tool shown in Figure 4.6 is an essential tool in the accurate alignment of the test pieces. The edges of the tool were manufactured to be perfectly flat in order to aid with accuracy of the alignment.

The digital inclinometer was used to ensure that both test pieces were placed at identical angles. The inclinometer gives readings to two decimal places. The absolute reference frame setting was used on the inclinometer.

Once both test pieces are positioned at identical angles and identical longitudinal positions the shock tube is prepared for testing. A test was performed and it was noticed after the test that the shock did not come into contact with both leading edges at exactly the same time. The shock appears to be slightly inclined.

The inclined wave is displayed in Figure 5.4. In Figure 5.4 a line is drawn which connects the two leading edges. Another line is drawn over the incident shock wave. As it is clear in the image the two lines are not parallel to each other, thus a clear indication that the test rig and test pieces are not accurately aligned. The angle was measured as 0.96^o using Autodesk Inventor.

In order to achieve an accurate alignment the entire rig needed to be rotated by 0.96^o anti-clockwise. This was achieved by rotating each test piece 0.96^o. The longitudinal positions of

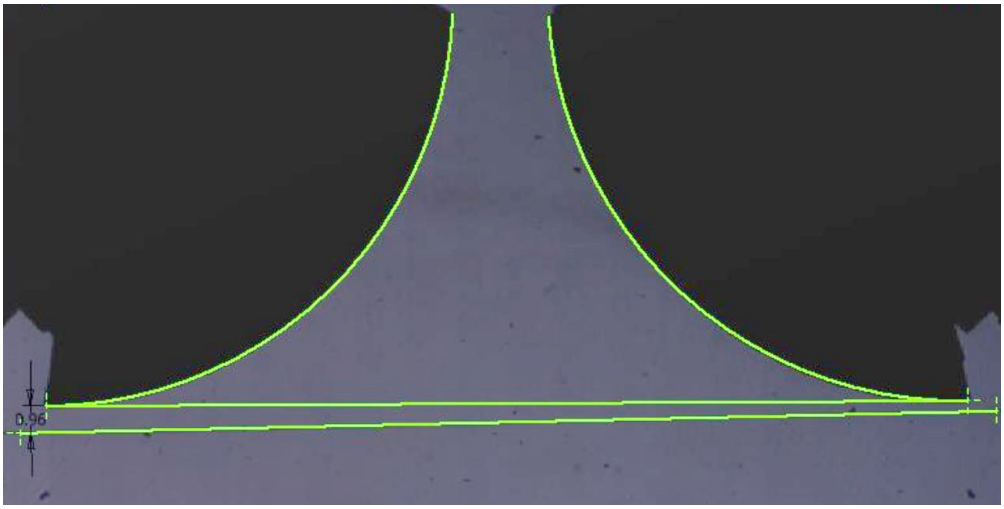

Figure 5.4: Image of Inclined Wave Entering the Test Rig

the test pieces had to be adjusted to account for the rotation. Once the changes were made the shock tube was prepared for testing.

The final aligned setup of the test rig is shown later in Figure 7.8. The test piece on the right is copper and on the left is the PVC test piece.

5.2.3 Improvements on Test Rig and Set Up

Based on the issues with the alignment discussed in detail in Section 7.1.1, two approaches can be followed to ensure that the alignment of the two test pieces is as accurate as possible. The first is to ensure that the rig is rigid and the second is to follow an iterative process to ensure both test pieces are in identical positions across a plane of symmetry.

Increasing the Rigidity of the Rig

When inspected for rigidity the rig had several concerning issues. The test rig is shown in Figure 4.3. The following issues were noticed: All of the supporting arms which connect the test mounts to the back mounting plate were loose, the supporting arm which connects the back mounting plate to the test pieces was not level, the majority of the cap screws on the rig were not properly tightened and the spacing arms were not rigid. A possible cause for these issues is the backlash experienced during testing.

All screw connections on the rig were found to be loosened. The cause of this can be explained by the vibration caused by the air following a shock wave during testing. Over time and during the course of many tests the screws are gradually undone. This reduces the rigidity of the rig which introduces inconsistencies into the results. There is no permanent solution to this

problem. However, the rig is inspected every 10 tests to make certain that the rig is rigid for all tests.

The supporting arms are tightened and checked for rigidity in the same way as all the screws. The supporting arms are levelled when the rig is out of the testing section. All the screws connecting the supporting arm to the back mounting plate are loosened. A spirit level is placed on the top surface of the supporting arm. The supporting arm is adjusted until the spirit level indicates that it is in a level position. The screws are then tightened. This is done on both supporting arms.

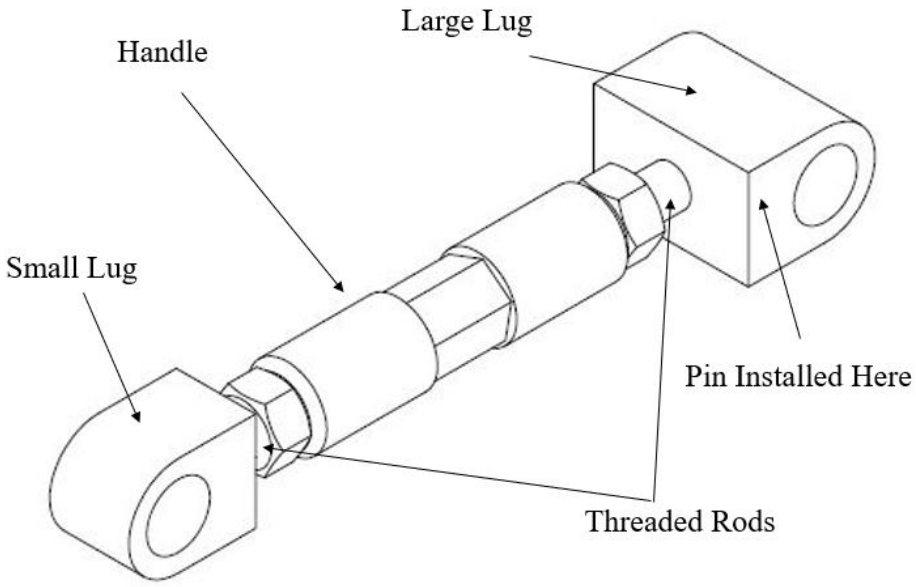

Figure 5.5: A Isometric View of the Spacing Arm [8].

The spacing arm consists of five components. There is the small lug, large lug, two threaded rods and the handle. Initially, when manufactured the threaded rod was screwed into the lugs and tightened with Loctite. However, after a considerable amount of use the threaded rods were no longer secure in the lugs. This meant that the air vibrations produced during testing have the ability to rotate the threaded rods and hence change the angle of the spacing arm. This immediately invalidates the experiment.

The rotation of the threaded rod in the lug was prevented by the installation of a pin in the lug and threaded rod. The pin prevents rotation of this crucial component of the test rig. The prevention of the rotation of the spacing arm during testing ensures consistent results.

Set Up of the Test Pieces

An image of the set-up test section is shown in Figure 5.6.

In undergraduate work an inclinometer and visual assessment of the test pieces were used to initially align the test pieces. Once this was done, experiments were performed to test the accuracy of the alignment. Images were used to determine the adjustments required, these changes were then implemented. After a few iterations a satisfactory alignment was achieved.

The use of a visual assessment in the alignment of the test pieces is a possible source of error. This is because the accuracy of the setup is dependant on the eye of the inspector and no physical measurement. Therefore, both test pieces are manufactured to be identical. This is done so that the physical measurements of the test pieces can aid in the accuracy of alignment.

The two test pieces were placed at an angle of 0.5° relative to the plane of symmetry. The decision to slightly open the two test pieces was made to ensure that a compression reflection would form on the reflection surface. The absolute reference frame was used on the inclinometer.

Once both test pieces had been positioned at the same angle using an inclinometer a flat block was placed on the back edge of the test pieces. The test pieces were moved longitudinally along the sliding mounts until the two back surfaces were flush to each other. The test pieces were made using the same computer code on the CNC milling machine. Therefore, the two test pieces are identical to each other. Based on the common physical dimensions of the test pieces if both test pieces are at the same angle and the back surfaces are flush to each other then the leading edges of both test pieces are in identical relative position and the setup is considered to be perfectly aligned. This alignment is perfected even further during an iterative process during testing.

During the polishing process of the copper test pieces, it was noted that the back edge of the copper test piece was blunted. This was caused directly by the polishing process. As a result it appears as if the copper test pieces are behind the PVC test piece. However, this is not the case as both test pieces are in identical positions as explained above.

Figure 5.6 shows a planar shock wave entering the test section. The copper test piece is on the right side of the image and the PVC test piece is on the left side of the image. It is evident from the image that the incident wave comes into contact with both leading edges at exactly the same moment in time. This image clearly shows that the test rig is correctly aligned. It also indicates that the shock is normal to the leading edge of the test pieces and the plane of symmetry.

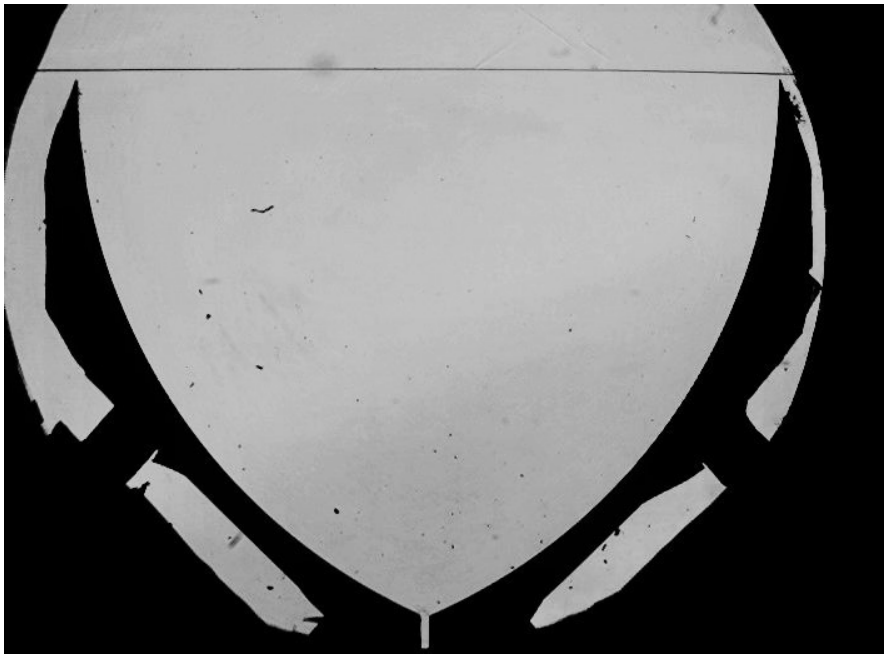

Figure 5.6: Image of a Incident Shock Entering the Test Section.

Upon a close inspection of Figure 5.6 it appears that the leading edge of the copper test piece is very slightly in front of the leading edge of the PVC test piece. This is because the leading edge of the copper test piece is sharper than the PVC. Due to the soft nature of the PVC a sharp edge like that of the copper is impossible to achieve in the manufacturing process. Therefore, though it appears that the copper test piece is slightly in front of the PVC, in actual fact the two test pieces are in identical positions along a plane of symmetry.

Weak Shock Wave Reflection off Curved Surfaces

5.3 Generation of Ultra Weak Shock Waves

One primary objective of this study was to generate ultra weak shock waves (M $<$ 1.03). As this had not been achieved before, new experimental methods had to be explored. The generation of the ultra weak shock waves was the central experimental challenge and the methods used to achieve it are briefly explained here.

5.3.1 Undergraduate Work Done by Blessing Chirewa

In an undergraduate study titled 'Generation of Weak Shocks and Compression Waves' several methods and techniques were used in an attempt to produce shock waves with a Mach number below 1.03. Various combinations of aluminium foil were used. Wire mesh was also used in

attempt to aid in the attenuation of the wave. The porosities of the wire mesh ranged from 34% to 65%.

The methods used in his experiments obtained shock waves with Mach numbers above 1.03. The wire meshes had little effect on the attenuation of the shock wave. The shock waves with the lowest Mach number were achieved with a combination of one piece of light duty aluminium foil and one piece of heavy duty aluminium foil.

5.3.2 Methods Used in Current Experimentation

In this study a wider range of diaphragms were used. The diaphragms used are mentioned in Section 4.6. Experimentation began with a newly sourced plastic sheeting with a thickness of 12μm and 23μm. Due to the material being so thin it lacked structural integrity and extreme care had to be taken when placing it in the shock tube. In order to assure that the diaphragm burst was symmetrical the diaphragm had to be placed on the tube without any creases.

The Mach numbers obtained from using the plastic sheeting were in the range of 1.06 - 1.09. This was higher than the desired Mach number of 1.03. The pricker was added to the rig and placed in an activated position. More tests were performed and the Mach numbers obtained ranged from 1.03 to 1.05. The plastic sheeting produced clean and well defined shock waves. However, since the lower limit of the Mach number is 1.03, further methods had to be explored.

In the experimentation done by Chirewa [16] a Mach number of 1.03 had been achieved using a combination of one piece of heavy duty foil and one piece of light duty foil. In this study various combinations of foil were used. The first being two pieces of light duty foil and the second being one piece of light duty foil. Mach numbers in the range of 1.02 to 1.035 were found. However, there was an issue with these tests. The aluminium foil diaphragm broke in an inconsistent and unpredictable manner. Upon an inspection after testing it was noticed that the rupture of the diaphragm was not a clean break along the length of the foil. Rather, what was noticed was that the bottom half of the diaphragm was intact and the top part was severely ruptured. Several cases similar to this were found. This resulted in a inclined shock with several transverse waves attached. In some cases the shock wave was barely visible on the images. Therefore, further diaphragms were explored.

Consistent results of Mach numbers below Mach 1.03 were obtained using wax paper. It was found that as a diaphragm the wax paper ruptures easily and is non-porous. The waves produced from the wax paper were well formed, defined and clean waves. The experiments were performed with prickers activated and nonactivated. The prickers didn't affect the way

the diaphragm broke. In all cases the diaphragm has one long break along the length of the diaphragm.

Table 5.1 lists several results from the testing. It is a record of the methods used in the experimentation and their resultant Mach numbers.

Table 5.1: Experimental Data and Notes for Low Mach Number Testing

Diaphragm	Thickness (μm)	Mach Number	Notes
Plastic Sheeting	12	1.068	Natural Burst
Plastic Sheeting	12	1.08	Natural Burst
Plastic Sheeting	12	1.036	Pricker Activated
Plastic Sheeting	12	1.05	Pricker Activated
Aluminium Foil	2 Sheets Light Duty	1.028	Pricker Activated
Aluminium Foil	1 Sheet Light Duty	1.021	Pricker Activated
Wax Paper	1 Sheet	1.021	Natural Burst
Wax Paper	1 Sheet	1.014	Pricker Activated

5.4 Testing Procedure

During testing the procedure outlined in the document LSDST-01 was carefully followed. This document can be found in the digital Appendix. These are documents which are provided by the Flow Research Unit. These documents cover the standard operating procedures of the shock tube. A summary of the operation procedures that were followed are listed below. All other documents relevant to the testing procedure can be found in the digital Appendix.

1. All loose objects must be removed from the area surrounding the shock exhaust.
2. A diaphragm of chosen thickness is cut and placed onto the driven section.
3. The driver and driven section are bolted together following the process outlined in LSDST-3.
4. Before testing can begin, the siren and the alarm in the room are activated. This warns people in the vicinity of the room that a test is about to take place.
5. The data acquisition system is activated.
6. The operator moves toward the control panel where preparation for the testing takes place. The supply and vent valved are closed.

7. A whistle blow is sounded and the gate valve is opened.
8. In order to pressurize the driver, the supply valve is gradually opened.
9. The whistle is sounded every time the pressure increase by 1 bar. This is done until the diaphragm bursts.
10. After the diaphragm has burst the gate valve and supply valve are closed immediately.
11. In order to remove the excess air the vent valve and supply valve are opened.
12. The driver is unbolted and removed from the driven section. The ruptured diaphragm is removed from the shock tube.
13. The tube is inspected for any pieces of diaphragm that may have broken off in the blast. These pieces are removed.
14. Once testing is done, the data is recorded and saved.

5.5 Data Acquisition

Data such as the high-speed pictures and the time between the two pressure traces is obtained during experimentation. This subsection will explain how the data was obtained and how it was recorded.

Before the test:

1. The camera is turned on and the image is calibrated by pressing the shading button.
2. The light source is turned on and the camera application is opened.
3. The operator inspects the image and if the quality is satisfactory.
4. All trigger units are armed.
5. The camera is set to the 'Trigger On' position.
6. The oscilloscope is set to record.

After the test:

1. The time between pressure traces is recorded.
2. All relevant images are saved.
3. The light source is turned off.

5.6 Safety Precautions

Operation of the Large Scale Diffraction Shock can be a dangerous activity with potentially harmful results if not operated properly. With the aid of a risk register potentially harmful scenarios are considered and several precautions are used to ensure the safety of the operator and people in the vicinity of the shock tube laboratory. These include:

- All loose items are cleared from the area around the exhaust.
- All ports are checked to be tightly secure.
- All components on the testing section are tightened.
- A whistle is blown during the pressurization of the vessel to alert people outside the laboratory of the impending blast.
- Hearing protection is worn by the operator and any person in the laboratory.
- Gloves are worn during the operation of the pneumatic wrench. This is done to prevent white knuckle syndrome.
- A buddy system is used, to ensure that in the case of a catastrophe all persons are accounted for.
- When working with the laser and light source, the appropriate eye protection is worn.

Chapter 6 Data Processing

This section elaborates and expands on the data processing and data capturing methods used throughout the course of this study. It covers the collection of experimental data, Mach number calculation, image processing and analytical methods.

6.1 Collection of Experimental Data

During experimentation the data was collected and observed in two ways. The data was entered into a log sheet and onto an Excel spreadsheet. This information was captured and entered after each and every experiment. The following details were recorded into the log sheet: the type of diaphragm used; date and time of the test; test number; burst pressure and time between transducers (see next section). The Excel spreadsheet contains the following details: test temperature; time between transducers; burst pressure and test number.

Once the data is collected the Mach number can be calculated. This calculation is explained in Section 2.1.1. Once calculated, the Mach number is entered into both the log sheet and the Excel spreadsheet. A sample log sheet can be found in Appendix B.

6.2 Calculation of the Mach Number

Two different methods were used to calculate the Mach number in this study. In the work on thermal conductivity, an oscilloscope and two pressure transducers were used to obtain the Mach number. In the work on ultra weak shock waves the high speed camera and distance travelled by the shock wave were used in the Mach number calculations. The methods used to obtain the Mach numbers are explained in detail below.

6.2.1 Pressure Transducers and Oscilloscope

In order to determine the Mach number of the passing wave two piezoelectric pressure transducers were connected to a digital oscilloscope. This is shown in Figure 6.1. As the moving shock passes each of the pressure transducers a pulse was recorded and sent through the signal conditioners to the digital oscilloscope. Using the digital oscilloscope software application, the time between the two pressure rises was obtained. Once obtained, the time was used to calculated the wave speed. It must be noted that the distance between the two pressure transducers is measured within +/- 0.1 mm.

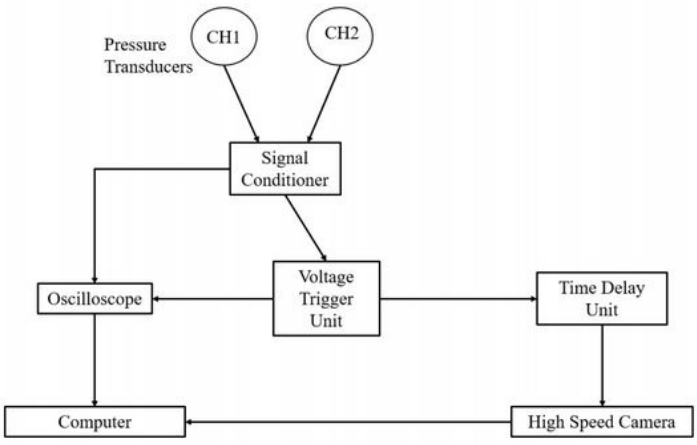

Figure 6.1: Flow Chart of the Imaging and Pressure Capturing System

Figure 6.2 illustrates the calculation of the Mach number. The distance (D) measured between the two pressure transducers and the time (S) taken for the shock to travel between the two transducers are used as inputs in the Mach number calculation. The temperature(T) in Kelvin is used to calculate the sonic speed in m/s. The wave speed is obtained from dividing the distance between the two pressure transducers (D) by the time taken for the wave to travel between the two transducers (S). The wave speed is then divided by the sonic speed in order to obtain the Mach number.

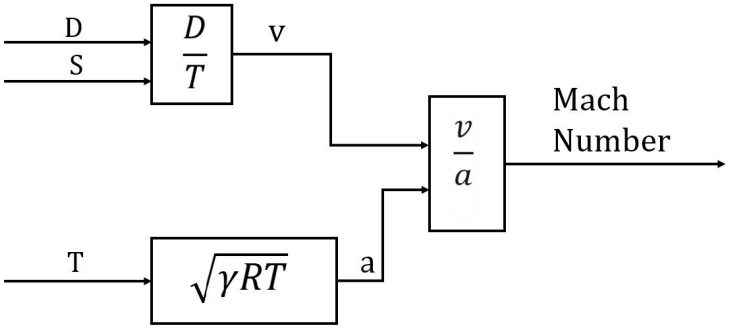

Figure 6.2: Flow Diagram of the Steps Taken to Calculate the Mach Number

6.2.2 High Speed Camera

The pressure transducers and oscilloscope are sufficient for measuring the wave speed for strong shock waves. However, the system is not accurate enough to measure the speed of the passing wave in the very weak shock wave case. The pressure rises are too sensitive to be picked up by the measurement system.

An alternative method of calculation is used. This is done calculating the time taken for the shock to travel between two distinct points. This is done by using the high speed camera and distinct marks on the image. Lines are drawn on the surface of a transparent sheet which is place over the optical window. These lines aid in the required calculations.

In order to obtain the distance the shock travels between the two distinct marks, points were drawn on these distinct marks using Autodesk Inventor. This is shown in Figure 6.3. The distance between the two lines is then measured. This is shown in Figure 6.4. This is the distance the shock travels between the two reference points. Once the distance has been obtained the time taken for the shock wave to travel between the two reference points is calculated using the frame rate and the number of frames between the two reference points. This is done using the following formula.

$$time = \frac{no\ of\ frames}{frame\ rate}$$

Where time is in seconds, frames is the number of frames between the two points and frame rate is the frame rate from the camera.

A detailed explanation of this process is given below:

1. A point is placed on the each of the two distinct marks/reference points.
2. Two lines are drawn on the reference points, these lines are parallel to each other.
3. The distance between the two lines is measured. This is shown in Figure 6.4.
4. The time taken for the shock to travel between these two points is calculated.
5. Using the distance between the points and the travel time between the points the shock wave speed is calculated.
6. Using the speed of the wave, the Mach number is calculated.

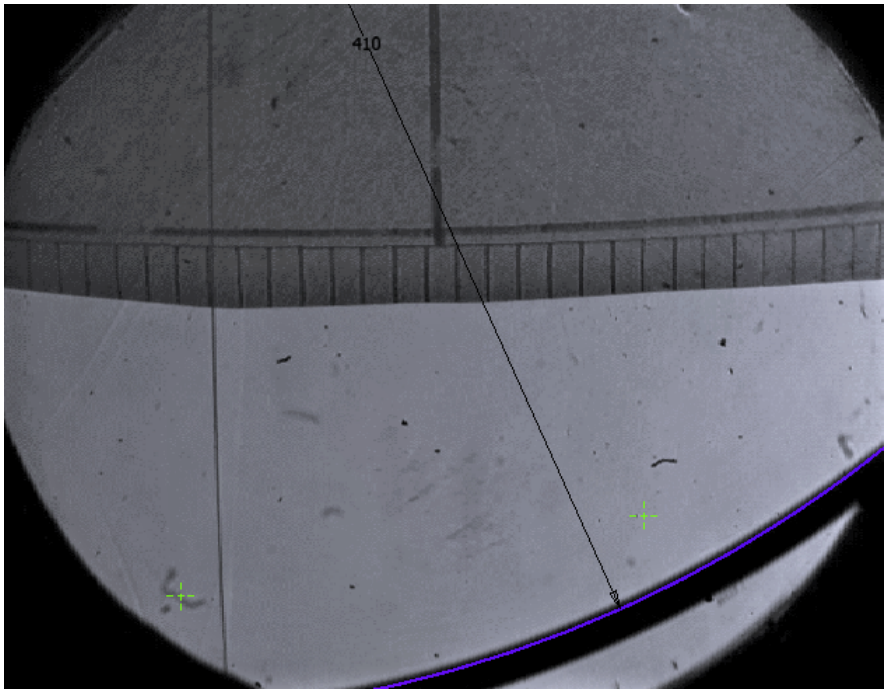

Figure 6.3: Points That are Drawn on an Image

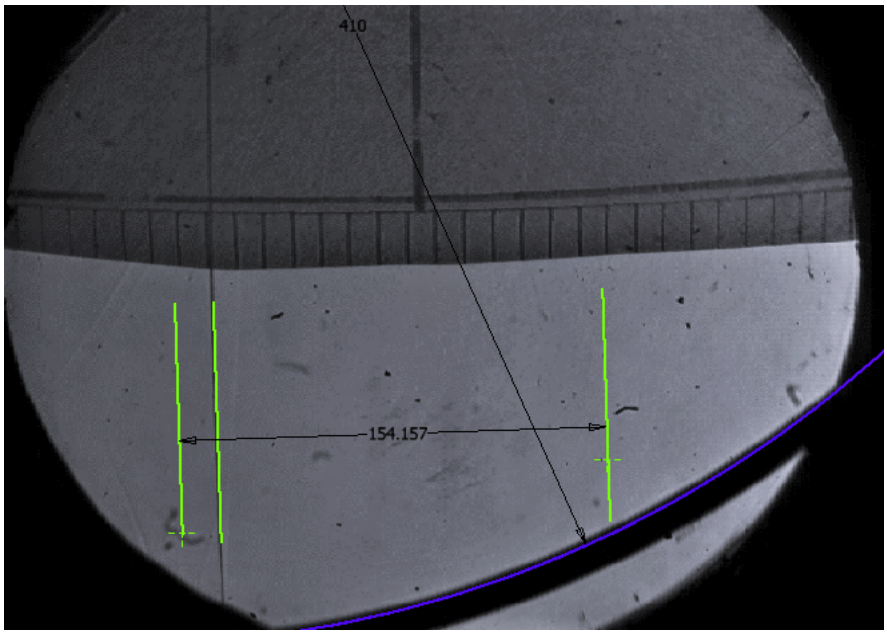

Figure 6.4: Distance between two Shock Waves

Before any measurements were performed on the images a simple check for image distortion was performed. By using the measuring grid with 10mm line spacings and comparing the measured distance between the line spacing in Autodesk Inventor to the actual distance it can be determined whether image distortion exists or not.

It was found that the image was magnified by a factor of 0.787. This was found by the comparison of the measurement of the distance between the spacing lines and the actual distance. Additionally, when the radius of the curve was measured it was measured to be 410mm. This distortion was corrected in Autodesk Inventory by increasing the size of the image. Once the radius of the curved was measured to be 520mm and the distance between the spacing lines was 10mm the correction was deemed satisfactory.

Distortion was minimal in tests done on the concave and convex test pieces. The curvature angle of the test pieces were correctly scaled in the images and the straightness of the shock waves infer that minor distortion is present.

6.3 Image Processing

In this study all information about the shock wave is obtained from the image. Therefore, it is important that the image is as clear as possible. This ensures that all data in the image can be seen and analysed. The following procedure is performed on the images:

1. The image is converted to a .png file.
2. If required, the image is rotated.
3. The image is imported into GIMP, an image manipulation program.
4. The image is converted into greyscale.
5. The exposure of the image is changed from 0.0 to 2.5.
6. The shadows of the image is changed from 0.0 to 35. This is done using the shadows and highlights tool to change the contrast of the image.
7. The saturation of the image is changed from 0.0 to 0.5.
8. Once the images has been changed, it is saved as a .png file.
9. If required, further editing is done to enhance the quality of the image.

6.4 Analytical Methods

The Effect of Wall Thermal Conductivity on Shock Wave Reflection

The reflection patterns produced are unique to the surface shape. Therefore, different methods were used in the processing and analysis of the images. The following section outlines the methods used for the concave and convex cases.

6.4.1 Quantitative Analysis (Concave Case)

In the Mach reflection case the angle between the incident wave and reflected wave are measured. Using an AutoCad package lines are drawn on the discontinuities and the angle between them is measured. This is shown in Figure 6.5.

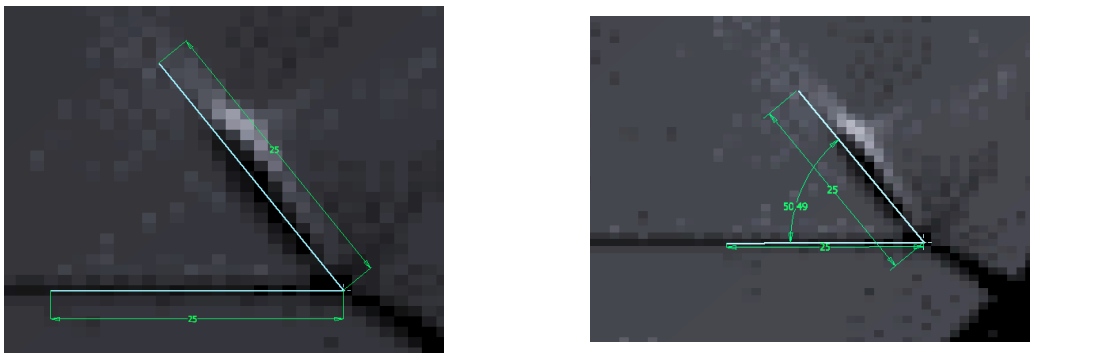

(a) The lines are drawn on the Waves.

(b) The angle between the Two Waves is Measured.

Figure 6.5: Methods Used to Obtain Data from Reflected Waves.

The following procedure is followed to obtain measurements from the images:

1. Open a new Autodesk inventor part file (.ipt).
2. Create a sketch.
3. Import the image into the sketch.
4. Rotate and enlarge the image.
5. Magnify the copper side.
6. Place a point on the triple point of the reflected wave.
7. Draw a line of 25mm over the reflected wave.
8. Draw a line of 25mm over the incident wave.
9. Capture the required measurements.
10. Remove the lines that were drawn.
11. Repeat three times.

12. Repeat the entire process on the PVC test piece.

6.4.2 Quantitative Analysis (Convex Case)

The reflected wave off the convex test piece was observed to be a curved wave. Therefore, a different image processing method was required. This was done to account for the curve of the reflection. Since multiple images would be analysed a template was created to aid is the measurement. The following process was followed to create the template:

1. Open an Autodesk Inventor file.
2. Create a new Sketch.
3. Import the image into the sketch.
4. Using the 'triple point centre' tool in Inventor, lines are drawn onto the two test pieces.
5. A rectangle is drawn over the image to give a boundary to the template.
6. The image is deleted and the template is saved.

6.4.2.1 Measuring Angle Between Incident and Reflected Wave

The following images have been displayed below to aid in the explanation of the process followed.

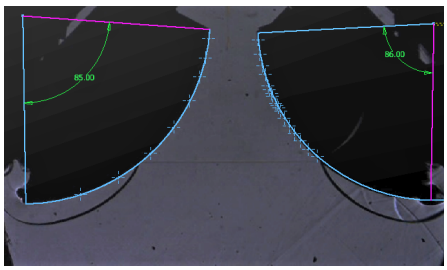

(a) Imaged Placed in Template.

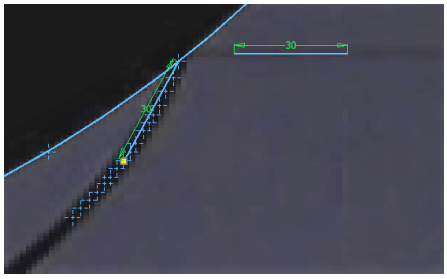

(b) Lines Drawn on Incident and Reflected Shock Waves.

Figure 6.6: Images of Steps Taken in the Measurement of Reflection Angles

The following process was undertaken:

1. The template is opened.

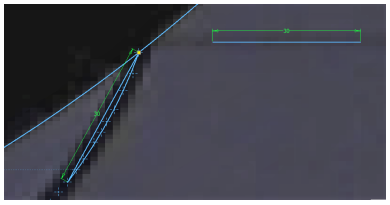

(a) Imaged Placed in Template.

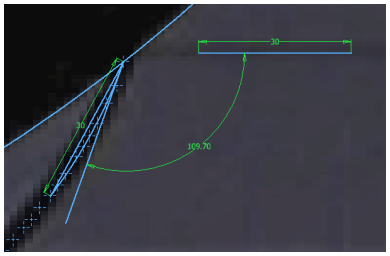

(b) Lines Drawn on Incident and Reflected Shock Waves.

Figure 6.7: Images of Steps Taken in the Measurement of Reflection Angles

2. The required image is inserted into the template. This is shown in Figure 6.6a.
3. A point is drawn on the reflection point.
4. Points are drawn along the curved reflection as shown in Figure 6.6b.
5. Lines of 30mm are drawn on the shock waves as shown in Figure 6.6b.
6. Using the start point and the end point of the line drawn on the curved wave a three point circle is drawn. This is shown in Figure 6.7a.
7. A straight line started at the point drawn on at the reflection point is drawn. It is constrained to be tangent to the curved drawn in Step 6.
8. The angle between the curve line drawn in Step 7 and the incident wave is measured. This is shown in Figure 6.7b.
9. The data is recorded in an Excel file.
10. The above process is repeated with lines of length 40mm and 50mm being drawn.

6.4.2.2 Measuring the $\omega - \theta$ Angle

The angle between the reflected wave and a line tangent to the curved surface (θ) is measured using the following procedure:

1. The template is opened.
2. An image is inserted into the template.
3. A point is drawn on the reflected point.
4. A line is drawn tangent to the curve at the point of reflection.

5. From the point of reflection a line of 30mm is drawn on the reflected wave. This line starts on the reflection point and measures 30mm along the reflected wave.
6. The angle between the line drawn in Step 4 and the line drawn in Step 5 is measured.
7. The angle is recorded in an Excel document.
8. The above process is repeated 4 times.

6.4.2.3 Measurement of the Triple Point Trajectory

In the measurement of the triple point the following procedure is followed:

1. The template is opened.
2. An image is inserted into the template.
3. A point is drawn on the triple point.
4. The image is deleted and the next image for that particular Mach number is inserted.
5. A point is drawn on the triple point. The above two steps are repeated for all the required images.
6. A line is drawn along the incident shock wave.
7. Lines are drawn which connect the points that have been drawn.
8. Angles are measured between the incident shock and the lines drawn in Step 7.

6.4.3 Qualitative Analysis

The following procedure is followed in order to draw a line along the plane of symmetry as accurately as possible.

1. An image is inserted into a sketch on Autodesk inventor.
2. A line is drawn along the incident shock wave.
3. Four lines are drawn parallel to the incident shock wave but above it.
4. Points are placed on the midpoint of the drawn lines.
5. All of the four lines are deleted.

6. A point is placed on each of the four lines.
7. A best fit line is drawn through the points.
8. If required equidistant lines are drawn at the desired point.

In order to check whether the line drawn on the image is accurate or not the following steps are followed:

1. An image is inserted into the sketch.
2. Using the three point arc tool, a circular arc is drawn on one of the test pieces.
3. The drawn arc is then mirrored using the line drawn above as the mirror line.
4. If the curve fits the test piece nicely, the line is accurate. If not, the above process must be repeated with more lines until a satisfactory line is obtained.

An example of how the the line drawn on then plane of symetry is done is shown below in Figure 6.8.

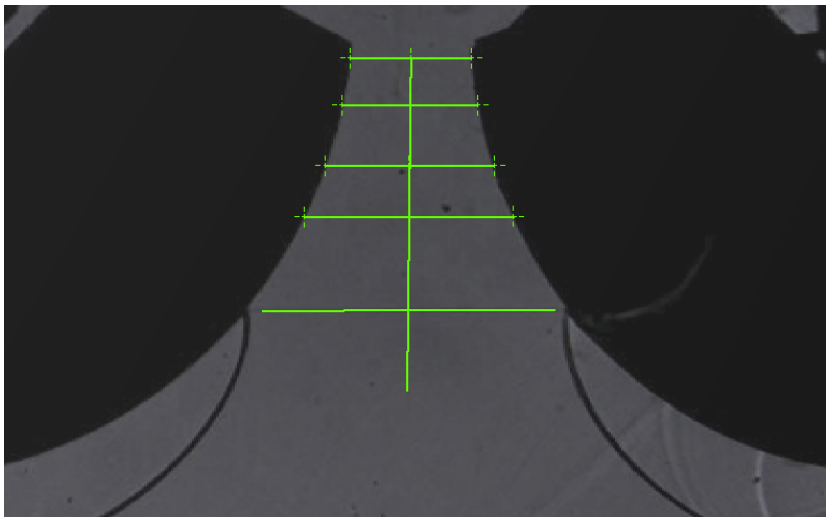

Figure 6.8: Screenshot of the Line Drawn Over the Plane of Symmetry.

Weak Shock Wave Reflection off Curved Surfaces

6.4.4 Quantitative Analysis (Weak Shock Case)

In the quantitative analysis, the image is imported into Autodesk Inventor and lines are drawn over the image in order to measure transition angles. The same method is followed for all transition cases. The process to measure the angles is outlined below.

1. Open a Autodesk Inventor file.
2. Create a sketch.
3. Insert the image.
4. Use the tool 'three point circle' to measure the radius of the test piece.
5. Correct the image distortion.
6. Draw a arc of radius 410mm along the curved test piece.
7. Draw a line along the incident shock.
8. Draw a line parallel to the incident shock which passes through the centre of the 410mm circle.
9. Save the position of the image by drawing a rectangle over the image.
10. Insert an image of a Mach reflection transition case.
11. Measure the angle of the transition.
12. Repeat steps 10 and 11 for the transition cases of regular reflection and transitioned regular reflection.

Figure 6.9 is an example of a measurement being taken in the case of a regular reflection.

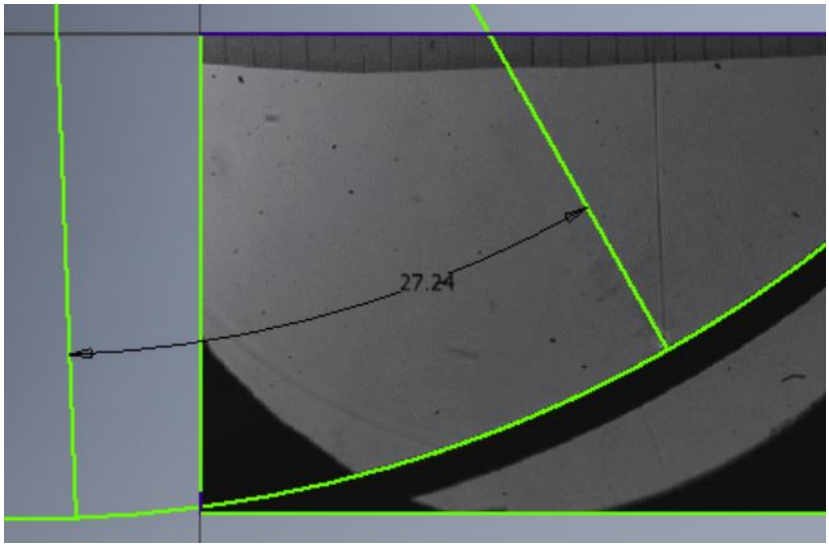

Figure 6.9: Measurement of the Transition Angle of Regular Reflection

Chapter 7 Discussion

In this dissertation, the results and discussion sections are merged together. This includes: the analysis, interpretation and conclusions from the data captured during the experiment. The discussion will cover both the effects of wall thermal conductivity on shock waves and very weak shock wave reflection.

The Effect of Thermal Conductivity on Shock Wave Reflection

7.1 Concave Curved Surface

This subsection covers all topics relevant to the tests performed on the concave curved surface. It will cover the motivation for further testing, validity of the results and include an in-depth discussion of the results.

7.1.1 Motivation for Further Testing

In undergraduate work [2] experiments were performed on the two concave test pieces. In these experiments, differences in the reflection properties of the reflected shock waves were observed. In the Mach reflection case the angle between the incident and reflected wave was measured. In addition, the ratio of the Mach stem length and the angle between the reflected wave and the shear layer was measured.

A review of the undergraduate work is found in Section 2.6.2. Differences of approximately 3^o to 5^o are present in the Mach reflection case. Images from the TRR reflection case are shown in Figure 2.28. These differences infer that the shock wave reflection properties are affected by the thermal conductivity of the reflecting wall. However, due to testing time constraints, these results are to be confirmed by more rigorous and accurate testing.

7.1.2 Collection of Concave Testing Images

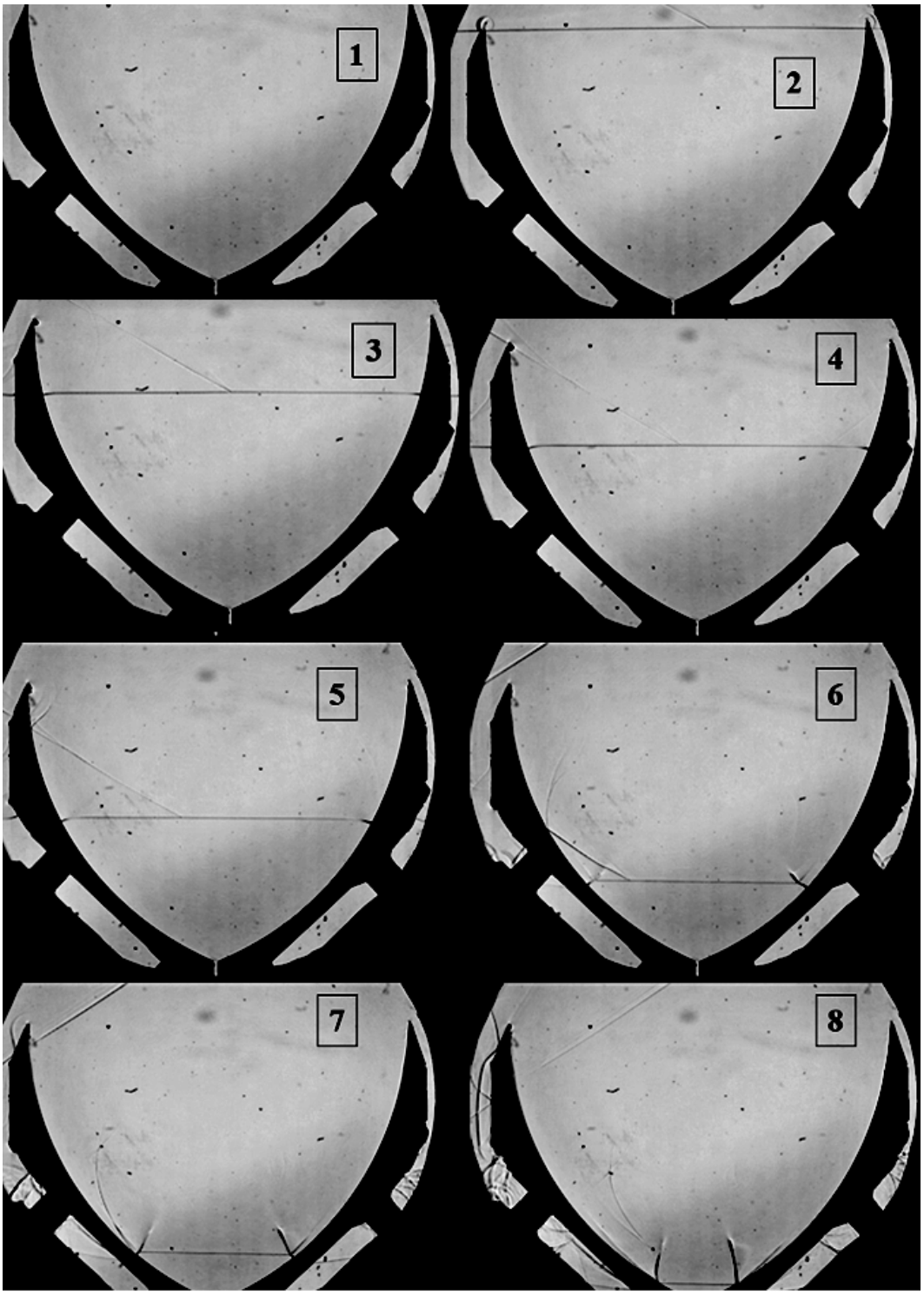

Figure 7.1: Shock Reflection Process Over A Concave Surface at Mach 1.37. The PVC and Copper Test Pieces are the the left and right sides of the image respectively.

Figure 7.1 above shows eight images of a typical test performed on the concave test piece set up. The shock wave comes into contact with the leading edges in frame 2. As the shock wave travels along the curvature of the test pieces the reflection patterns experience the evolution of a shock wave on a curved surface as mentioned in Section 2.3.2.1. The time interval between each image is 25μs.

Expanding on the previous comment, in image 5 the compression reflection is clearly visible as there is a kink in the incident wave present where it is adjacent to the reflecting surface. The image is not sensitive enough to observe any corner signals. A Mach reflection is clearly visible in image 6 from the presence of a shear layer, Mach stem and reflected wave. This is also present in image 7. There is a subtle difference in the Mach reflections in image 6 and 7 where the reflection patterns are direct Mach reflection (DiMR) and inverse Mach reflection (InMR) respectively. This observation is made based on the angle of the shear layer relative to the reflection surface at different points in time. In image 8 it appears as the reflected wave emanates from the reflecting surface. However, this is not the case as there is the presence of a shear layer. Therefore, at this point the reflection pattern is a TRR in its infancy.

7.1.3 Validity of Tests

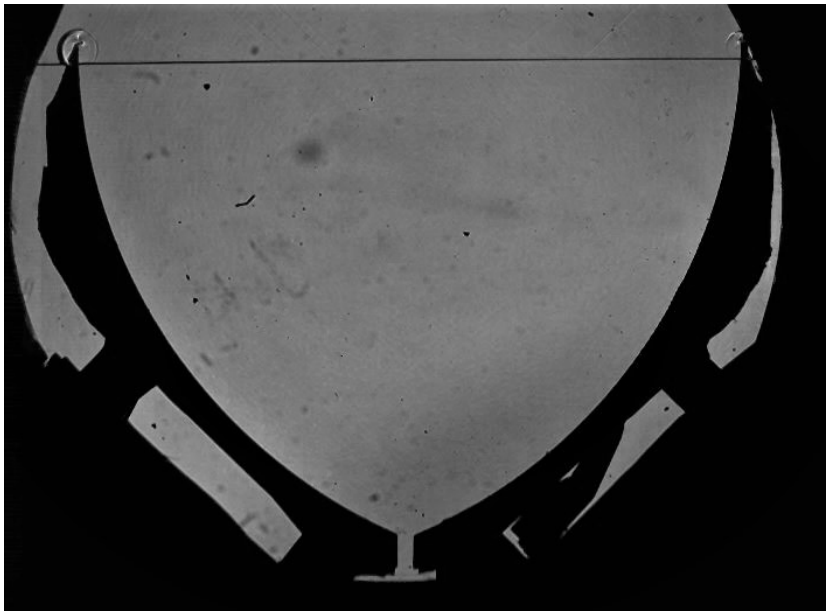

Figure 7.2: A Valid Test: Shock Coming Into Contact with Both Leading Edges at the Same Point in Time.

Since the diaphragm does not rupture in an identical manner every time, a final validity check is done after testing. This is a visual test to ensure that the incident shock wave comes into

contact with the leading edges of both test pieces at the same time. An example of a valid test is shown in Figure 7.2. Only these tests are used in the analysis.

7.1.4 Angle Between the Incident and Reflected Waves

An example of measured angles between the incident and reflected waves is shown in Figure 7.3. This measured angle will be referred to as the RI angle angle. The measurement is performed by following the process outlined in Section 6.4.1.

Figure 7.3: Measurement of the Angle Between the Incident and Reflected Shock Waves at Mach 1.47 on a Mach reflection. (Left is PVC and Right is Copper)

Tests were performed at Mach numbers of 1.26 to 1.5. Figure 7.4 shows a scatter plot of the RI angle measured between copper and PVC test pieces at Mach numbers of 1.26, 1.36, 1.38, 1.42, 1.47 and 1.5. All measurements were taken at a similar wall angle.

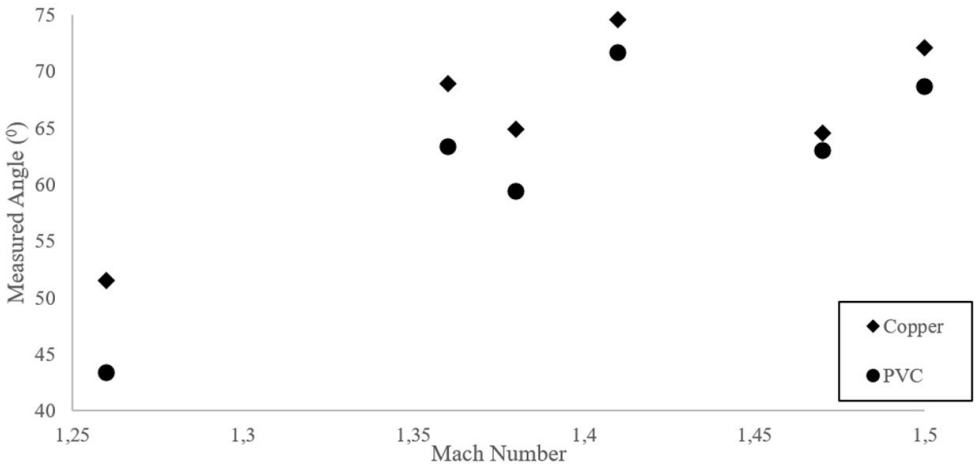

Figure 7.4: Scatter Plot of RI Angle measured at 1.26< M < 1.5.

At all six Mach numbers there is a noticeable and significant difference in the RI angles measured. These differences range from 1.61° to 8.14°. At all Mach numbers the Copper RI angle was consistently larger than the RI angle measured on PVC. This is consistent with the results obtained by Berry [1] in the Mach reflection case. In addition, this also confirms the results obtained in undergraduate work by the author [2].

In Figures (7.4, 7.5 and 7.7) it must be noted that the Mach number is used as the x-axis. Although the normalised penetration from the leading edge was not used as the x-axis, all featured measurements were taken at similar wall angle positions. This is crucial in ensuring that the measurements are comparable to each other as the shock reflections are not psuedo-steady along the curved surface. In addition, the camera captures 9 or 10 usable images during a test. Since the Mach number of the shock wave is different at each test, the reflection patterns and transition points occur at different point along the curve.

Figure 7.4 with error bars can be found in Appendix C. Error bars have not been included in this section as the errors bars are small and have a minute effect on the interpretation of results.

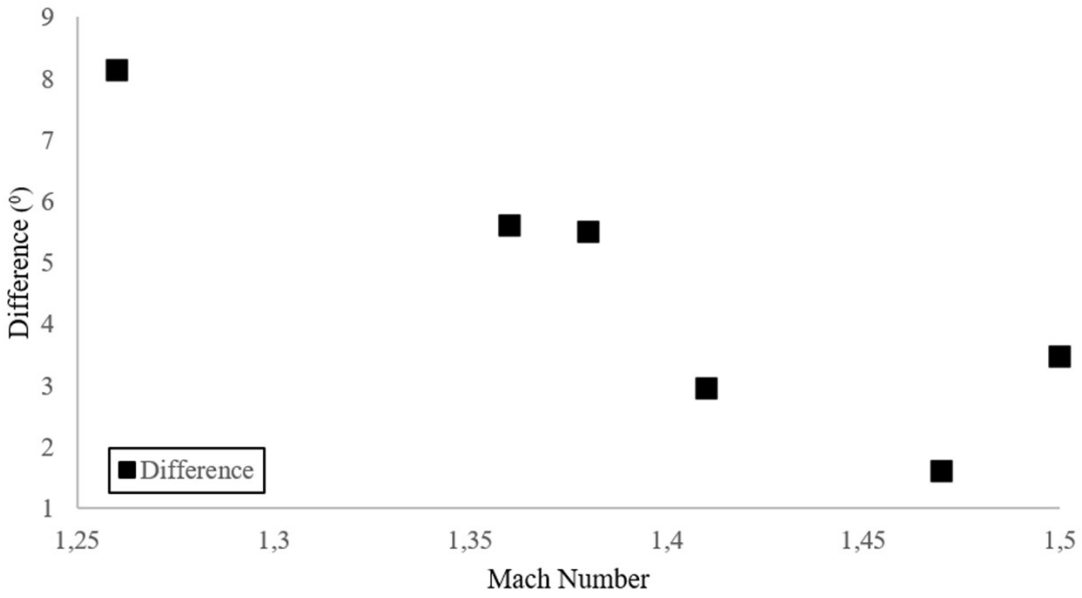

Figure 7.5: Scatter Plot of the Differences in RI Angle Between the Copper and PVC surfaces.

Figure 7.5 shows a scatter plot of the differences in the RI angle. The PVC angle is subtracted from the Copper angle. The difference between the reflection patterns decreases as the Mach number increase.

7.1.5 Angle Between the Shear Layer and the Reflected Wave

In addition to the measurement of the RI angle. In the case of the Mach reflection the only point of contact that the shock reflection has with the reflecting surface is the Mach stem. Although the shear layer does not come into direct contact with the reflecting surface it acts as a separation between air which flows along the reflecting surface. Therefore, it is indirectly in contact with the reflecting surface. Therefore, the effects of heat transfer into the reflecting surface may exhibit themselves in the position of the shear layer.

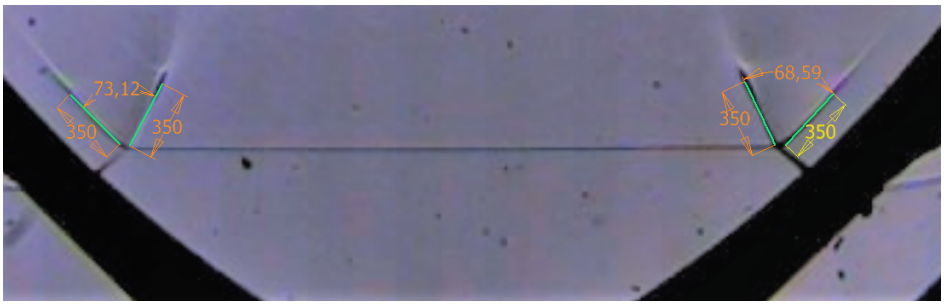

Figure 7.6: Measurement of the Angle Between the Shear Layer and Reflected Wave at Mach 1.47.

Figure 7.6 shows the measured angle in the Mach reflection case. For simplicity, this angle will be referred to as the SL-RW angle. A plot of the angle measured between the shear layer and the reflected wave is shown in Figure 7.7.

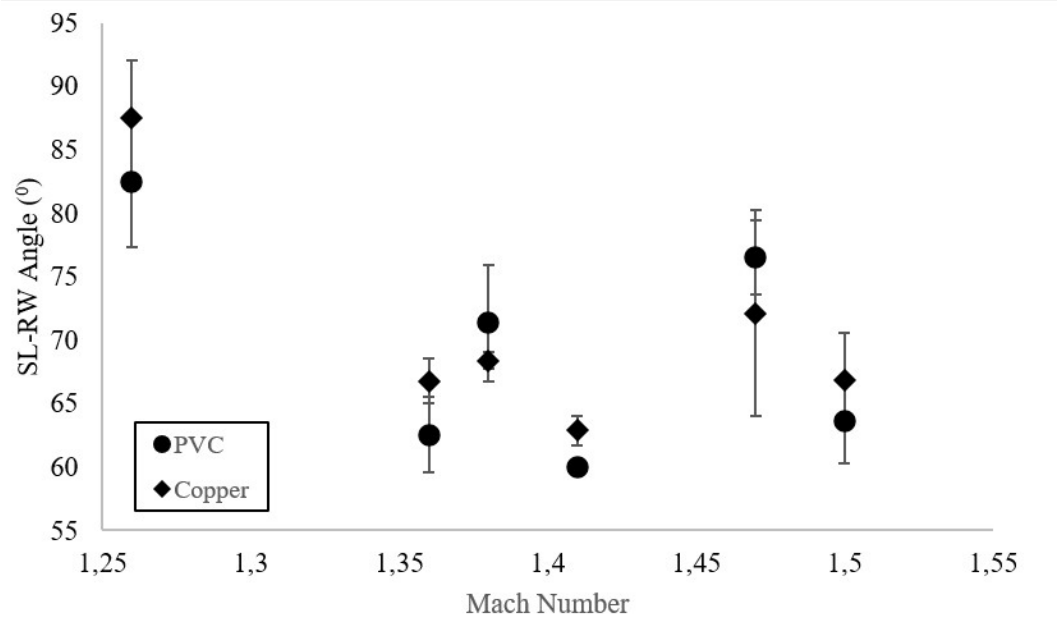

Figure 7.7: Scatter Plot of the SL-RW angle at a Mach Reflection.

At each of the six data points in Figure 7.7 there is a difference between the measured angles. The differences range from 3° to 5.5°. However, inconsistencies are present. At Mach numbers of 1.38 and 1.47 the angle measured in the reflection from the PVC test piece is larger than that from the copper test piece. At all the other four measurements the opposite is true.

The inconsistencies in the measured differences do not support the hypothesis that the thermal conductivity of the reflecting surface affect the shock wave reflection properties. These inconsistencies also do not disprove this hypothesis. Rather they can be explained as inaccurate measurements taken with an insufficient measurement technique. The error bars in Figure 7.7 are large and significant. At Mach numbers 1.26, 1.38, 1.47 and 1.5 the error bars overlap. These large error bars indicate that the measurements are inaccurate. Therefore, no conclusions on whether the reflection properties are effected by thermal conductivity can be made from these unreliable measurements. Furthermore, the shear layers are slightly curved which lead to decreased measurement accuracy.

Despite the unreliable test results from the measurement of the SL-RW angle, the tests performed on concave surfaces provide strong evidence that in the concave curved surface case the thermal conductivity of the reflecting surface affects the curved shock wave reflection properties. The measurement of the SL-RW angle did not provide conclusive results. However, the results obtained from the measurement of the RI angle provided enough conclusive results. These results also agreed and confirmed what had been found in undergraduate work.

As the purpose of the testing on concave test pieces was to confirm the findings from previous work, a comprehensive analysis such as that performed on the convex case was not required as the findings confirm the results from previous work.

7.2 Convex Curved Surface

This subsection will cover the tests performed on the convex test piece. It will include the motivation for testing, the validity of the experiment and the analysis of the results (both qualitative and quantitative).

Throughout the analysis an apparent regular reflection pattern is present in the images. Although the pattern can be clearly visually identified as a regular reflection there is the possibility that the reflection pattern is a Mach reflection with a small Mach stem which cannot be recognized. During the following sections, the reflection pattern will be referred to as a regular reflection.

7.2.1 Motivation

In Section 7.1.4 it is clear that the thermal conductivity of the reflecting surface has an effect on the reflection properties of curved shock wave reflection. However, the tests in Section 7.1.4 are performed only on concave surfaces. Therefore, tests on convex test pieces are crucial in ensuring that a comprehensive study on curved surfaces is completed.

The nature of the reflection patterns present on a convex surface could be useful in the achieving the objectives of this study. Therefore, for a more comprehensive and complete study tests on convex test pieces were required.

7.2.2 Validity of Tests

An image of an incident shock entering the test section is shown in Figure 7.8. It can be seen from the image that the shock wave is equidistant from the leading edges of both test pieces. This is an example of a successful and accurate test. The correct alignment ensures that any differences found in the reflection patterns are caused by the thermal conductivity and not a misalignment. Valid tests were obtained at Mach numbers of 1.22, 1.37, 1.38 and 1.5

A small transverse wave can be noticed on the top left-hand corner of the image. It must be noted that although the transverse wave is visible, it is a very weak wave and has no effect on the incident shock wave and resultant reflections and can therefore be ignored.

However, after several tests, inconsistencies in the angle of the incident shock wave were noticed. The waves would enter the test rig slightly inclined. Although the waves are only

Figure 7.8: Image of Incident Wave at Mach 1.38 Entering the Test Rig in an Aligned Position.

slightly inclined the results obtained from these tests are not valid. The inconsistencies were present at all Mach numbers. Examples of inclined waves are showed in Figure 7.9.

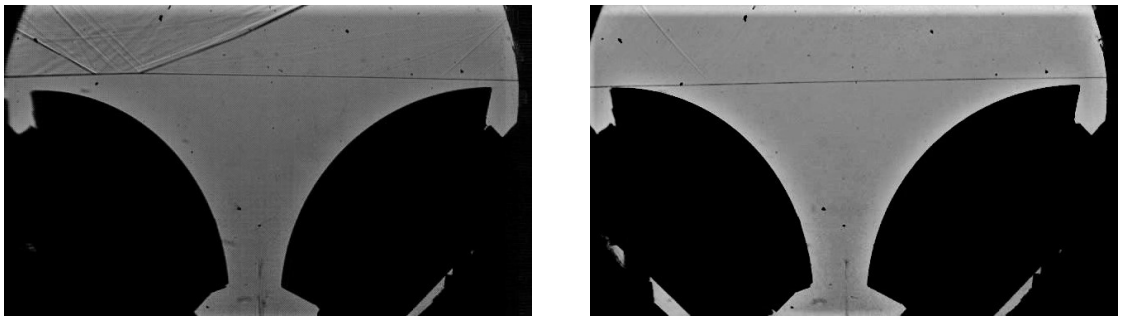

(a) An Inclined Wave at Mach 1.36.

(b) An inclined Wave at Mach 1.46.

Figure 7.9: Inclined Waves at Mach 1.36 and Mach 1.46.

The inclined waves observed had random inclinations. In one set of images the wave would be inclined to the right and in another set of images the wave would be inclined to the left. Figure 7.9a shows an example of an image inclined to the right. The shock wave will come into contact with the right test piece first. Figure 7.9b is an example of a shock wave which is inclined to the left.

The inconsistencies found in the angle of the incident shock wave are a result of the nature of the diaphragm rupture. The diaphragm ruptures in a different manner each time. This has a direct effect on the angle of the incident shock wave and is the cause of the inclined waves. Attempts were made to minimize the effects which were partially successful.

Obtaining an image of a valid test proved to be difficult. The approach taken was to perform many tests in the hope of a valid test. This method proved effective but highly inefficient. Overall 39 tests were performed and only 6 of the 39, (15%) were satisfactory for analysis.

In addition to performing many tests to get a valid result a pneumatic pricker was used to burst the diaphragm. This ensured that the diaphragm begins breaking at the exact same point.

7.2.3 Collection of Convex Test Images

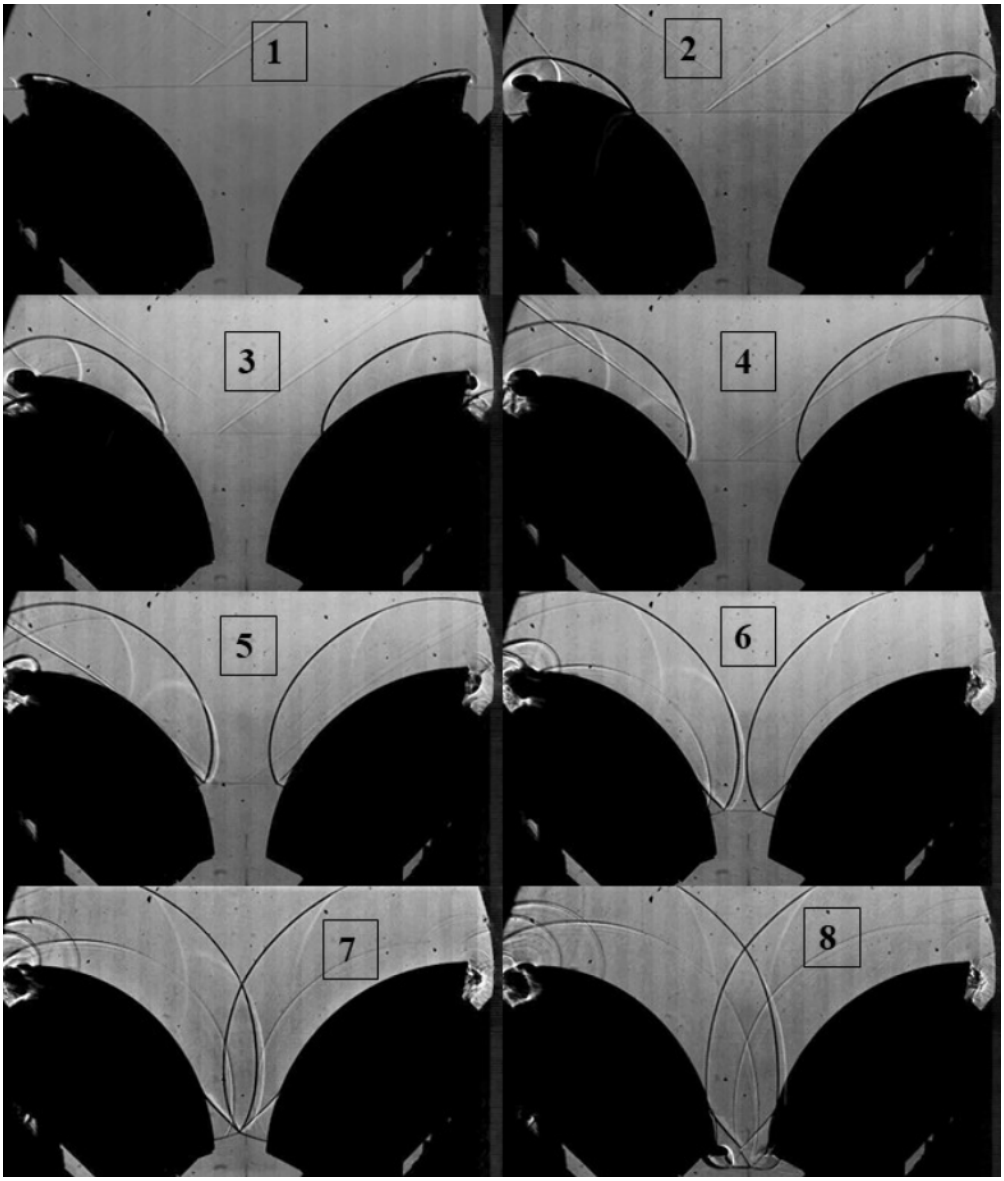

Figure 7.10: A Collection of Images of a Test Done on a Convex Test Pieces at Mach 1.36. The material choice on the left of the image is copper and on the right of the image is PVC.

Figure 7.10 shows eight images of a shock entering the test section. The time interval between images is 25μs. In images 1 to 3 a regular reflection is observed. Between 40^o and 50^o the reflection pattern transitions from regular to Mach reflection. In image 4 the shear layer starts to build which is an indication of the beginning of a Mach reflection. In image 6 the Mach reflection is clearly visible with the shear layer, Mach stem and reflected wave clearly visible. The reflected waves intersect in image 7.

7.2.4 Quantitative Analysis

A comprehensive quantitative analysis is performed on the results. The analysis focuses on the angle between the incident wave and reflected wave (RI angle), angle between the wall angle and reflection angle (ω - θ) and the triple point trajectory.

7.2.4.1 RI Angle Measurment

It is of great importance to compare angles from PVC and Copper at similar wall angles. Figure 7.11 shows measurements taken from PVC and Copper at all three different Mach numbers. At different positions along the curve the value of the measured RI angle changes significantly, thus highlighting the importing of comparing measured angles from PVC and copper and similar wall angles.

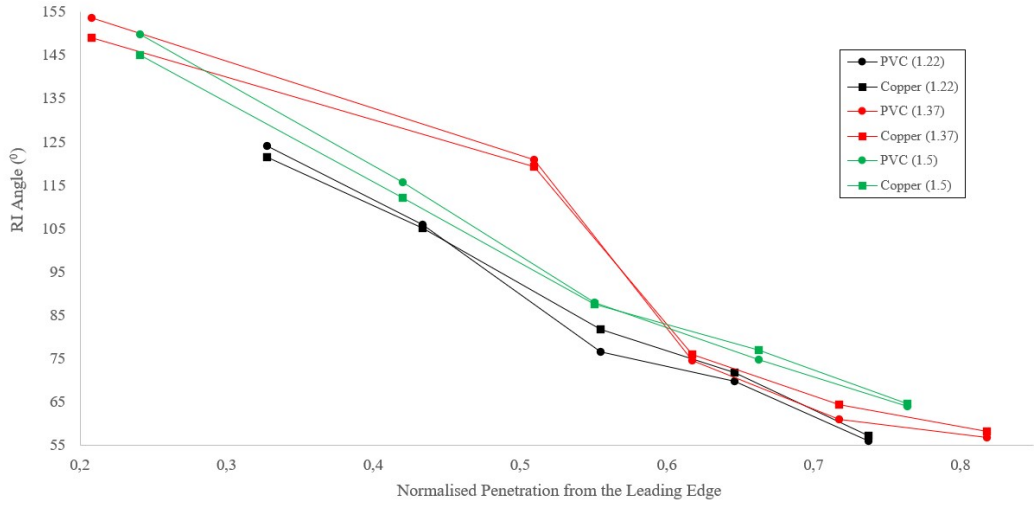

Figure 7.11: Measured RI Angles Along the Normalised Penetration from the Leading Edge.

7.2.4.2 Regular Reflection

Angle Between the Incident and Reflected Wave

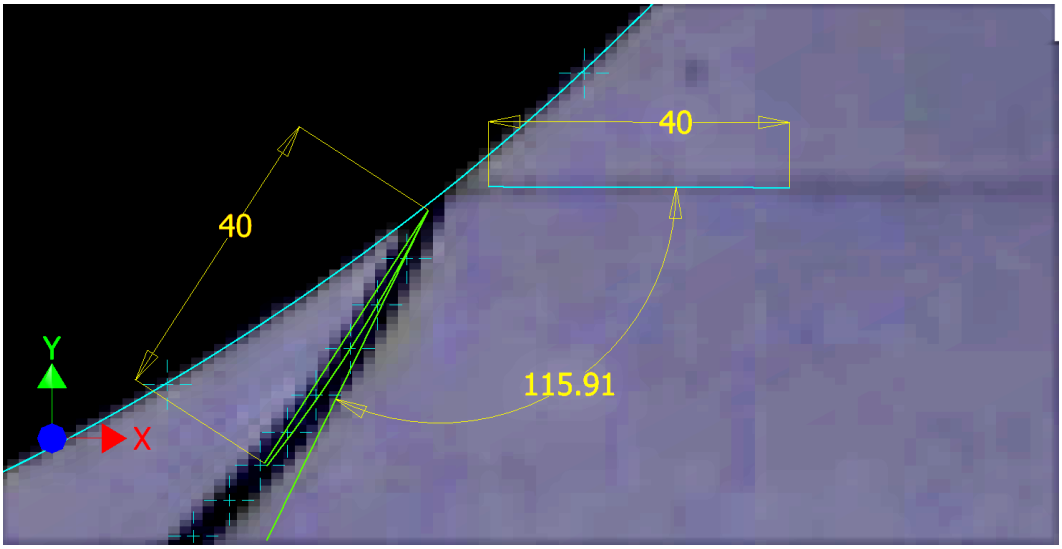

Figure 7.12: Image of the Angle Measured Between the Incident and Reflected Wave.

The angle between the incident and reflected wave is measured using a similar approach as the one taken in Section 7.1.4 and outlined in detail in Section 6.4.2. The angle will be referred to as the reflected angle or (RI). An example of the measured angles is shown in Figure 7.12.

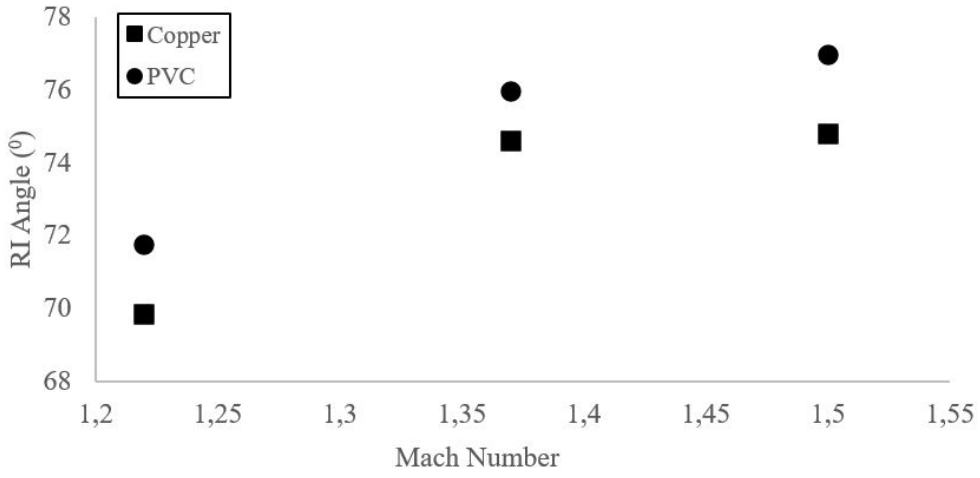

Figure 7.13: Scatter Plot of Measured RI Angles at Various Mach Numbers.

Figure 7.13 shows a scatter plot of the measured RI angle at the different Mach numbers. All results are measured at a wall angle between 30^o and 40^o. It can clearly be seen from the scatter plot that there is a significant difference in the RI angle between copper and PVC. The differences range from 1.3° to 2.2°.

Figure 7.13 with error bars can be found in Appendix C. Error bars have not been included in this section as the errors bars are small and have a minute impact on the interpretation results.

It can also be noted that at all three Mach numbers the RI angle recorded on the PVC test piece is larger than that measured on the copper. This agrees with the results found in the testing of the concave test piece and align to the conclusions made by Berry [1]. These significant differences are a clear indication that the thermal conductivity of the reflecting surface has an effect on the reflection topology

$\omega - \theta$ *Angle*

In addition to the analysis done on the angle between the incident and reflected wave, the angle between the reflection wave and reflecting surface (ω) is measured and analysed. This is done to provide additional insight and knowledge on the thermal effects of the reflecting surface. Figure 7.14 shows how the angles were measured and recorded.

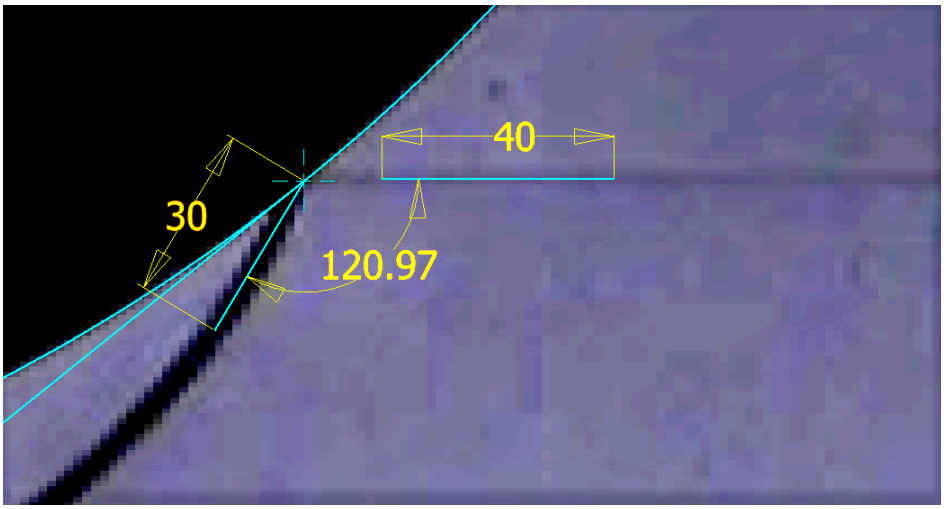

Figure 7.14: Measurement of ω and θ Angle.

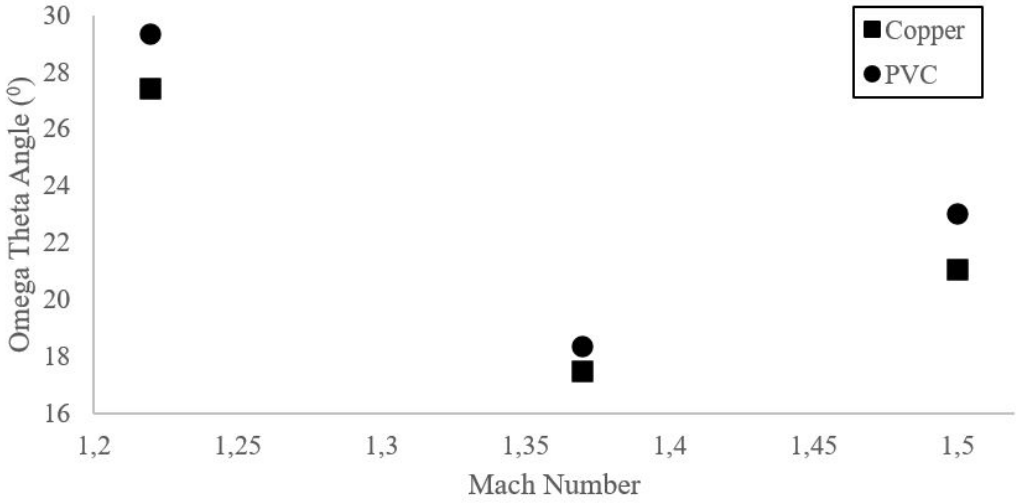

Figure 7.15: Scatter Plot of the Measured ω Angles for Copper and PVC in the Regular Reflection Case.

Figure 7.15 shows a scatter plot of the ω angles plotted against the Mach number. At each Mach number there is a detectable difference in the data. The differences range from 1° to 4°. The differences indicate that the thermal conductivity of the reflecting surface has a direct and significant impact on the reflection properties.

The ω angle measured from the PVC test piece has a greater value than the ω angle measured from the copper test piece. This can be seen in Figure 7.15. This is consistent at all four Mach numbers. The lower ω angle reflected from the copper is caused from heat transfer being absorbed into the copper test piece.

7.2.4.3 Mach Reflection

Angle Between the Incident and Reflected Wave

From a wall angle of around 55^o, a Mach reflection was present on the convex curved surface. It was observed that the reflected wave was slightly curved. This subsection covers and discusses the results obtained from the Mach reflection case.

The graphs displayed represent the angle between the incident and reflected wave (RI angle) of the PVC and copper test pieces at similar points on the curved surface and against the normalised penetration from the leading edge. Tests were done at Mach numbers of 1.22, 1.37 and 1.5.

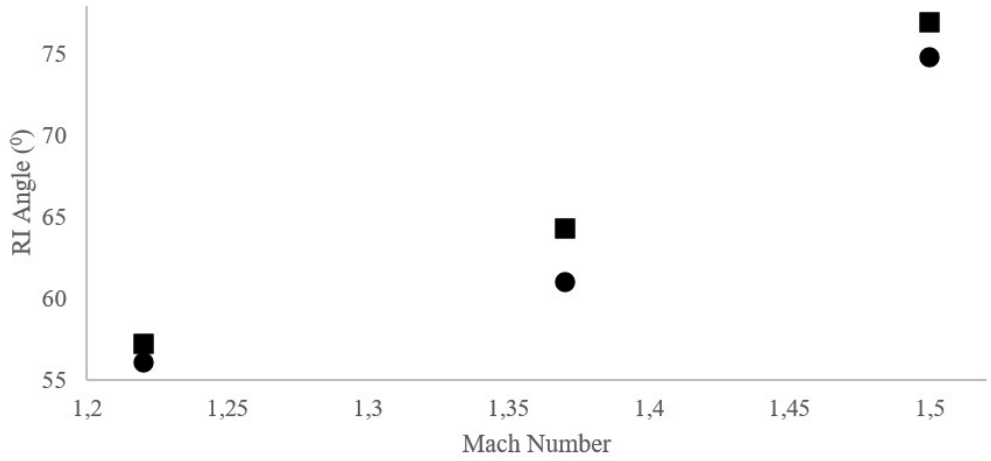

Figure 7.16: Scatter Plot of the RI Angle Measured at Various Mach Numbers.

Figure 7.16 shows a scatter plot of the measured RI angles from the copper and the PVC test pieces. The differences range from 1.2° to 3.1°. The differences increase as the Mach number increases. These differences strongly indicate that the thermal conductivity of the reflecting surface has an influence on the shock wave reflection properties.

Figure 7.16 with error bars can be found in Appendix C. Error bars have not been included in this section as the errors bars are small and have a minute impact on the interpretation of the results.

At all three Mach numbers (1.22, 1.37 and 1.5) the value of the measured angle from the copper surface is larger than the measured RI angle from the PVC surface. The correlates with the results obtained in the concave tests and in the tests done by Berry [1]. In the regular reflection case, the PVC has a larger RI angle than the copper. In the Mach reflection case the opposite is true.

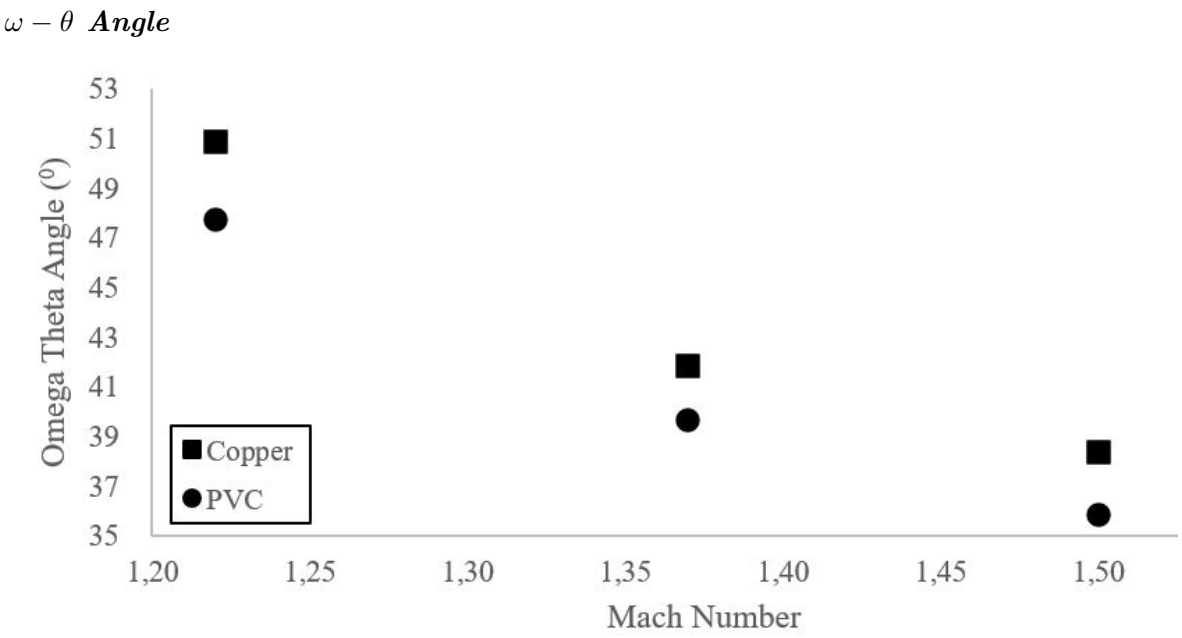

Figure 7.17: Scatter Plot of the Measured ω Angles for Copper and PVC in the Mach Reflection Case.

At Mach numbers of 1.22, 1.37 and 1.5 detectable differences in the measured ω angle are found. This implies that in the Mach reflection case, the effects of thermal conductivity on the reflection topology exist. It can also be noticed that the angle measured of the copper is higher than that measured from PVC. This is also the case in the measurement of the RI angle as shown in Figure 7.16. An explanation as to why this is the case cannot be given as the flow properties behind the Mach reflection are unsteady in both space and time. In Figure 7.17 there is a distinct difference in the measured ω angles.

7.2.4.4 Difference Between the Reflected Angles

The difference between the copper and PVC reflected angles was calculated by subtracting the PVC angle from the copper angle. These differences were plotted along the normalised penetration from the leading edge.

RI Angle

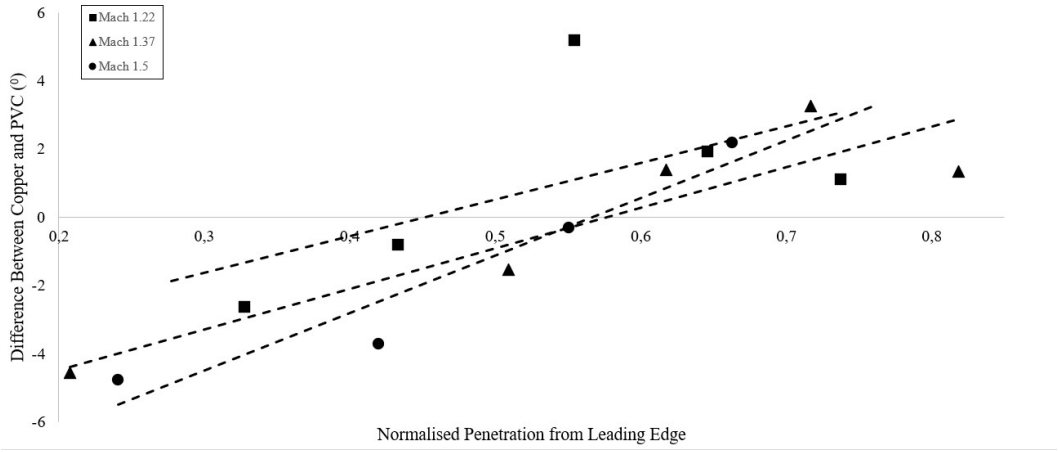

Figure 7.18: Scatter Plot of the Measured RI Angles for Copper and PVC in the Regular Reflection Case.

The trend lines in Figure 7.18 show the value of the difference in the RI angle of the copper and PVC decreases as the wave moves along the curved surface. Although there are limited data points the trend lines give an indication of how the differences change as the shock propagates along the curved surface. What can be seen from the limited data points is that the largest differences are present closer to the extreme values of the normalised penetration (0 and 1). At a normalised penetration value of approximately 0.5 the values of the differences invert and become negative. This is an indication that the nature of the reflection has changed from regular reflection to Mach reflection. The change of sign correlates to the transition point.

$\omega - \theta$ Angle

Figure 7.19 shows the differences between the ω angles from the copper and PVC test pieces (trend lines are added into the graph). The differences are plotted along the normalised penetration from the leading edge.

It is clear from the graph that all along the curved surface there is a significant difference in the reflection patterns caused by heat transfer between the reflecting wave and the reflecting surface. It can also be noticed that the trend lines pass through zero at an approximate NP value of 0.55. This switch between negative and positive differences reflects the transition

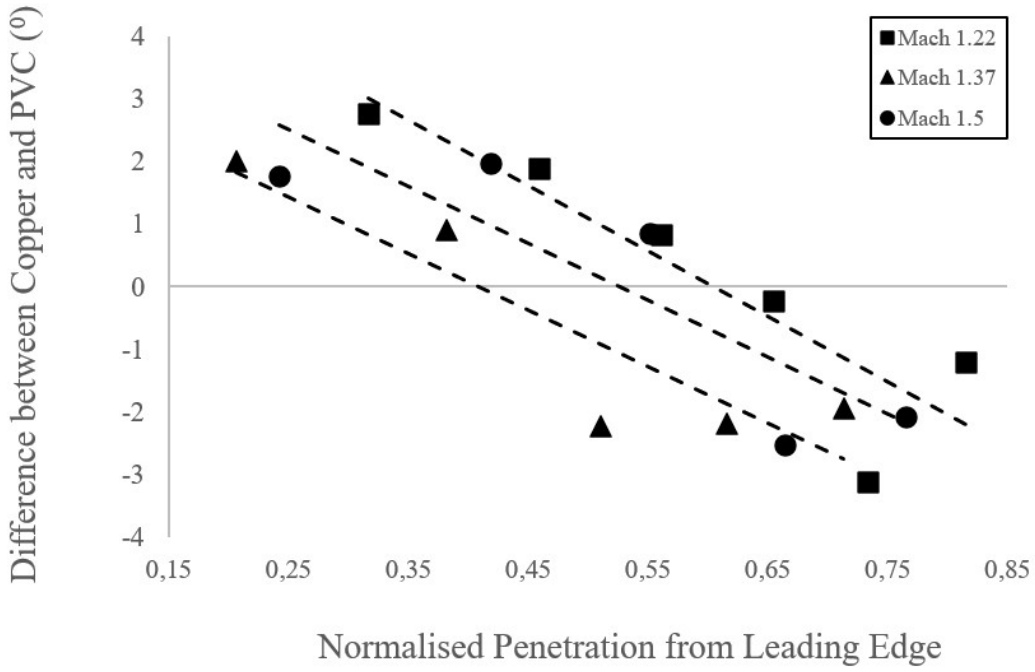

Figure 7.19: Scatter Plot of the Measured ω Angles for Copper and PVC in the Regular Reflection Case.

point on the reflection evolution. Although there are limited data points used here, the trends in Figure 7.19 give an indication of the differences between the reflections off the two surfaces as the shock propagates along the curved surface.

7.2.4.5 Triple Point Trajectory

In this subsection the analysis of the triple point trajectory of the Mach reflection is used to determine the effect that the thermal conductivity of the reflecting surface has on the reflection topologies. The triple point trajectory is calculated using the method in Section 6.4.1 and an example of the measurement is shown below in Figure 7.20.

The trajectory of the triple point was mapped in the analysis. A point was placed at the triple point of the Mach reflection. Once that had been done, using the same Autodesk file another image was inserted and a point was drawn on the triple point. This was done for as many images as possible. Once these were drawn on the image, straight lines were drawn which connect the points. Another straight line was drawn on the incident shock wave. The angle between the incident shock wave and the line connecting the triple points is measured.

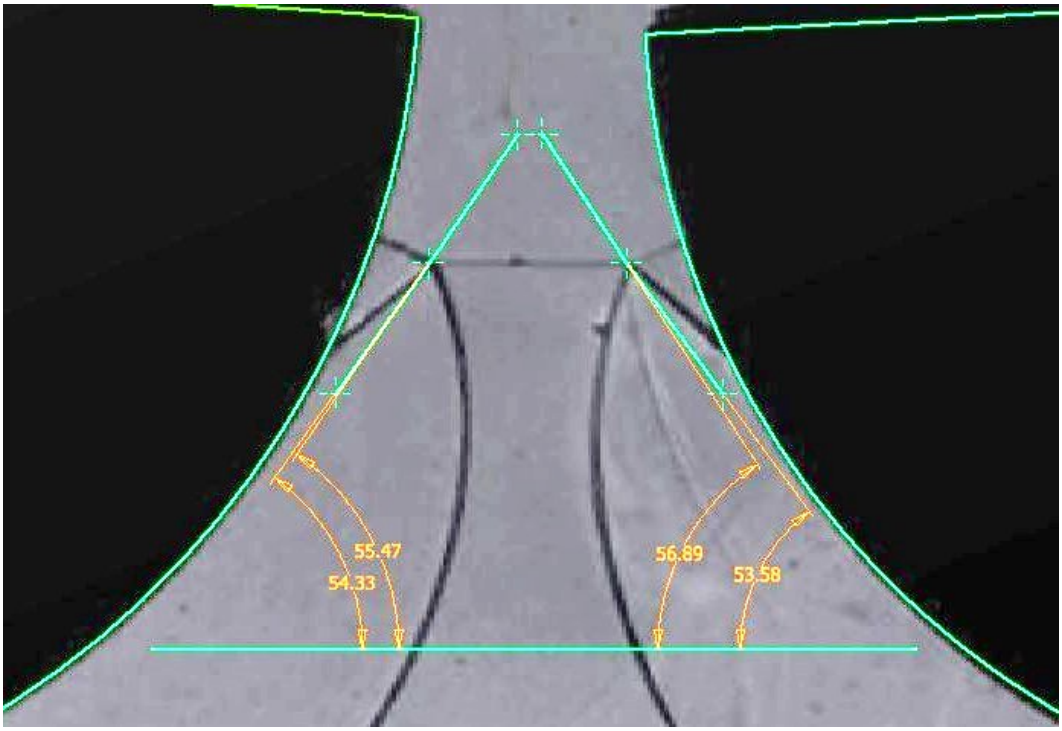

Figure 7.20: Angle Measured Between the Triple Point Trajectory and the Incident Shock Wave.

Table 7.1: Trajectory Angles.

Mach Number	PVC (°)	Copper (°)	Difference (°)
1.22	56.98	58.52	1.54
1.37	55.38	56.74	1.36
1.43	46.34	50.21	3.87
1.5	53.20	55.28	2.08

Table 7.1 shows the average trajectory angles measured from the convex test pieces. At all four Mach numbers the copper trajectory angles are larger than the PVC trajectory angles. There is no correlation between the Mach number and the difference in the trajectory angles. This measurement only aims to determine whether there is a difference in the triple point trajectories. However, due to a limited number of data points these results are inconclusive.

7.2.5 Qualitative Analysis

In addition to the quantitative analysis performed in Section 7.2.4 a qualitative analysis is performed on the images obtained in in the tests. In the qualitative analysis the physical properties are analysed and compared to each other. To aid this, a line has been drawn along the line of symmetry. This is done using the method shown in Section 6.4.3.

7.2.5.1 Regular Reflection

In order to aid in identifying a possible difference between the reflection patterns equidistant lines are drawn perpendicular to the line drawn over the plane of symmetry. This line is used as a reference point when comparing the reflection patterns to each other.

Figure 7.21 shows a regular reflection at Mach 1.22. The lines drawn on the image aid in identifying an asymmetry in the image. At point 1 (PVC) in Figure 7.21 the green line is touching the reflected wave but at point 2 (copper) there is a clear gap between the green line and the reflected wave. This is a clear difference and a visual suggestion that the thermal conductivity of the reflecting surface affects reflection topologies.

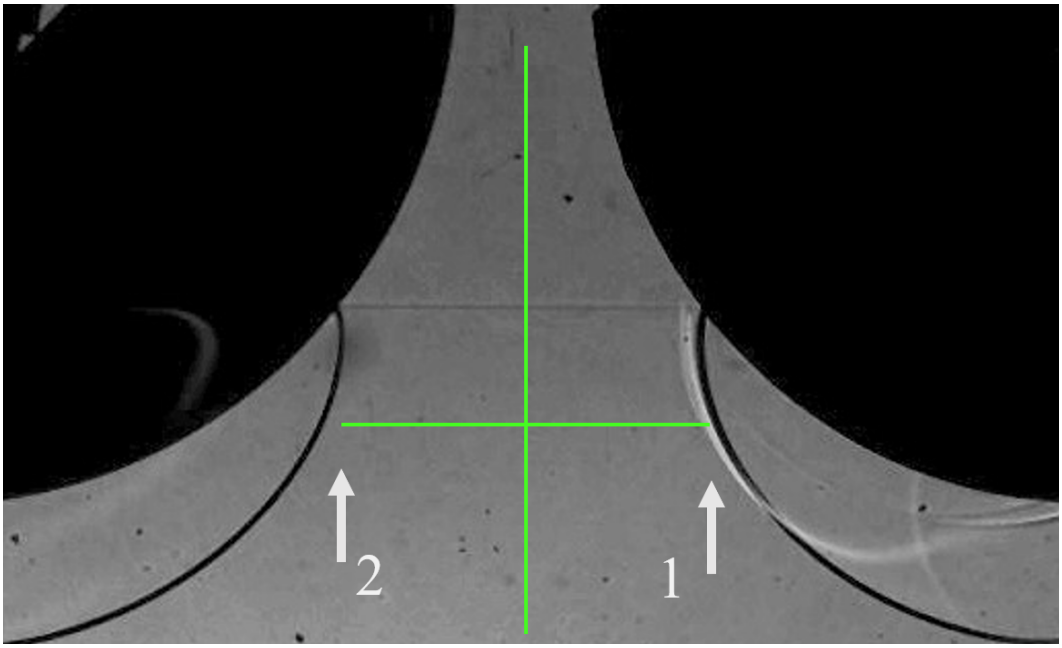

Figure 7.21: Shadowgraph of a Regular Reflection Case at Mach 1.22.

Regular reflection at Mach 1.37 is shown in Figure 7.22. At point 2 a detectable difference is visible. The difference is not as noticeable as the difference at Mach 1.22 but it is still significant and clearly visible in the image.

Figure 7.23 shows the regular reflection case at Mach 1.5. Just as in the tests at Mach 1.22 and 1.37, there is a detectable difference at point 2 (copper). Upon a visual inspection, the gap between the line and the reflected wave is not as large as the gap at Mach 1.22.

In the regular reflection case, clear detectable differences were found at Mach numbers of 1.22, 1.37 and 1.5. The asymmetry was characterised by the reflected wave from the PVC surface being further away from the plane of symmetry than the reflected wave from the copper surface.

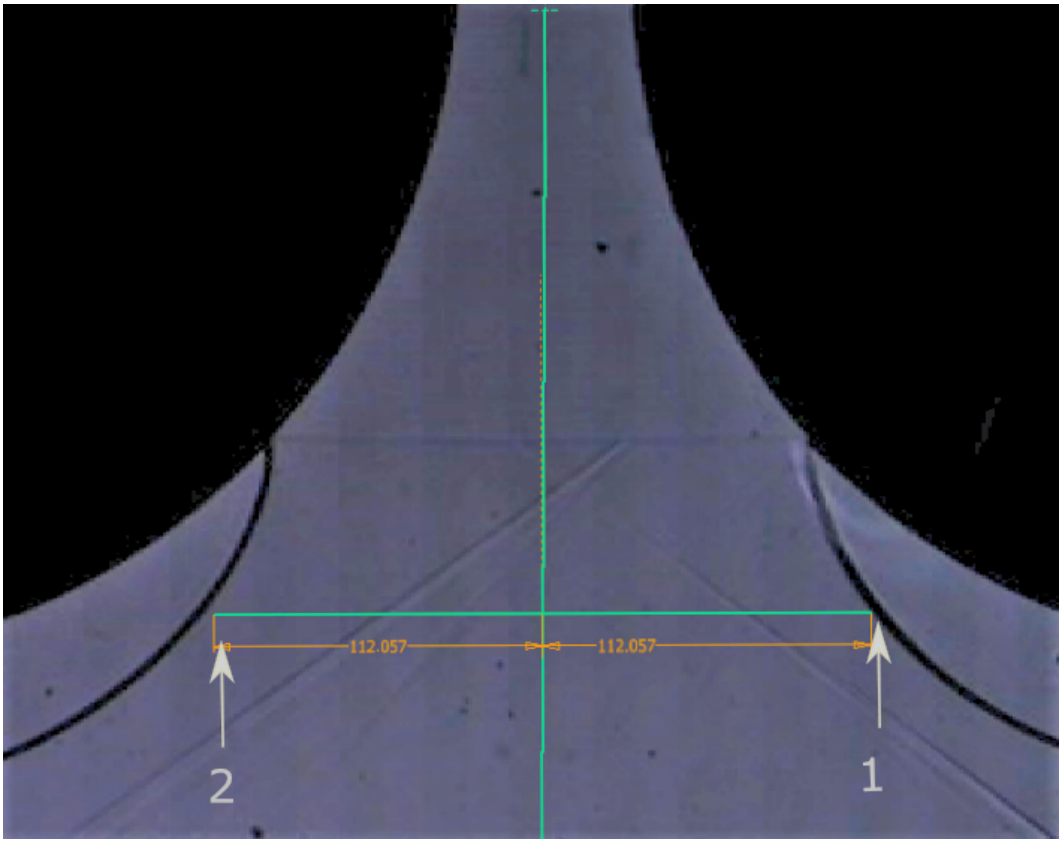

Figure 7.22: Shadowgraph of a Regular Reflection Case at Mach 1.37.

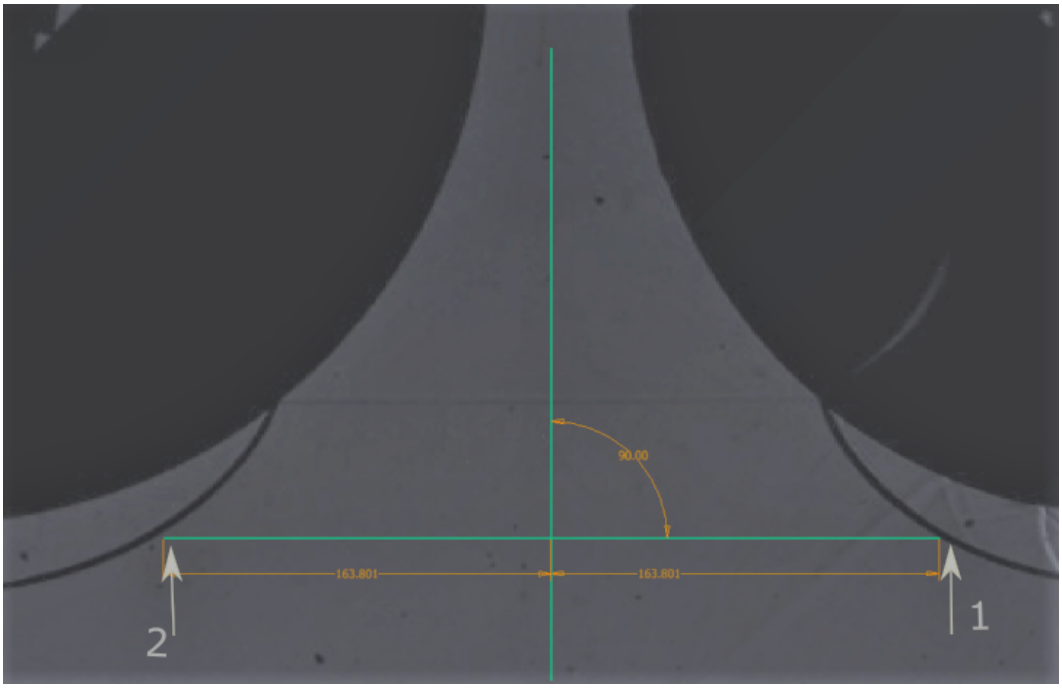

Figure 7.23: Shadowgraph of a Regular Reflection Case at Mach 1.5.

7.2.5.2 Mach Reflection

In the Mach reflection case, the reflected wave patterns intersect. In the case that the reflection patterns are identical, the intersection of the triple points and reflected waves would intersect on the plane of symmetry. In order to determine whether this is the case or not, a line is drawn along the plane of symmetry and a line connecting the intersection points is drawn.

Figure 7.24 shows a Mach reflection at Mach 1.22. At this Mach number there are two indications of the effect of thermal conductivity. There is a clear difference between the line joining the intersection points and the plane of symmetry. The area on the copper side (left) is larger than the area on the PVC side (right).

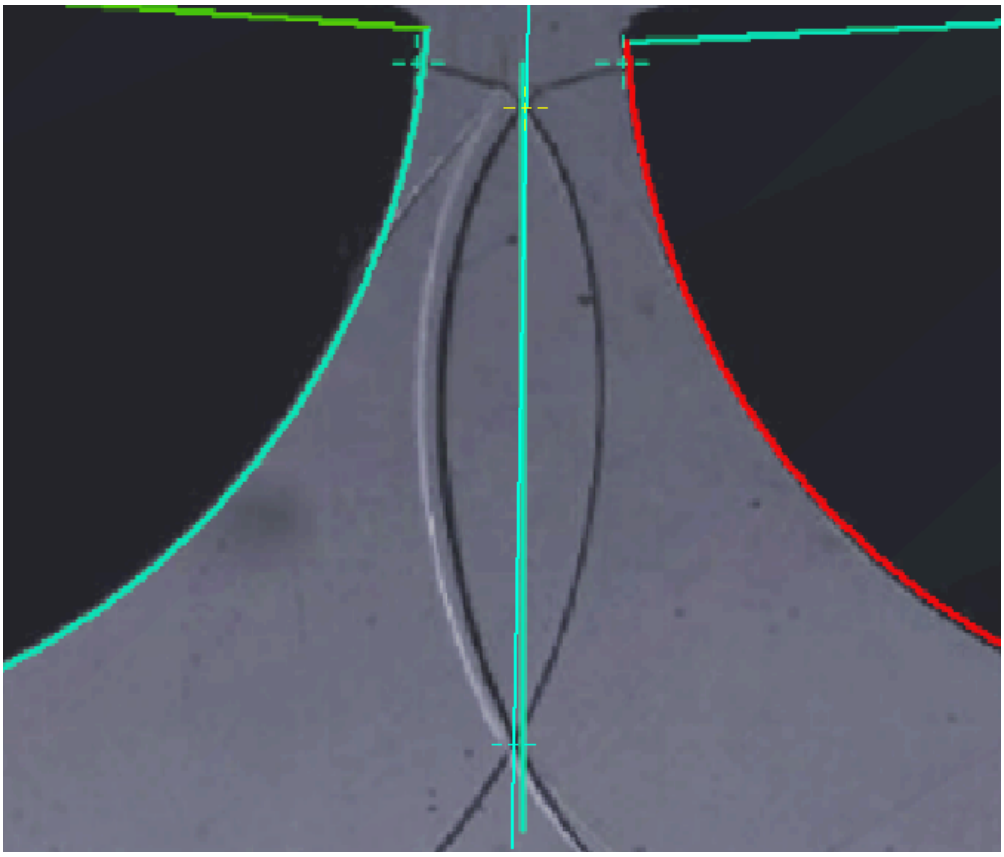

Figure 7.24: Shadowgraph of a Mach Reflection Case at Mach 1.22.

In Figure 7.25 there is a slight difference between the drawn lines. In addition, two corner signals are visible. The signals are shown with grey arrows. The corners signals are clearly asymmetrical, as the PVC corner signal is close to the plane of symmetry while the copper signal is further away.

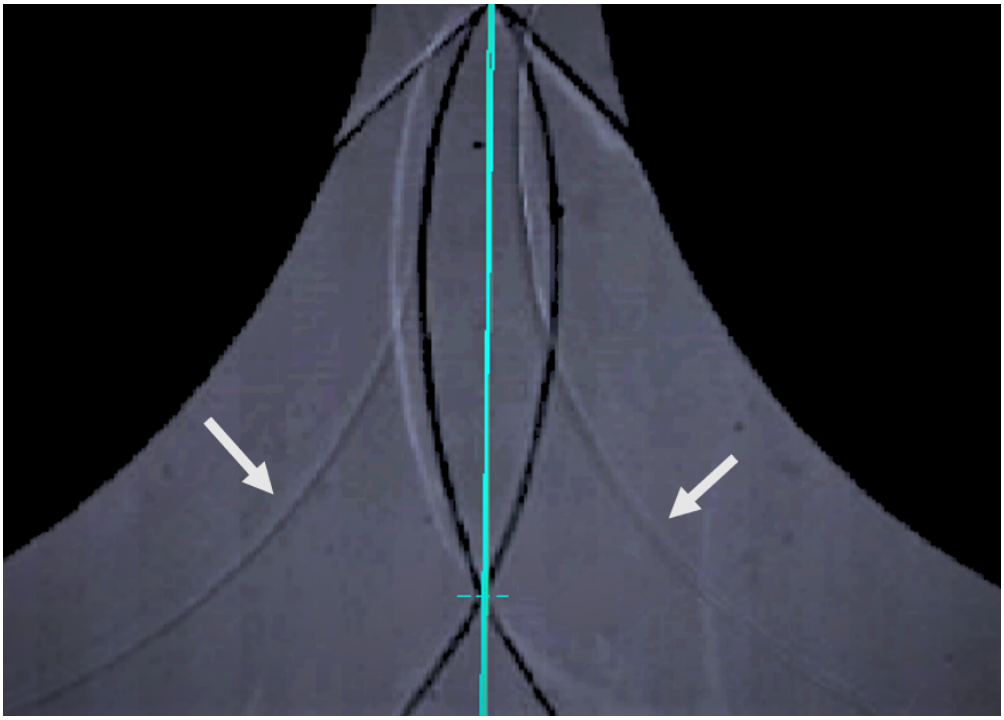

Figure 7.25: Shadowgraph of a Mach Reflection Case at Mach 1.37.

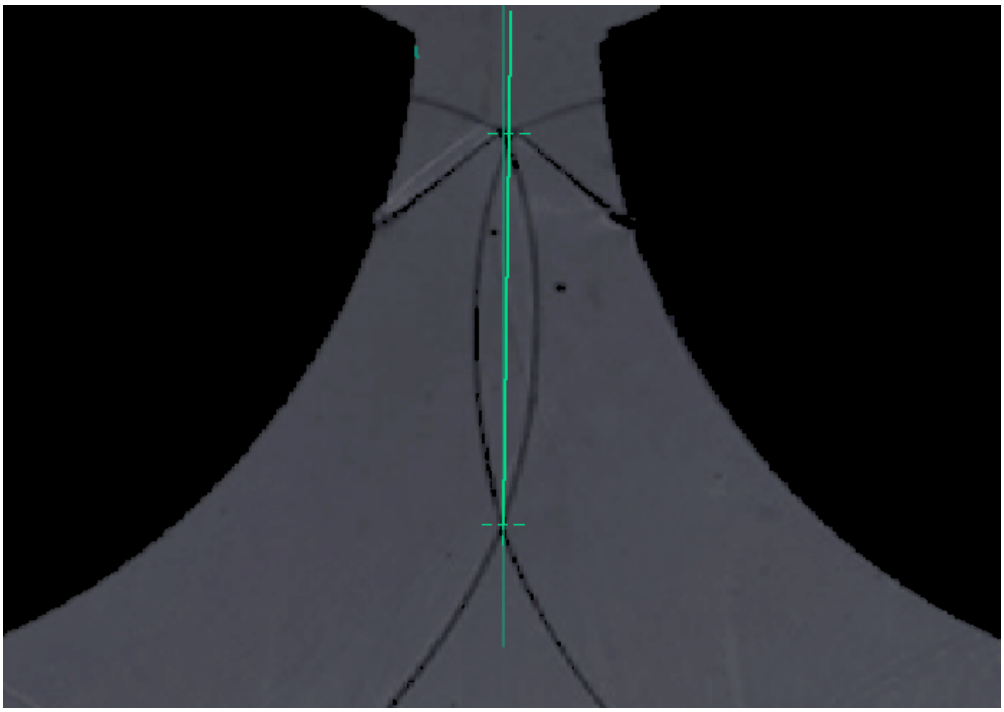

Figure 7.26: Shadowgraph of a Mach Reflection Case at Mach 1.5.

Figure 7.26 shows a distinguishable gap between the two drawn lines at the point of intersection between the triple points. When inspecting the area between the reflected waves and the intersection points, the area on the PVC side is larger than the area on the copper side.

There are detectable and clear differences in the reflection topologies in the Mach reflection case. The differences are present at all four Mach numbers. Differences include the intersection of the triple point not on the plane of symmetry, intersection of the reflected wave not on the plane of symmetry, intersection or corner signal offset from plane of symmetry and differences in the size of area enclosed between the reflected wave and intersection points.

7.2.6 Asymmetry of Reflected Waves

Figure 7.27 shows the reflected waves re-reflecting off the surfaces. It clearly shows a lack of symmetry between the reflection patterns. This image clearly shows different reflection patterns in the left and right side.

Figure 7.27 shows clear shear layers on both the left and right hand sides where the reflected waves cross. The difference in these reflection patterns could suggest that a Mach reflection is forming on the right hand side and a regular reflection is forming on the left hand side.

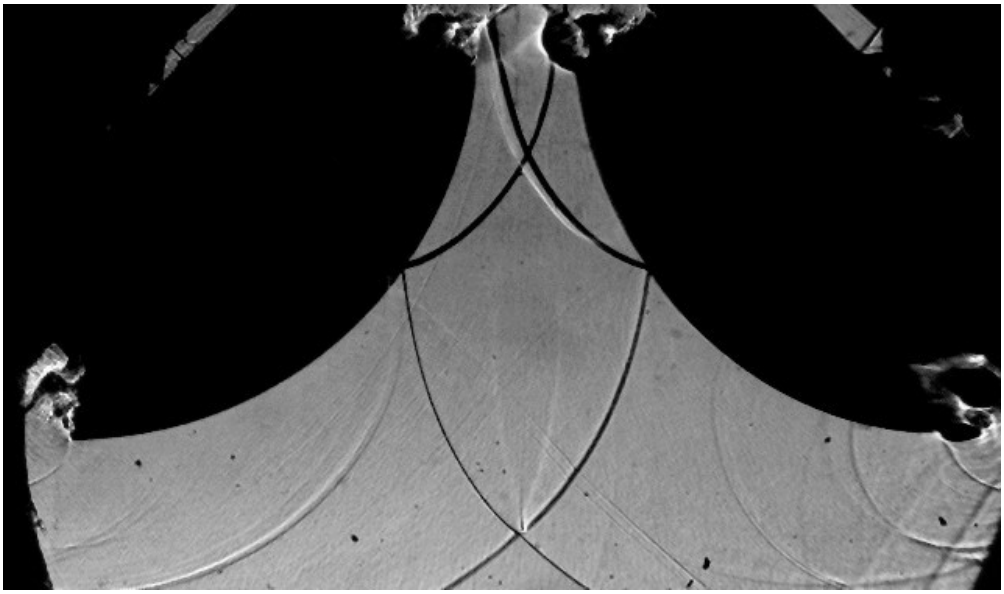

Figure 7.27: Shadowgraph Highlighting Assymetry of Reflected Waves at Mach 1.5.

7.3 Weak Shock Wave Reflection

In this subsection the results obtained with regards to very weak shock wave reflection off curved surfaces will be discussed. The following topics will be covered: calculation of very weak shock wave Mach numbers, analysis of obtained data and inspection of very weak shock wave reflection properties.

7.3.1 Calculation of the Mach Number

The calculation of the Mach number using the digital oscilloscope proved to be a challenging task. At low Mach numbers the pressure pulse on the pressure transducers is minimal. Therefore, in order for the digital oscilloscope to capture a pulse, the trigger setting had to be extremely sensitive. However, at a sensitive setting the oscilloscope was easily triggered by external disturbances which made recording the shock wave information difficult.

An additional method of the Mach number measurement was used. Using the frame rate on the camera and the measurment of the distance the shock travelled between frames provided enough information to calculate the Mach number. The method is explained in Section 6.2.2. Although more time consuming than using the oscilloscope this method proved more consistent and provided more accurate Mach number results.

The Mach numbers obtained using the high speed camera were used in the experiment and the Mach numbers obtained from the oscilloscope were used as back up values. The pressure transducers are designed for a much higher range of pressures and their accuracy of measuring pressure traces is questionable. The frame rate of the camera is reliable and can therefore be used in the measurement of the Mach number with confidence.

7.3.1.1 Very Weak Shock Reflection Test Images

In Figure 7.28 there are ten images which represent a typical test done in the weak shock experiments. In image 1 the shock has started travelling along the curved surface. A small kink in the wave representing a compression reflection is observed. An irregular reflection is observed in image 4. A Mach stem is clearly visible. There is no Mach stem present in image 9 but a well formed reflected wave and shear layer are present indicative of a developing TRR.

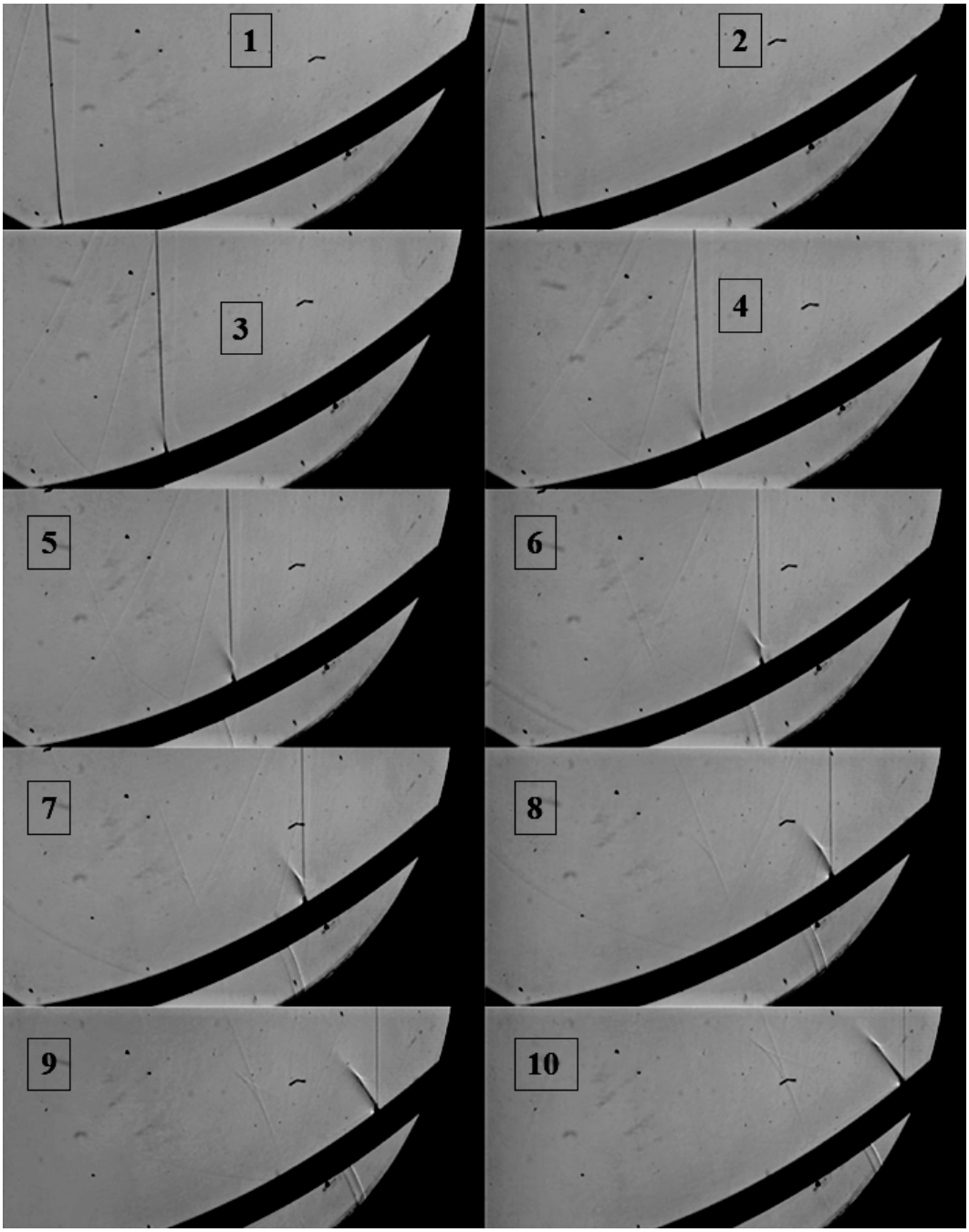

Figure 7.28: A Collage of a Weak Shock Wave Test at M 1.05.

7.3.2 Quantitative Analysis of Very Weak Shock Data

In the quantitative analysis of the ultra weak shock wave data the transition points between different reflection patterns were recorded. In this analysis the results from previous testing and the results from current testing will be combined to aid in the understanding the shock wave reflection evolution. The previous testing data was in the range of Mach 1.03 to 1.06.

This data is obtained from the work done by Chirewa [16]. In total data for 24 different tests is used. This is shown in Figure 7.29.

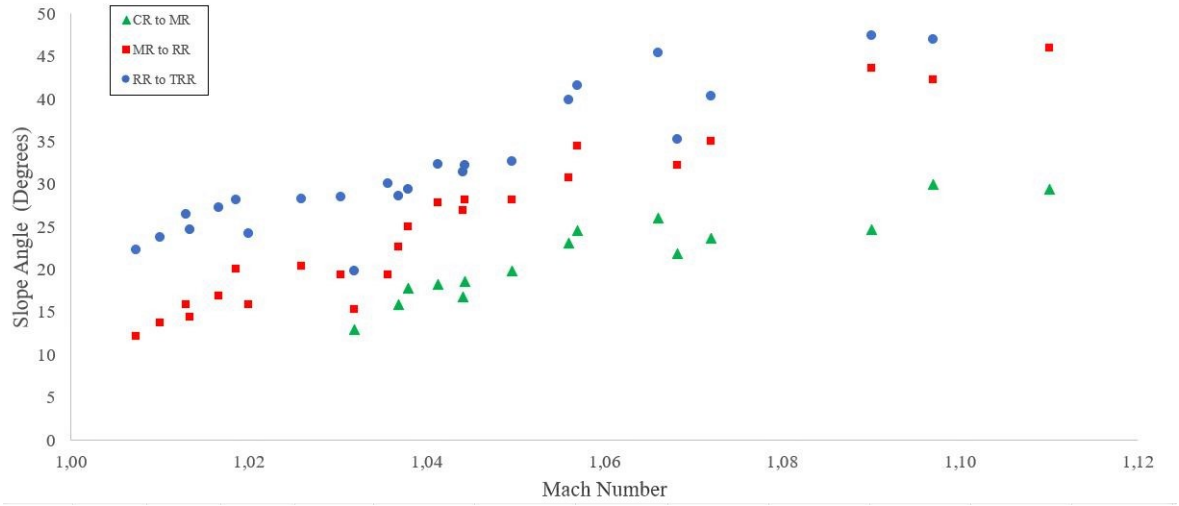

Figure 7.29: Scatter Plot of Transition Points of Weak Shock Wave Reflection Plotted Against the Mach Number.

At the TRR transition point there is a slight disagreement between the data from current tests and previous tests. It can be seen in Figure 7.29 that in the region between Mach 1.035 and Mach 1.05 the data points are lower than the general data trend. As two different people did the analysis in the different data sets a slight difference in judgement could be the cause. The TRR transition point may be identified differently between different people as it requires the judgment of the viewer to determine at what point the reflection case transitions. However, despite the slight differences these two data sets are comparable.

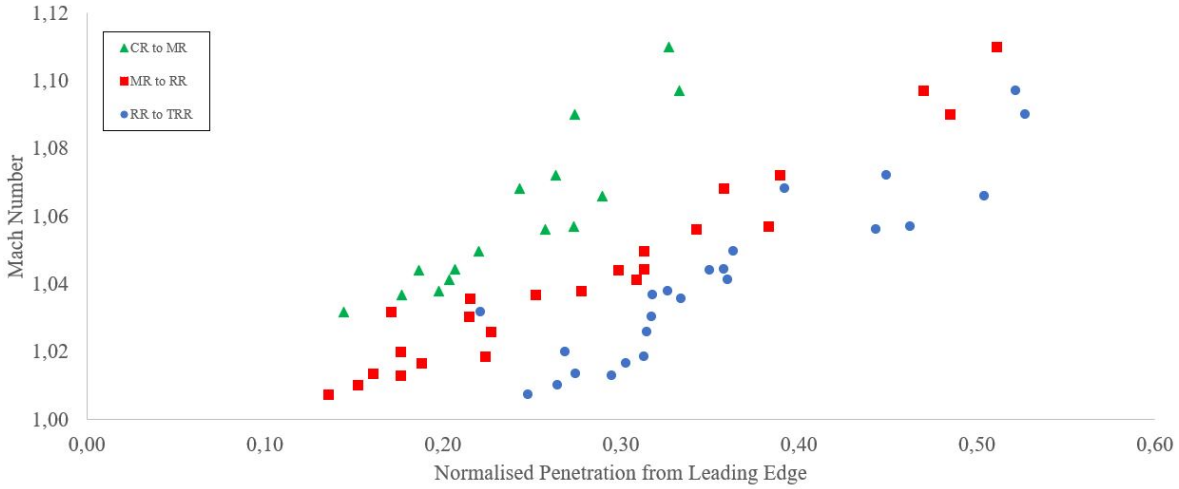

Figure 7.30: Scatter Plot of Transition Points of Weak Shock Wave Reflection Plotted Against the Normalised Penetration From the Leading Edge.

Figure 7.30 shows the transition points plotted along the normalised penetration from the leading edge. This is a similar plot as the one created by Gruber in Figure 2.31. The novel data obtained in the experiments in this study are at a Mach number below 1.03.

A line of best fit is added to the data in Figure 7.31 and Figure 7.32. These lines give an indication of the behaviour of the transitions points and give perspective across various Mach numbers and the angle of curvature. In general, the data in Figure 7.31 exhibits consistent behaviour. All three transition cases show a gradual decrease in slope angle values over Mach numbers of 1.007 to 1.11. Overall the data from this experiment and previous experiments agree and connect with each other succinctly.

The R-squared value for the CR to MR, MR to RR and RR to TRR data points are 0.83, 0,95 and 0.84 respectively. The R-squared values indicate that for all transition cases the trend shown in the graph is a strong trend.

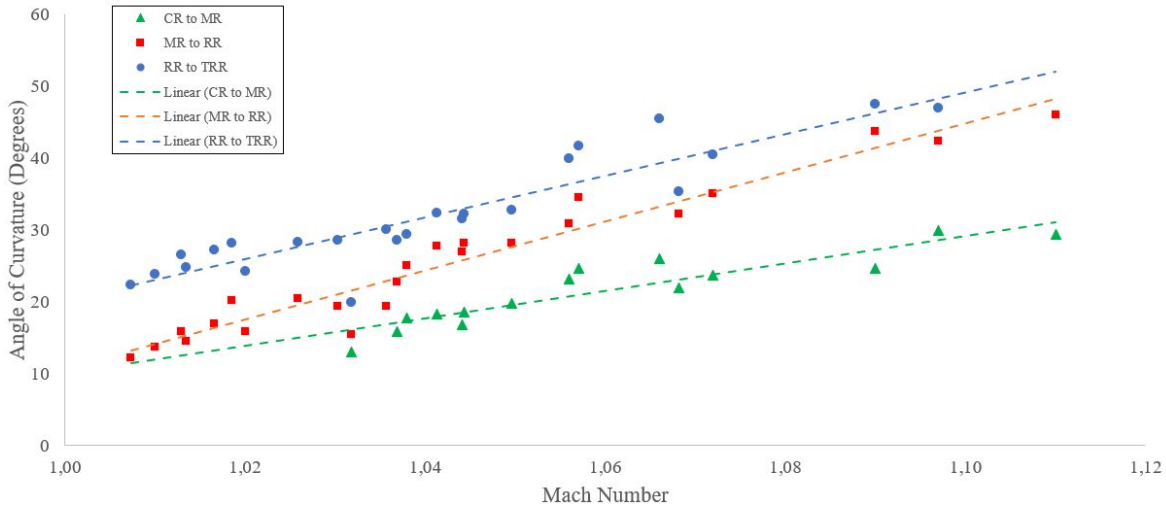

Figure 7.31: Scatter Plot of Transition Points Between Reflection Types of Weak Shock Wave Reflection Plotted Against the Mach Number.

The trend exhibited by the TRR transition point is gradual. However, it follows the same pattern as the trends of the other transitions point. As the Mach number increases the slope angle of the transition point increases.

The points which represent the transition between Mach reflection to Regular reflection show a clear trend over the entire data set. This provides a clear picture of the behaviour of the transition point for weak shock waves. The angle of curvature of the transition point increases as the Mach number increases.

The difference between the regular reflection transition point and the TRR transition point decreases as the Mach number increases. At Mach numbers below 1.03 the difference between

the transition points has an approximate average value of 10°, whereas at higher Mach numbers the difference decreases to approximately 4°. The hypothesis can be made that at lower Mach numbers the reflection evolution happens at a slower pace than at higher Mach numbers.

The gradual increase in the data suggests that there is a correlation between the slope angle at which the Mach reflection forms and the Mach number. The higher the Mach number the larger the slope angle at which the transition points occur. This is true in the region of Mach 1 to Mach 1.1, but more data is required to make conclusions about this correlation after Mach 1.1.

At Mach 1, the reflection pattern will always be a regular reflection. It is therefore important to understand the behaviour of the reflecting wave as the Mach number approaches 1. At Mach 1, there will be no CR, therefore the CR to MR line will level out as the Mach number approaches Mach 1. Although a regular reflection will be present at Mach 1, a prediction of the behaviour of the MR to RR line cannot be made due to the lack of data points closer to Mach 1.

In Figure 7.31 there is no data on the transition point between a compression wave and a Mach reflection below a Mach number of 1.03. This is because the compression reflection had transitioned to a Mach reflection before reaching the viewing window.

Consistent trends are displayed in Figure 7.32 across all three transition points. From the graph there is the possibility that at Mach 1 the transition points will converge at the leading edge. However, there is not enough data at the Mach number close to Mach 1 which would be able to confirm this.

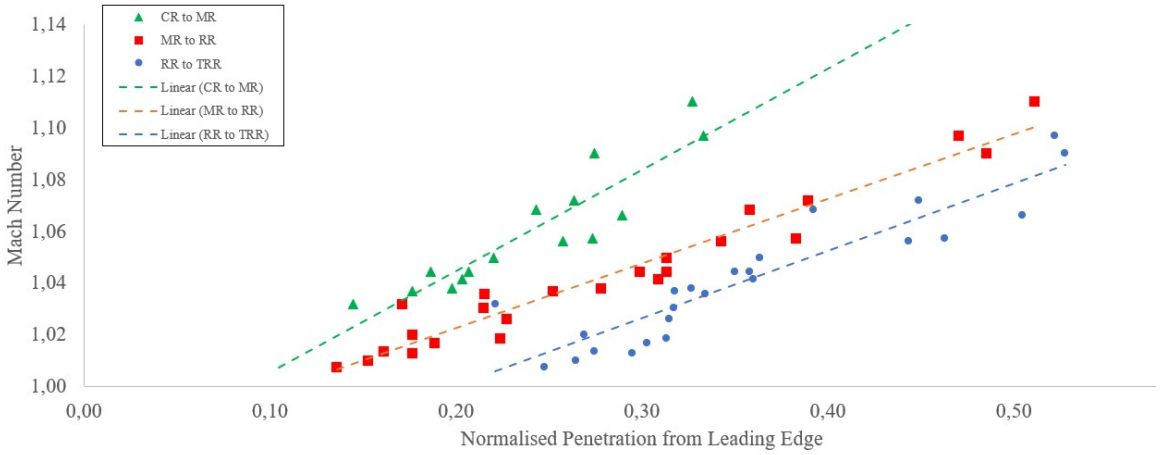

Figure 7.32: Scatter Plot of Transition Points of Weak Shock Wave Reflection Plotted Against the Normalised Penetration from the Leading Edge.

The lines of best fit which have been added into Figures 7.31 and 7.32 are useful in understanding the behaviour of the reflection evolution. The line representing the transition point between CR and MR and the line representing the transition point between the MR and RR intersect in Figure 7.31. This intersection suggests that at Mach numbers close to Mach 1 a Mach reflection doesn't form. This suggestion is backed up from the images at Mach 1.007 and Mach 1.026. In the images, the reflected wave is not clear and well defined.

The line of best fit representing the transition point between RR and TRR suggests that at Mach 1 the TRR will form at 18°. This is obviously impossible as at Mach 1 only regular reflection exists. It could be hypothesized that at very low Mach numbers (Mach number close to 1), the TRR reflection pattern is absent.

7.3.3 Qualitative Analysis of Very Weak Shock Waves

In order to better understand the behaviour of weak shock waves reflecting off concave curved surfaces a comprehensive analysis of the images was undertaken. Through an analysis of images of very weak shock waves at different Mach numbers an understanding of the reflection behaviour will be explored.

7.3.3.1 Mach 1.007

The lowest Mach number that was attainable was Mach 1.007. This test is shown in a series of images in Figure 7.33. The four different reflection patterns are noted on the images (c - compression reflection, m - Mach reflection, r - regular reflection and t - transitioned regular reflection).

The development of the reflected wave happens gradually, a fully formed reflection wave is only visible after a number of frames. The absence of a shear layer and a small Mach stem make it challenging to identify a Mach reflection. Before the development of the TRR there is an apparent regular reflection for a few frames. The reflection pattern identified by Gruber in Figure 2.30 as a regular reflection has the same physical appearance as the RR in Figure 7.33. The identification of the TRR is easy as the reflection pattern is well developed. It must be noted that there is an absence of a shear layer. There is not enough information on the shadowgraph whether the shear layer is absent or just is not visible.

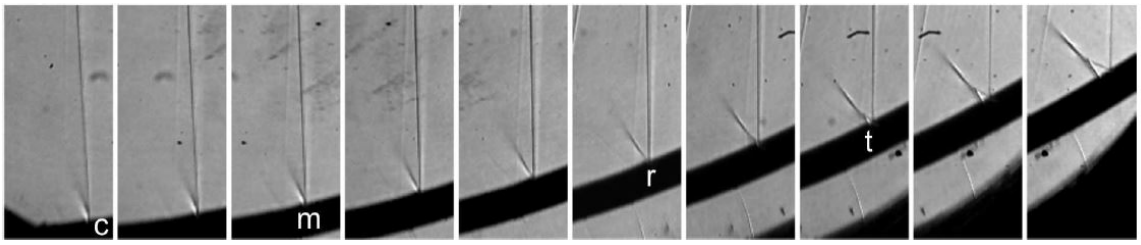

Figure 7.33: A Series of Images at Mach 1.007, Images are 50μs Apart.

7.3.3.2 Mach 1.026

Figure 7.34 is a series of images at Mach 1.026. The results from these images are similar to those at Mach 1.007. There is the absence of a shear layer in the MR. Although not fully formed, the reflected wave is more defined than the reflected wave in Figure 7.33. Once again, there are a few frames of regular reflection which are present. It is clear that there is no visible shear layer on the TRR.

A weak transverse wave can also be seen in the images. This is a result of an imperfect diaphragm burst. The transverse wave is weak and has no effect on the reflection properties of the incident wave.

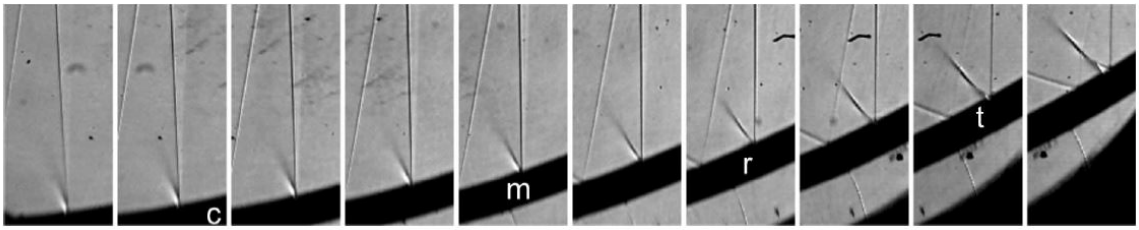

Figure 7.34: A Series of Images at Mach 1.026, Images are 50μs Apart.

7.3.3.3 Mach 1.056

The compression reflection has a well defined and clear kink in the base of the wave. The CR is also much higher up the curve than in the tests at lower Mach numbers. A shear layer is still missing from the MR. However, the Mach stem and reflected wave are more defined than in the previous two cases. Regular reflection is present in a few frames before the reflected wave evolves into a TRR. The TRR still lacks a shear layer.

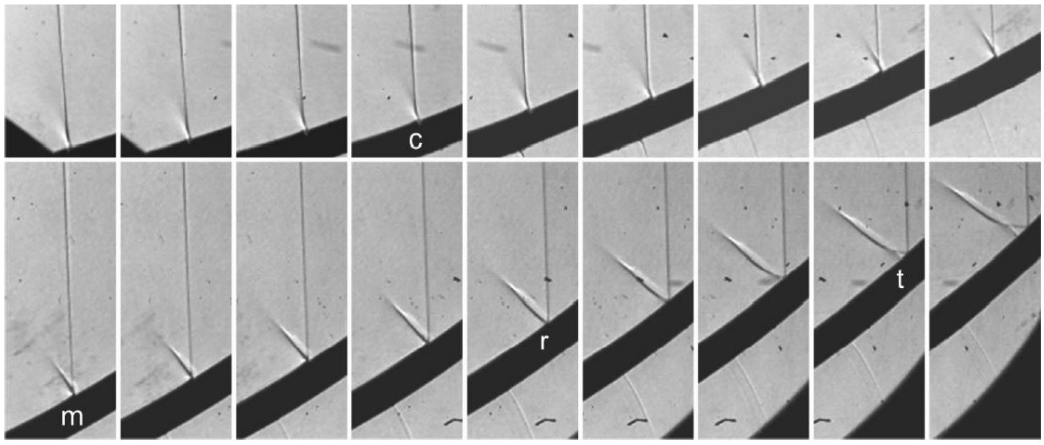

Figure 7.35: A Series of Images at Mach 1.056, Images are 33μs Apart.

7.3.3.4 Mach 1.09

Figure 7.36 shows images from the test done at Mach 1.09. At this Mach number, the reflection features associated with stronger shocks are present. There is a noticeable shear layer in the MR and the reflected wave is well defined. The identification of the regular reflection is not clear. Since for experiments with stronger shocks there is no evidence of a regular reflection as is to be expected from previous studies.

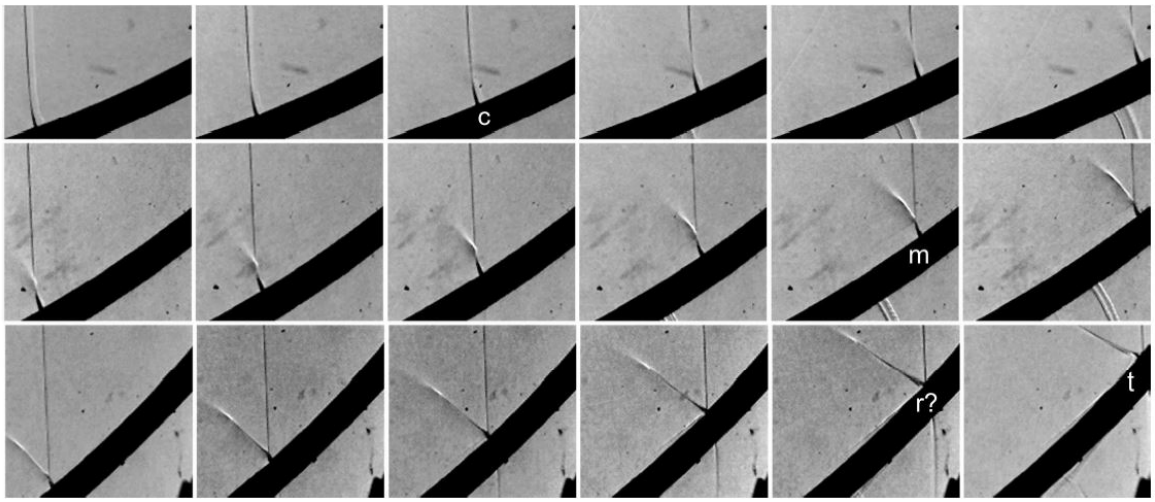

Figure 7.36: A Series of Images at Mach 1.09, Images are 33μs Apart.

In the second last frame a regular reflection appears to be present. However, due to the presence of a shear layer the reflection pattern cannot be regular but rather the early stages of a TRR. A reflection pattern which resembles a TRR is shown in the last image. The image does not contain enough information to exactly determine the geometry of the reflection pattern. There is a the slight resemblance of a shear layer, which would be expected for TRR from stronger shocks.

From the qualitative analysis it is clear that at the Mach numbers tested, all reflection patterns in the shock wave reflection evolution from a curved surface are present. It is clear that there is an apparent regular reflection pattern present at the lower Mach numbers. When the reflection angles of the apparent regular reflection are compared to theoretical and experimental reflection angles of a regular reflection the reflection patterns resembles a Mach reflection in the plane wall case. This suggests that the regular reflection present in the reflection from a curved surface is either different from the plane case regular reflection due to the history of the wave or that what appears to be a regular reflection is a Mach reflection with a small Mach stem. Although the reflection pattern consistently resembles a regular reflection, the only way to determine what type of reflection pattern it is, is by performing a high resolution CFD model to determine whether there is a Mach stem or not.

Chapter 8 Conclusions

This work explores two different studies: The Effect of Wall Thermal Conductivity on Shock Wave Reflection and Weak Shock Wave Reflection. The purpose of the thermal conductivity study is to determine whether the thermal conductivity of the reflection surfaces affects the reflection angles of a shock wave reflecting off a curved surface. The purpose of the Weak Shock Wave Reflection Study is to obtain very weak shock wave ($M < 1.03$) results and to better understand the reflection off curved surfaces of these waves. Once obtained the experimental results were analysed qualitatively and quantitatively.

All experimentation were performed in the Large Scale Diffraction Shock Tube. The length of the shock tube allowed a long enough distance for the very weak waves to form before entering the testing section. However, the viewing window restricted the size of the test pieces and the size of the observable flow field.

A shadowgraph optical setup was used with high speed imaging. The resolution of the images was satisfactory and the high-speed imaging allowed multiple images of a single test to be analysed.

It was found that depending on the manner in which the diaphragm would rupture, the plane shock would enter the testing section at slightly different angles to the floor of the shock tube. An attempt to increase the consistency of the diaphragm rupture was made by using a pneumatic pricker with little success.

Very weak shock waves were obtained by using wax paper as a diaphragm material. During these test the pricker was activated. Although other diaphragm materials were used (12μm polyester film and light tin foil), the wax paper was the only diaphragm material that consistently produced shock waves in the range of 1.007 to 1.03.

8.1 Quantitative and Qualitative Results

The Effect of Thermal Conductivity on Shock Wave Reflection

Differences in the shock wave reflection patterns were found in both the quantitative and qualitative analysis performed. The qualitative analysis performed showed asymmetrical shock reflection patterns for both regular reflection and Mach reflection cases at all tested Mach numbers. The results from the testing done confirm the results obtained in past work.

The quantitative analysis highlighted the effect heat transfer has on the reflection patterns through the measurement of the reflection patterns angles. Differences in the Measurement of the RI angle and the ω - θ angle showed that the thermal conductivity of the reflecting surface has an effect on the reflection patterns. Tests on the concave tests pieces produces differences in the Mach reflection angles of 1.61° to 8.14° at Mach number of 1.26 to 1.5. On the convex test piece tests were performed at Mach numbers of 1.22, 1.37 and 1.5. In the regular reflection case, differences of 1.3° to 2.2° and 1° to 4° were found in the RI and ω - θ angles respectively. In the Mach reflection case differences in the reflection angels of 1.2° to 3.1° and to 2.1° to 3.1° in the RI and ω - θ angles were found respectively. The triple point was also mapped and measured, differences were found at all Mach numbers. The qualitative analysis performed provides a clear and conclusive case that the reflection properties of shock wave reflections off curved wall are affected by heat transfer, this conclusion is supported by the qualitative analysis.

Consistent results were found throughout testing, in the regular reflection case the measured RI angle on the PVC was larger than that of the copper in all measured cases. The measured RI angle on the copper was larger than the PVC in all Mach reflection cases. This is also consistent with the results obtained in undergraduate studies. The shock wave reflections from the convex case pass through an inflection point at a wall angle of 40° – 50°.

A trend was found in the concave case, as the Mach number increased the magnitude of the differences in the measured angles decreased. However, the opposite was found in the Mach reflection from the convex test piece. As the Mach number increases the difference in the reflection angles increases.

Weak Shock Wave Reflection

Ultra weak shock waves were produced in the experimentation. Mach numbers of 1.007 to 1.03 were achieved during testing which is novel data. In addition, tests were performed that covered a Mach number range of 1.007 to 1.1. A qualitative and quantitative analysis was performed on the results.

An apparent regular reflection exists at very weak Mach numbers. However, it cannot be confirmed if this reflection pattern is identical to a regular reflection in the plane wall case.

During the quantitative analysis the transition points over this Mach number range displayed a gradual trend representing a linear variation. The wall angles of all three transition points exhibit a directly proportional relationship to the Mach number. From the data, the hypothesis can be made that the reflection evolution happens at a slower pace at lower Mach numbers.

At Mach numbers close to Mach 1, it can be concluded that no Mach reflection forms. It can also be hypothesized that at close to Mach 1 the TRR reflection patterns ceases to exist.

At all Mach numbers the entire reflection evolution is observed in the qualitative analysis. At Mach numbers below 1.03 the regular reflection pattern has a curved reflection wave. No shear layer is present in the Mach reflection or transitioned regular reflection at these ultra low Mach numbers. However, a shear layer is found in tests with a Mach number higher than 1.08.

Across all Mach numbers there is a reflection pattern that visually represents a regular reflection. However, when the reflection angles are measured and compared to theoretical and experimental results, the reflection pattern represents a Mach reflection in a plane wall case. The reflection patterns strong visual resemblance to a regular reflection suggests that the regular reflection from a plane wall cannot be compared to the regular reflection from a curved wall. The similarity of the regular reflection to the Mach reflection in the plane wall case could be a result of physical history present in the wave.

8.2 Validation of Previous Work

The studies performed on the effects of thermal conductivity on shock wave reflection confirms the results suggested in previous work. It was shown conclusively through differences in the measured shock reflection angles and asymmetry in the reflection patterns that heat transfer into the reflecting surface effects the properties of shock wave reflections off curved surfaces.

Chapter 9 Recommendations

Effect of Wall Thermal Conductivity on Curved Shock Wave Reflection

- Tests at higher Mach numbers can be done. This will give insight into how heat transfer affects reflection properties at higher Mach numbers.
- A CFD analysis can be done on the experimental setup where the two different reflecting surfaces are modelled with different thermal conductivities.
- A measuring technique with increased accuracy for the concave SL-RW angle can be developed. This will aid in understanding how the shear layer is affected by heat transfer in the reflecting surface.
- The test pieces can be switched around and the results of both sets of testing can be compared to each other.
- Further study must be performed on the asymmetry found in the reflection patterns at high Mach numbers.

Weak Shock Wave Reflection off Curved Surfaces

- A CFD analysis could be performed to determine whether the apparent regular reflection is regular reflection or Mach reflection with a small stem. A CFD analysis could also investigate the curved reflected wave found.
- More tests can be done to obtain the transition point of CR to MR at Mach numbers below 1.03.
- Tests with schlieren optical setup could be done to better understand the reflection patterns. This will give insight into the existence of a shear layer.

Bibliography

[1] B. Skews and R. Berry. 'Experimental study of wall conductivity influence on shock wave reflection'. In: *Experiments in Fluids* 58.12 (2017), pp. 1–9. ISSN: 07234864. DOI: 10.1007/s00348-017-2454-3.

[2] A. Cohen. *Effect of Thermal Conductivity on Shock Wave Reflection Patterns on Curved Surfaces*. October. Johannesburg: Undergraduate Report, 2018.

[3] S. Gruber and B. Skews. 'Weak shock wave reflection from concave surfaces'. In: *Experiments in Fluids* 54.7 (2013). ISSN: 07234864. DOI: 10.1007/s00348-013-1571-x.

[4] M. Potter, D. Wiggert and B. Ramadan. *Mechanics of Fluids*. 4th. Cengage Learning, 2012. ISBN: 978-1-4390-6203-6.

[5] B. Skews. *Course Notes - Compressible Flow*. 2nd. Johannesburg: University of Witwatersrand, 2018, pp. 33–78.

[6] V. Peterson. *Equations for Isentropic and Plane Shock Flows of Mixtures of Undissociated Planetary Gases*. Washington DC: NASA, 1965.

[7] G. Settles. *Schlieren and Shadowgraph Techniques: Visualizing Phenomena in Transport Media*. 1st. Berlin, 2001. ISBN: 9783642630347.

[8] R. Berry. *The Effect of Wall Thermal Conductivity on Shock Wave Reflection*. Johannesburg: Masters Dissertation, 2017.

[9] G. Ben Dor. *Shock Wave and High Pressure Phenomena Shock Wave and High Pressure Phenomena*. 2nd. Springer, 2008. ISBN: 9783540745686.

[10] S. Gruber. *Weak Shock Wave Reflections from Concave Curved Surfaces*. February. Masters Dissertation, 2012.

[11] L. F. Henderson and A. Lozzi. 'Experiments on transition of Mach reflexion'. In: *Journal of Fluid Mechanics* 68.1 (1975), pp. 139–155. ISSN: 14697645. DOI: 10.1017/S0022112075000730.

[12] B. Schmidt. *Students Handbook (GALCIT 6-Inch Shock Tube)*. 1st. Pasadena: Caltech, 2013, pp. 2–5.

[13] J. M. Desse and R. Deron. 'Optical Diagnostics of Flows Shadow , Schlieren and Color Interferometry'. In: *Aerospace Lab Journal*. 01. 2009, pp. 1–10.

[14] B. W. Skews et al. 'New flow features in a cavity during shock wave impact'. In: *Proceedings of the 16th Australasian Fluid Mechanics Conference, 16AFMC*. January. 2007, pp. 414–420. ISBN: 9781864998948.

[15] Engineering ToolBox. *Thermal Conductivity of common Materials and Gases*. 2003.

[16] B. Chirewa. *Generation of Weak Shocks and Compression Waves*. Tech. rep. Johannesburg: University of Witwatersrand, 2017.

[17] L. Kirkup. *Experimental Methods*. Wiley, 1994. ISBN: 9780471335795.

Appendix A Apparatus

This Appendix contains details about the equipment used in the experiment. It also includes the technical drawings of the designed test pieces. It must be noted that the large curved surface was designed by Russell Hall, the drawing has been included.

Experimental Equipment

Camera: Photron SA5 Ultra High Speed Camera Model: 775K-C1 Serial Number: 362429074

Light Source: Megaray Lablight Model: MR-LL17 Serial Number: LL175-002-15

Laser: KRYPTON Spyder III Model: KPN5323S Serial Number: 64553

Oscilliscope: Hantek Digital Osciliscope Model: PP-80/150/200 Serial Number: V 00 002662

Signal Conditioner: PCB Piezotronics Model: 482A04 Serial Number: 2257 (F482A04)

Technical Drawings

Akiva Cohen

937491

076 33 88 570

Shock Wave Reflections Off Curved Surfaces

Note: Links are Joined to Test Piece Using Glue aswell

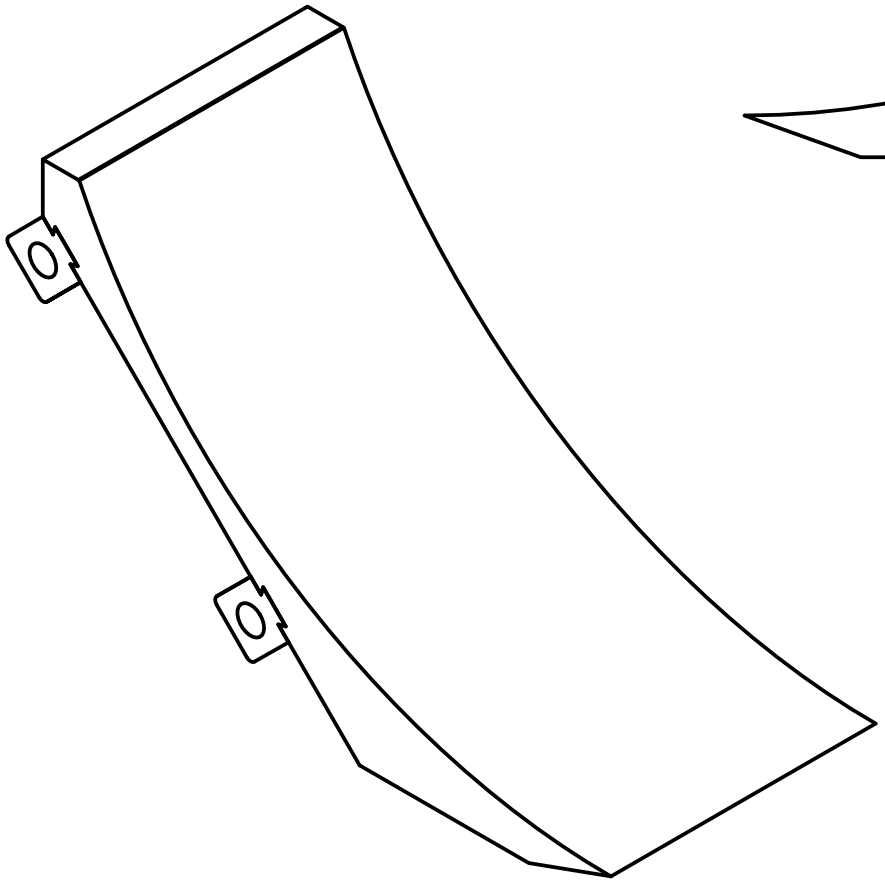

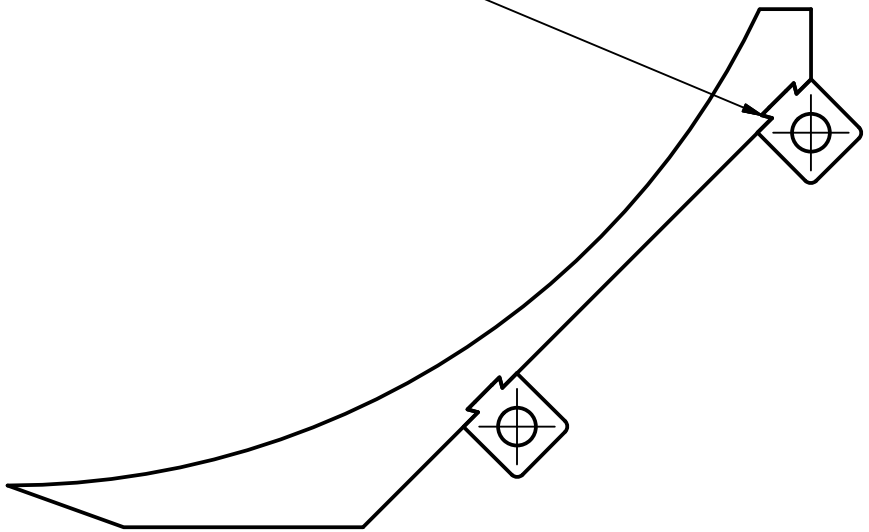

REVISION HISTORY	
SCALE 1:2	
NOTES: SURFACE FINISH ✓ UNLESS OTHERWISE STATED. DIMENSIONS IN mm. DO NOT SCALE. ALL THREADS MEDIUM FIT.	
APPROVED:	
CHECKED:	
DATE: 13/05/2018	
DRAWN BY: Akiva Cohen	
SHEET SIZE:	

DRG NO: Asembly	REV NO.		SHEET 1 OF 3
DESCRIPTION: Assembled Test Piece			
MATERIAL: Steel			

SCHOOL OF MECHANICAL, INDUSTRIAL AND AERONAUTICAL ENGINEERING.
UNIVERSITY OF THE WITWATERSRAND, JOHANNESBURG.

UNIVERSITY OF THE WITWATERSRAND JOHANNESBURG

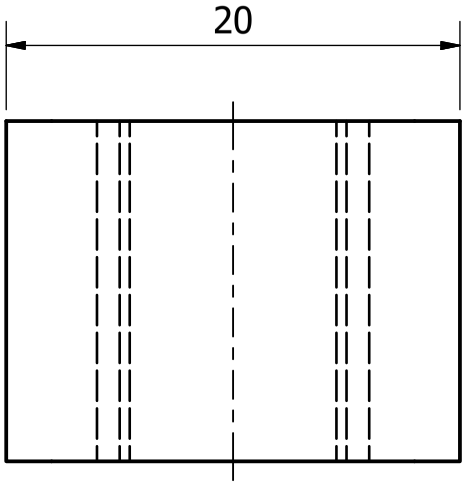

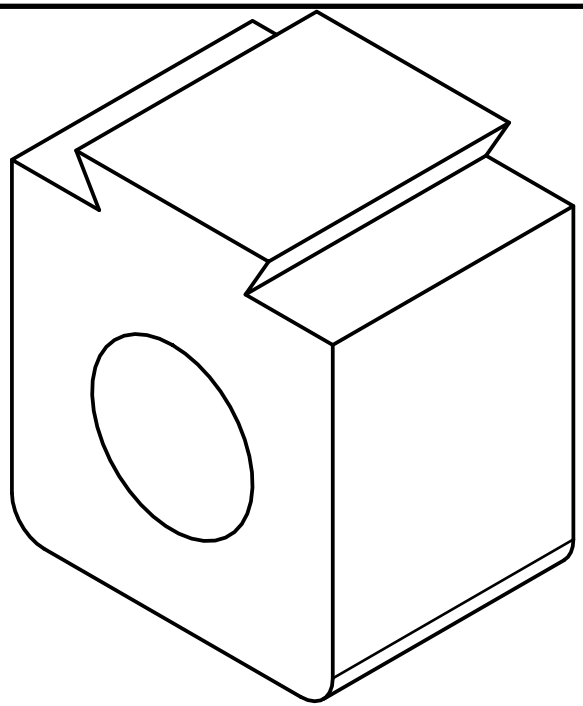

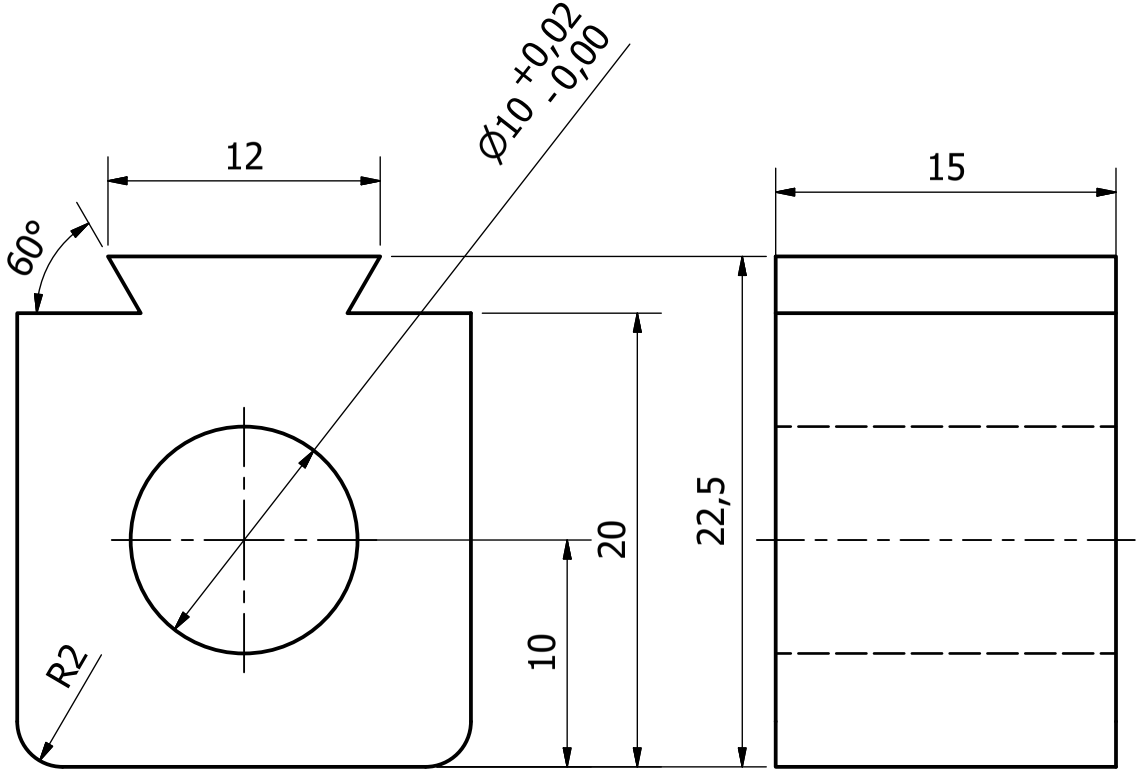

Quantity: 16

REVISION HISTORY
SCALE 1:1
NOTES: N/A SURFACE FINISH ▽ UNLESS OTHERWISE STATED. DIMENSIONS IN mm. DO NOT SCALE. ALL THREADS MEDIUM FIT.
APPROVED:
CHECKED:
DATE:
DRAWN BY: Akiva Cohen
SHEET SIZE: A4

DRG NO: Bottom Join	REV NO.	SHEET 2 OF 3
DESCRIPTION:		
MATERIAL: Steel		

SCHOOL OF MECHANICAL, INDUSTRIAL AND AERONAUTICAL ENGINEERING.
UNIVERSITY OF THE WITWATERSRAND, JOHANNESBURG.

Surface Roughness Must Be Below 50 microns

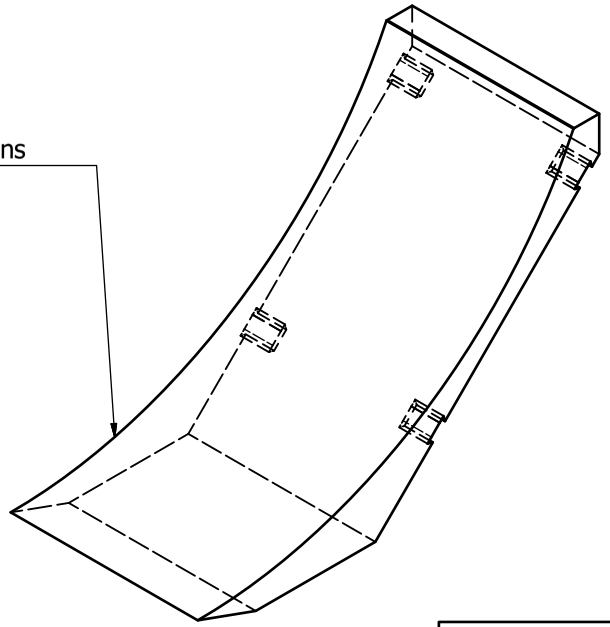

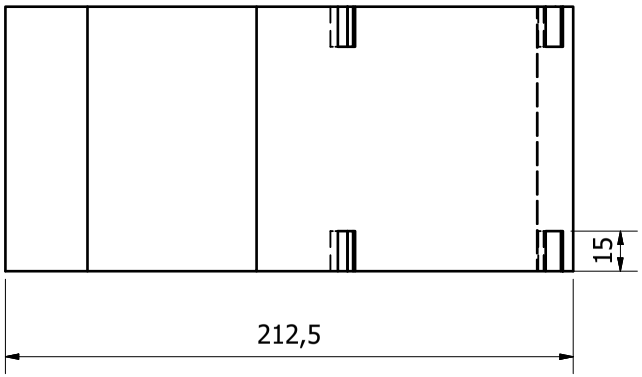

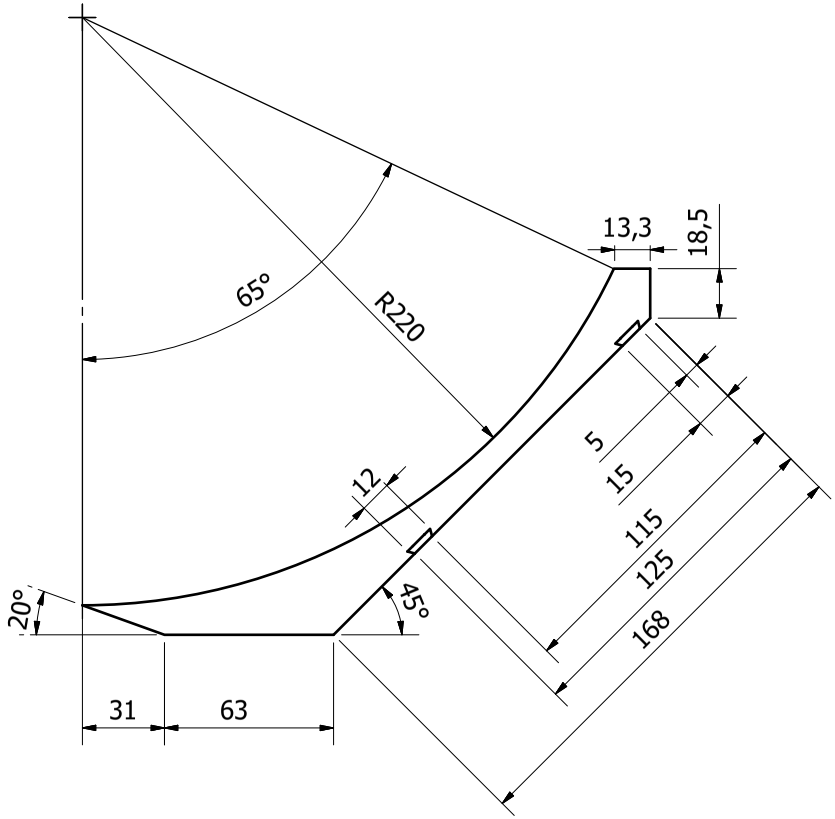

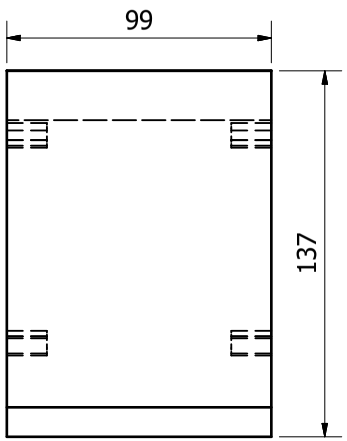

Note: Four Identical Test Pieces. One of each of the following materials:

- Steel
- Copper
- Aluminium
- PVC

REVISION HISTORY
SCALE 1:2
NOTES: N/A SURFACE FINISH UNLESS OTHERWISE STATED. DIMENSIONS IN mm. DO NOT SCALE. ALL THREADS MEDIUM FIT.
APPROVED:
CHECKED:
DATE: 13/05/2018
DRAWN BY: Akiva Cohen
SHEET SIZE: A4

DRG NO: 3mayDiagram	REV NO.	SHEET 3 OF 3
DESCRIPTION: Test Piece Drawings		
MATERIAL: **See Note		

SCHOOL OF MECHANICAL, INDUSTRIAL AND AERONAUTICAL ENGINEERING.
UNIVERSITY OF THE WITWATERSRAND, JOHANNESBURG.

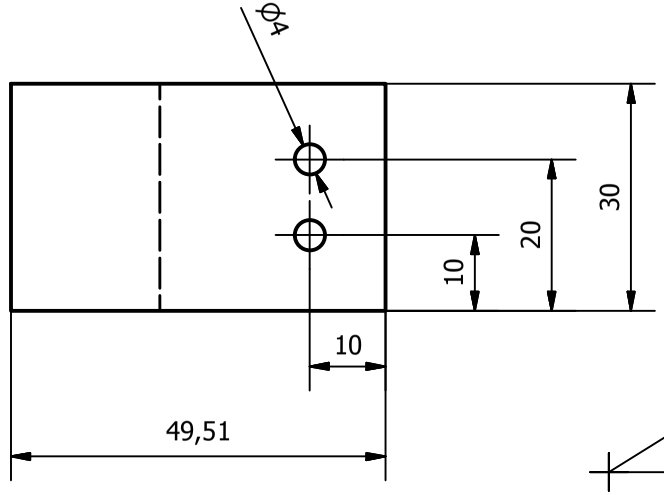

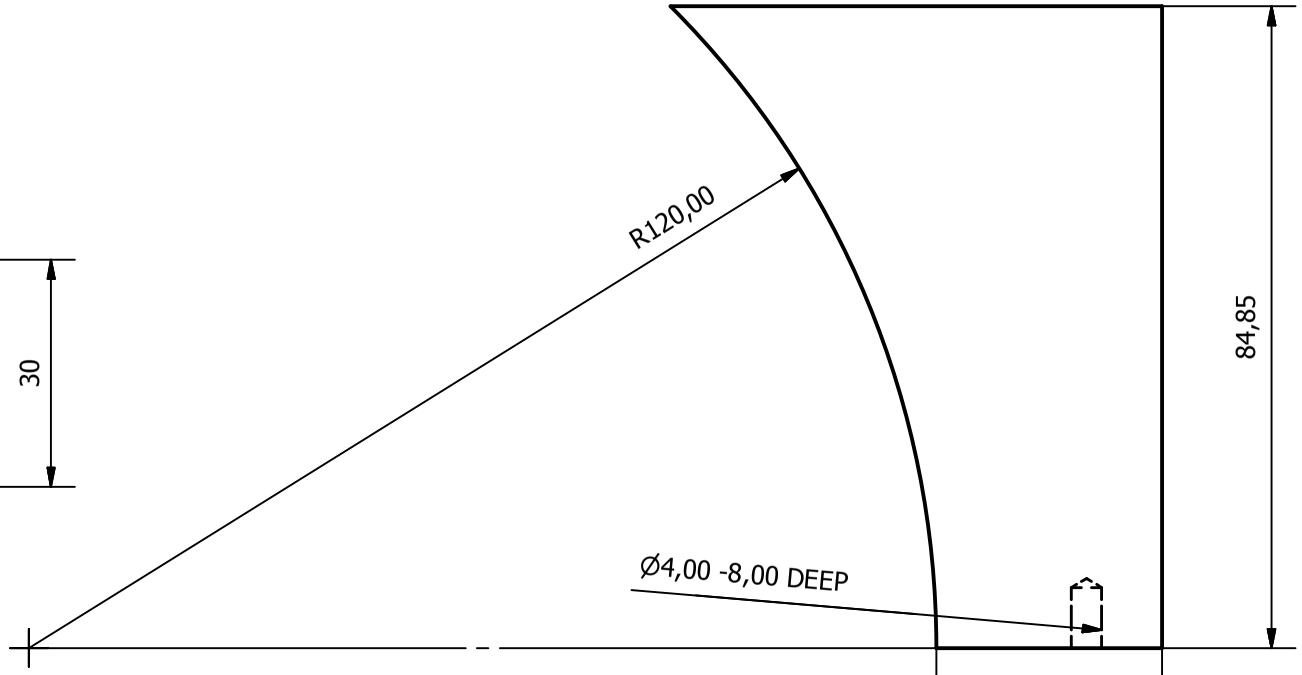

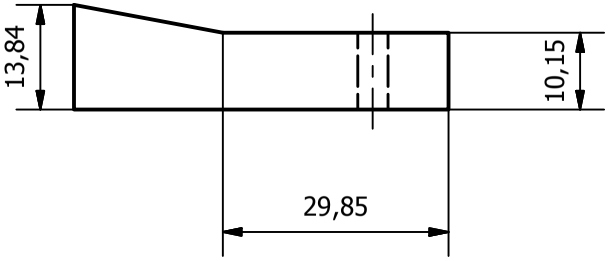

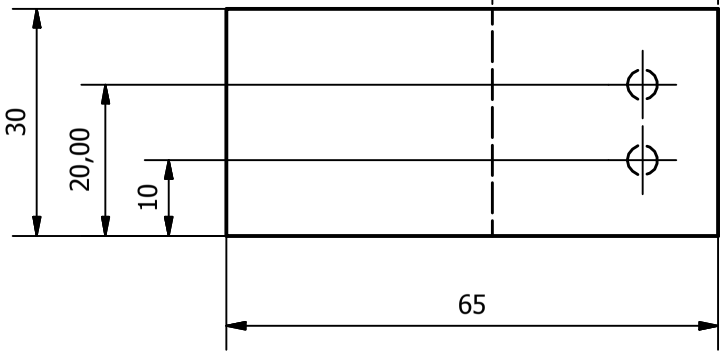

Alignment Tester

Designed by	Checked by	Approved by	Date		Date	
A0050058					2019/12/09	

	Scale 1:1	Edition	Sheet 1 / 3

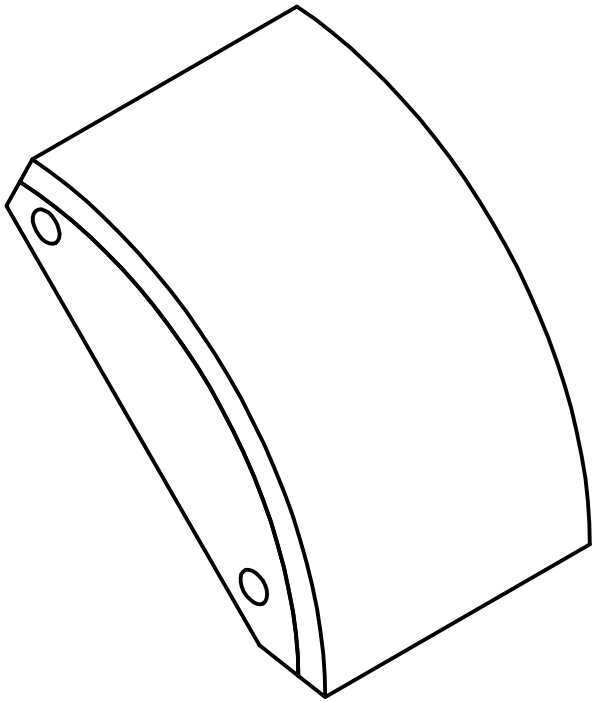

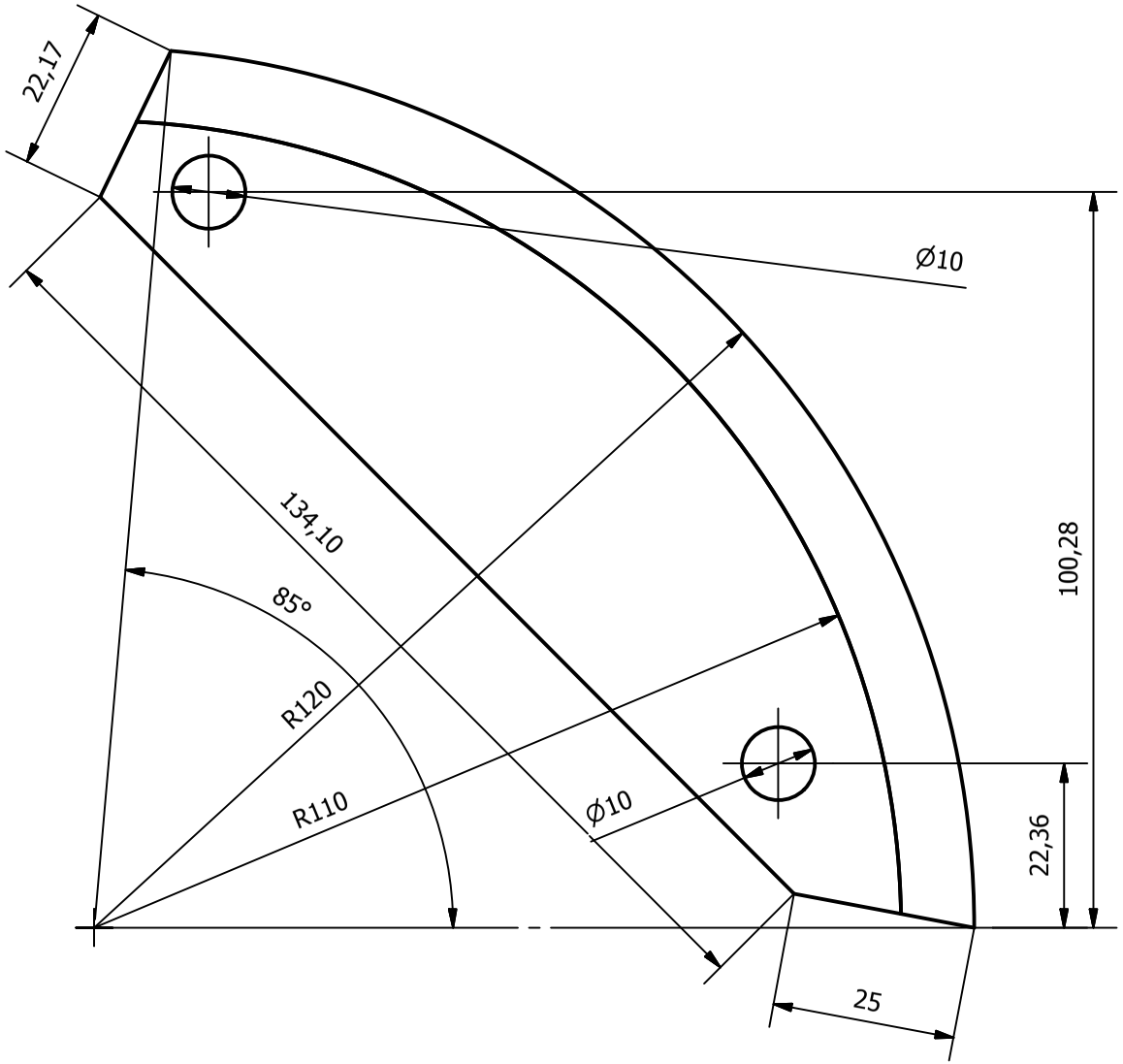

Designed by	Checked by	Approved by	Date		Date	
A0050058					2019/12/09	

	Scale 1:1	Edition	Sheet 2 / 3

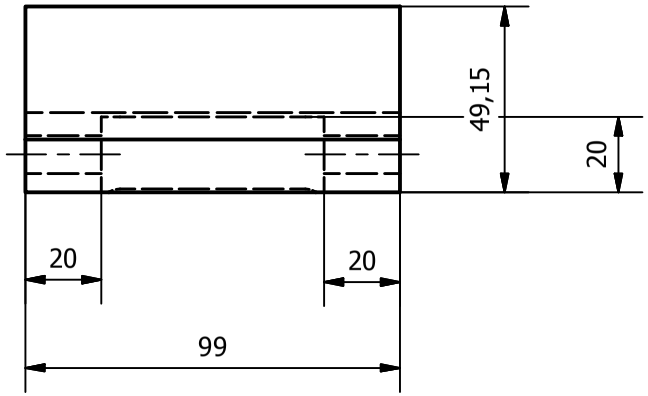

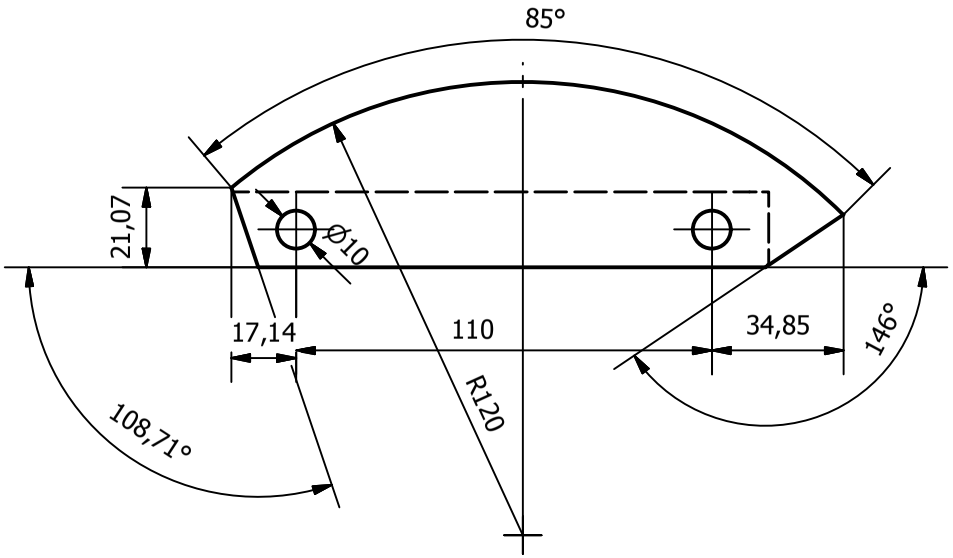

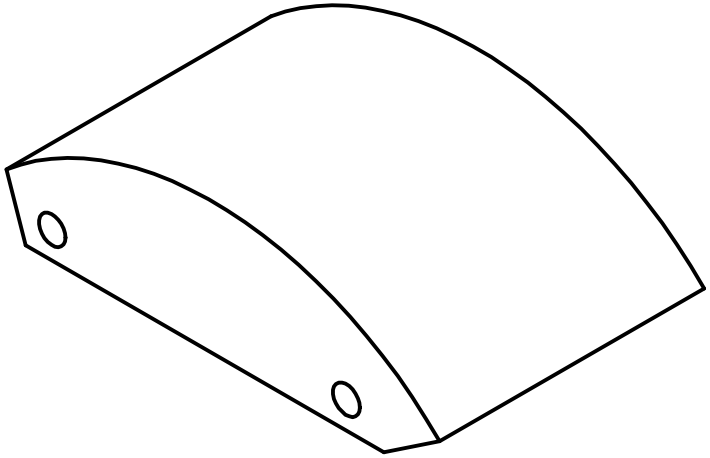

PVC Test Piece

Designed by	Checked by	Approved by	Date		Date	
A0050058					2019/12/09	

	Scale 1:2	Edition	Sheet 3 / 3

A (2 : 3)

PARTS LIST			
ITEM	QTY	PART NUMBER	DESCRIPTION
1	1	C_BP	Bottom Plate
2	1	C_RS	Rear Support
3	1	C_RSB	Rear Support Brace
4	1	C_WS	Circular Arc Surface
5	1	C_RWP	Rear Weld Plate
6	1	C_WAL	Wedge Attachment Left
7	1	C_WAR	Wedge Attachment Right

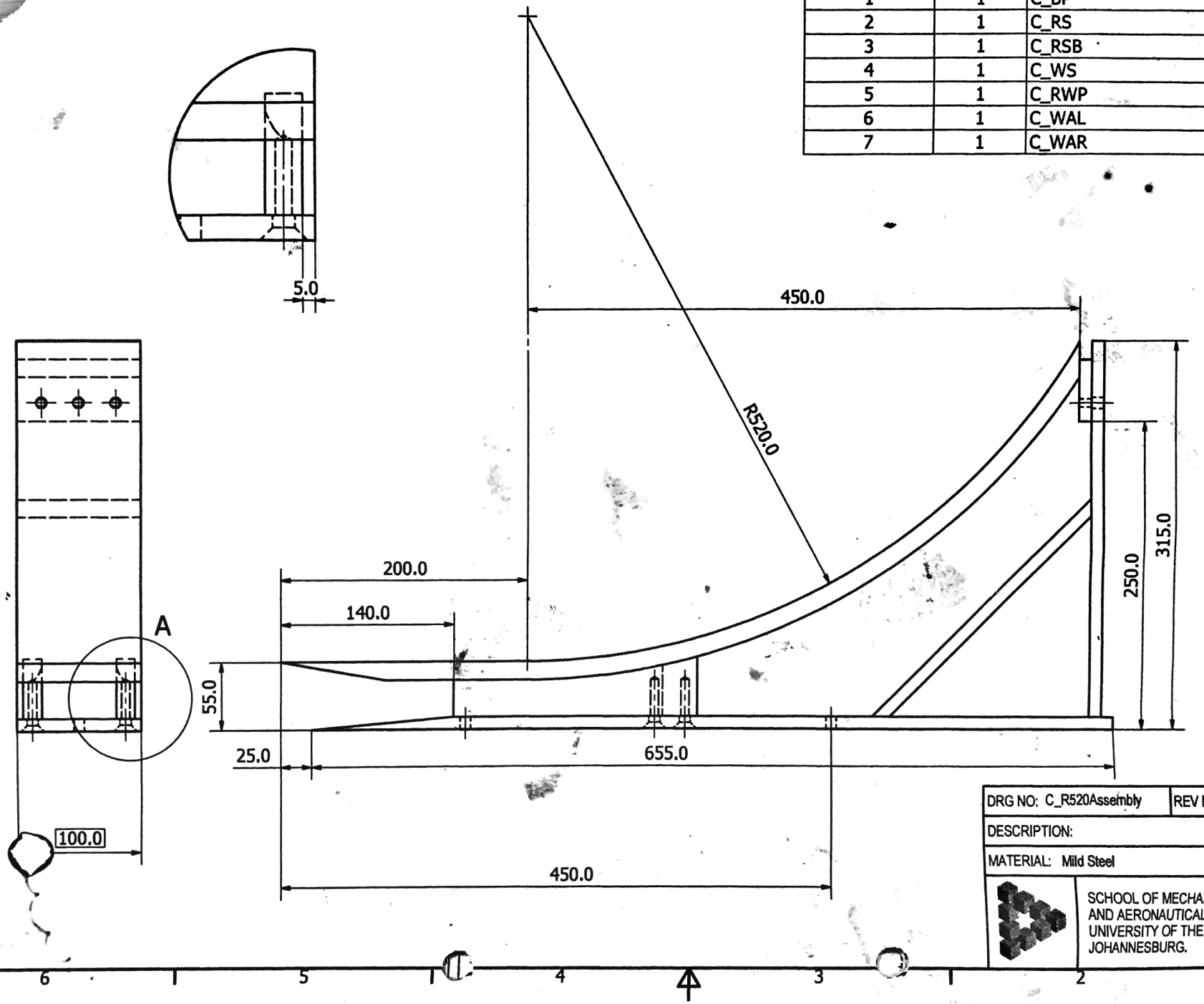

REVISION HISTORY

NOTES:
SURFACE FINISH ∇ UNLESS OTHERWISE STATED.
DIMENSIONS IN mm.
DO NOT SCALE.
ALL THREADS MEDIUM FIT.

APPROVED:

CHECKED:

DATE:

DRAWN BY: Russell Hall

SHEET SIZE: A3

DRG NO: C_R520Assembly | REV NO. | SHEET 1 OF 2

DESCRIPTION:

MATERIAL: Mild Steel

SCHOOL OF MECHANICAL, INDUSTRIAL AND AERONAUTICAL ENGINEERING.
UNIVERSITY OF THE WITWATERSRAND, JOHANNESBURG.

Appendix B Sample Test Log Sheet

This Appendix includes a sample of how the data was recorded to an Excel document during testing. The complete files can be found in the digital appendix (Appendix C). Table B.1 shows five rows of sample data for each test.

Table B.1: Sample Test Data

Delta X	Test Number	Temperature		Driver Pressure	Time		a	v	Mach Number
0,988		C	K	bar	ms	s	m/s	m/s	
Concave Curved									
	8	23	296	5,2	1,91	0,00191	344,09	517,28	1,503
	9	23	296	1,8	2,24	0,00224	344,09	441,07	1,282
	17	23	296	3,2	2,07	0,00207	344,09	477,29	1,387
	18	24	297	3,2	2,07	0,00207	344,67	477,29	1,385
	19	23	296	2,7	2,14	0,00214	344,09	461,68	1,342
Convex Curve									
	12	20	293	1,8	2,29	0,00229	342,34	431,44	1,260
	13	21	294	2,2	2,14	0,00214	342,93	461,68	1,346
	14	21	294	2,8	2,02	0,00202	342,93	489,11	1,426
	21	21	294	4,9	1,92	0,00192	342,93	514,58	1,501
Weak Shock									
	11	17	290	0,18	2,76	0,00276	340,59	357,97	1,051
	12	17	290	0,05	2,85	0,00285	340,59	346,67	1,018
	14	18	291	0,06	2,83	0,00283	341,17	349,12	1,023
	47	13,4	286,4	0,35	2,72	0,00272	338,47	363,24	1,073
	49	14,1	287,1	0,09	2,85	0,00285	338,88	346,67	1,023

Appendix C Uncertainty Analysis

A method shown in the book Statistical Approach to Variability in Data by L Kirkup [17] is to calculate the uncertainty of the measurements in data obtained in this work. By calculating error bounds of +/-2σ (the standard deviation), a confidence limit of 95% that the true mean lies between the error bounds is obtained.

The mean $\bar{x}$ is calculated by:

$$\bar{x} = \frac{\sum x_i}{n} \tag{C.1}$$

The standard deviation σ is calculated by:

$$\sigma = \sqrt{\frac{\sum (x_i - \bar{x})^2}{n}} \tag{C.2}$$

Five measurements were taken on each image, the mean and standard deviation are calculated. These are shown in the Excel file attached in the digital Appendix. Table C.1 shows an example of the calculated error bounds on a test at Mach 1.37.

Table C.1: An Example of the Error Bounds for Measurements Taken at Mach 1.37

Normalized Penetration	0.24	0.42	0.55	0.63	0.77
PVC	0.26	0.63	0.9	0.37	0.49
Copper	0.44	0.39	0.71	0.37	0.71

Angles Measurements with Uncertainties

Figure C.1 below shows the measured RI angle of a Mach reflection off a curved surface.

Figure C.2 below shows the measured RI angle of a regular reflection off a convex surface:

Figure C.3 shows the measured RI angle of a regular reflection off a convex surface:

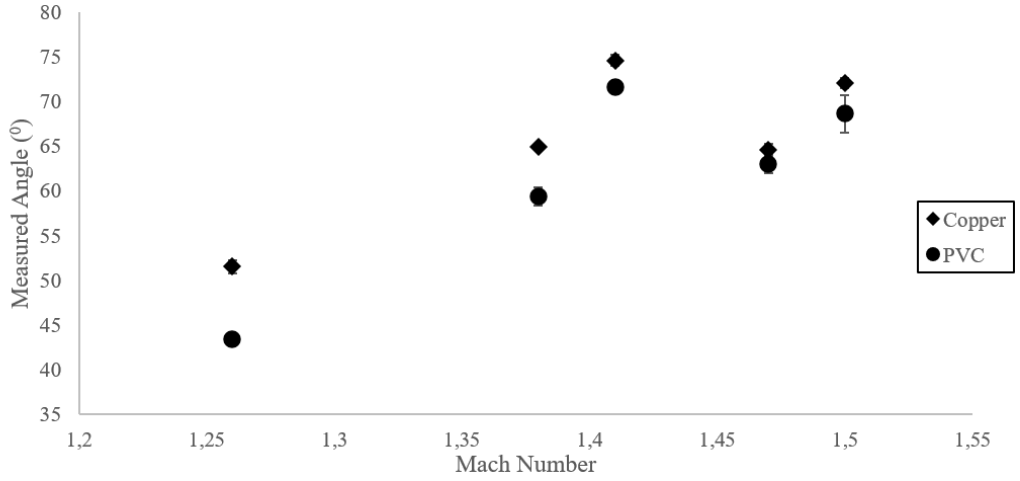

Figure C.1: Scatter Plot of the RI Angle of a Mach Reflection with Error Bars (Concave Case).

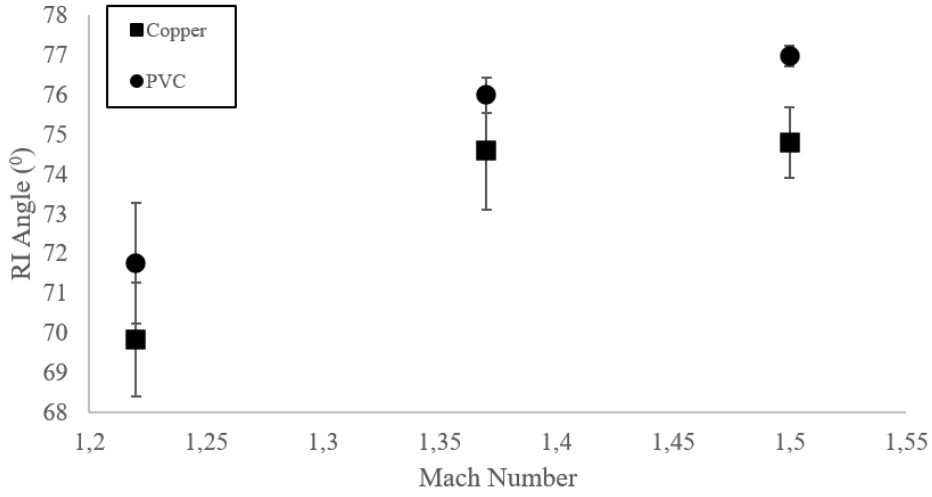

Figure C.2: Scatter Plot of the RI Angle of a Regular Reflection with Error Bars (Convex Case).

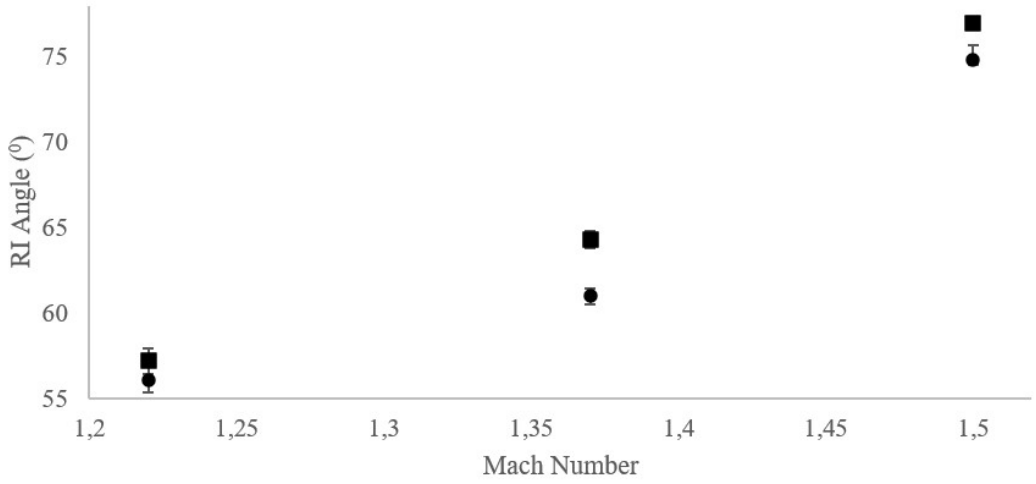

Figure C.3: Scatter Plot of the RI Angle of a Mach Reflection with Error Bars (Convex Case).

Appendix D Digital Appendix

This serves as a guide and explanation to the digital files used in this work. The digital files are found with the project supervisor.

- **Images:** This folder contains all the images in the work. There are three subsections: Concave Curve, Convex Curve and Large Curve.
- **Testing Records:** This folder contains excel documents which contain the testing records of the tests.
- **Shock Tube Documentation:** This folder contains all documentation relative to the operation of the shock tube.
- **Autodesk Inventor Files:** This folder contains the Autodesk Inventor Files relative to this work.